Theses and Dissertations

2016

Regulation of Chronic and Acute Inflammatory Disease by microRNA and Microbiota

Pegah Mehrpouya-Bahrami
University of South Carolina

Regulation of Chronic and Acute Inflammatory Disease by microRNA and Microbiota

By

Pegah Mehrpouya-Bahrami

Bachelor of Science
University of Isfahan, 2006

Submitted in Partial Fulfillment of the Requirements

For the Degree of Doctor of Philosophy in

Biomedical Science

School of Medicine

University of South Carolina

2016

Accepted by

Prakash Nagarkatti, Major Professor

Mitzi Nagarkatti, Chairman, Examining Committee

Daping Fan, Committee Member

Angela Murphy, Committee Member

Ho-jin Koh, Committee Member

Cheryl L. Addy, Vice Provost and Dean of The Graduate School

ii

DEDICATION

       Foremost, I would like to dedicate my dissertation work to my mentors Dr. Mitzi Nagarkatti and Dr. Prakash Nagarkatti who empowered me to be strong by following their guidance and footsteps. Also I dedicate the work to seven people that I love the most in the world: My Dad (Gharib Mehrpoya), My Mom (Ameneh Shahparikhaefi), my dearest sister (Neda Mehrpooya), My brother-in-law (Massoud Mansouri), My adorable nieces (Lily and Rosina), and my all-loving partner-in-everything Behnam.

ACKNOWLEDGEMENTS

daughter. I also thank Lee Ann Faulling, Judy Lawrence, and Tina Akers for all their help.

Finally, and most importantly, a special feeling of gratitude to my loving parents, Ameneh and Gharib whose words of encouragement and push for tenacity ring in my ears. I cannot thank them enough for their support, unconditional love, and their sacrifices for me. I am truly thankful for having my dearest sister in my life. Neda is the source of encouragement and support during all the challenges in my life. Words cannot express how grateful I am to my dear husband Behnam for encouraging me with his intellect throughout this experience. I also would like to thank Lily and Rosina, my beloved nieces for cheering me up and boosting my energy with their funny video clips during long nights of writing.

Dozens of people have helped me throughout my journey at USC, and even though I could not mention their names due to space, I am thankful for all that you have done!

ABSTRACT

Inflammation is implicated in cancer development, degenerative diseases, allergies as well as artherosecelorsis. Dysregulated immune responses lead to chronic inflammation and tissue damage. Finding the ways to terminate inflammatory responses when no longer needed, demands further investigation. Herein, we investigated the modulation of acute and chronic inflammatory disease models by inducing anti-inflammatory state. Acute inflammatory model was induced with SEB, an enterotoxin produced by a ubiquitous Gram-positive coccus, *Staphylococcus aureus (S. aureus)*, which exerts profound toxic effects on the immune system, which leads to the cytokine storm and adverse immune response. SEB is the main cause of nosocomial infections, acute and fatal respiratory distress and toxic shock syndrome.

Regulatory T cells (Tregs) are well characterized for their role in maintaining immunological tolerance and immune homeostasis. The immunosuppressive function of T regulatory cells correlates with the expression of the forkhead transcription factor (Foxp3) in these cells. However, the precise regulatory mechanisms which govern the expression of Foxp3 remain unclear. Herein, for the first time, we uncovered the complex interaction of DNA methyltransferase (DNMT) and/or histone deacetylase (HDAC) which leads to the reactivation of transcription of Foxp3 mRNA and induction of Tregs. More specifically, for the first time, we demonstrated the differential regulation of microRNA following administration of an immuno-suppressive environmental contaminant, 2,3,7,8-Tetrachlorodibenzo-p-dioxin (TCDD) in SEB-primed mice. We

identified the dual role of miR-31 in induction of Tregs by targeting Foxp3 and CYP-1A.

Because there is a growing incidence of obesity in the last 25 years which defines it as an epidemic condition all over the world, we characterized the mechanism of chronic inflammatory disease in Diet-Induced Obesity (DIO) model. Chronic low-grade, systematic inflammation associated with obesity plays a major role in the development of various chronic disease states, including type 2 diabetes, metabolic syndrome and atherosclerotic cardiovascular disease, which contribute to high rates of mortality and morbidity.

Endocannabinoid system consisting of exogenous and endogenous ligands as well as associated receptors, play a major role in diet intake, energy balance, and regulating of immune functions. In the current study, we offer a better understanding in the underlying mechanism of blockade of cannabinoid CB1 receptor with SR141761A in attenuation of DIO phenotype. We revealed that modulation of neuroimmune guidance cue (Netrin-1) and its related receptor (Unc5b), via blockade of cannabinoid CB1 receptor, leads to less retention of macrophages in adipose tissue, and subsequently causes improvement in metabolic functions. In the current study, we have attempted to investigate the impact of CB1 receptor antagonist, on gut microbial community in DIO phenotype. Herein, for the first time, we identified a rise in Akkermansia muciniphila bacterial community, following blockade of CB1 receptor. Interestingly, we uncovered that therapeutic properties of SR141716A at microbial level can be attributed to the suppression of immunogenic bacteria, Lanchnospiraceace and Erysipelotrichaceae community, in DIO phenotype. Furthermore, we found that SR141716A altered microRNA profile in adipose tissue macrophages and skewed the balance of adipose tissue macrophages to more anti-

inflammatory M2 macrophages. These studies provide novel mechanistic information on how microbiota and microRNA can be modulated to suppress acute and chronic inflammation thereby providing new tools to prevent and treat inflammatory diseases.

TABLE OF CONTENTS

LIST OF TABLES

LIST OF FIGURES

CHAPTER I: INTRODUCTION

1.1 STAPHYLOCOCCAL ENTEROTOXIN B (SEB)-INDUCED ACUTE INFLAMMATION

SEB, is an enterotoxin produced by a ubiquitous Gram-positive coccus, *Staphylococcus aureus (S. aureus)*, which has been classified as a super antigen [1] that exerts profound toxic effects on the immune system, which leads to the cytokine storm and adverse immune response [2]. SEB is listed as a category B priority agent by Center for Disease Control and Prevention due to its usage in a bioterrorist attack [3]. SEB is the main cause of nosocomial infections, acute and fatal respiratory distress and toxic shock syndrome[4,5,6]. SEB can activate ~ 20% of T cells by binding both to the non-polymorphic regions of the Major Histocompatibility Molecules (MHC)II on Antigen Presenting Cells (APC), and to the variable region of the β chain of the T cell receptor (TCR) such as Vβ8 TCR [7].

Activation of Mitogen-activated protein kinase (MAPK), extracellular signal regulated kinase (ERK),and c-Jun N-terminal kinase (JNK) , and NF-κB pathway in triggered T cells leads to massive systematic release of pro-inflammatory cytokines such as IL-1β, TNF-α, IFN-γ, IL-2 and IL-4 following exposure to SEB [8].Consequently, the circulating leukocytes are attracted to the site of inflammation and cause more damage to the tissue [9]. Therefore, in order to uncover the immunosuppressive properties of TCDD

on robust T cell responses, we designed an acute-inflammatory model by sensitizing in vivo with SEB.

1.2 REGULATORY T CELLS AND 2,3,7,8-TETRACHLORODIBENZO-P-DIOXIN (TCDD)

Regulatory T cells (Tregs), formerly known as suppressor T cells, are well characterized for their role in maintaining immunological tolerance to the self- antigen and immune homeostasis, the essential allies in regulating autoimmunity, cancer, as well as inflammatory diseases. Depletion of Tregs is associated with breakdown in immune tolerance and sever autoimmunity [10,11,12,13,14,15]. Tregs are characterized as small proportion of CD4^{+} T cells (5-10%). Thymus-derived natural Treg (nTreg) and the peripherally induced Tregs, are subpopulations of T cells with immunosuppressive function. Genetically hypoplasic thymus in DiGeorge syndrome and neonatal thymectomy in mice causes defects in Tregs differentiation and peripheral tolerance [16,17]. Scurfy mutant mice (Foxp3 knock-out) can be rescued from lymphoproliferative autoimmune syndrome by bone marrow reconstitution from wild type mice [18,19].

Cortical epithelial cells in thymus interact with naïve CD4 T cells with their MHC-II molecules, and facilitate their differentiation into nTregs [20]. Other stimulatory signals from co-stimulatory molecules (CD40 ligand, and CD28), and cytokines (TNF-α, and TGF-β) are involved in Tregs expansion [21]. TGF-β is also known as an essential cytokine in mediating peripheral Treg differentiation from the mature conventional T cells, and their homeostasis [22]. IL-2 is a master regulator of Tregs survival in periphery [23,24].

2

Numerous surface markers are associated with Tregs such as CD25 (the IL-2 receptor α-chain), CTL-associated antigen 4 (CTLA4), and glucocorticoid-induced TNF receptor (GITR). However, these markers cannot be considered as exclusive markers for Tregs. For example, other immune cells such as activated B cells, T cells and macrophages also express surface marker CD25. The forkhead/winged-helix family transcription factor (Foxp3), which contributes to development and immunosuppressive function of T regulatory cells, is being considered as an exclusive and specific marker for Tregs [25,26]. However, the precise regulatory mechanisms which govern the stable expression of Foxp3 remain unclear. Accessible demethylated locus of Foxp3 gene for transcription factors, and other epigenetic regulators such as Histone deacetylases (HDAC), phosphorylase and ubiquitin ligase are integral mediator for the stable expression of immunosuppressive Tregs [27,28,29,30,31]. Tregs can trigger suppression of immune responses in direct-contact manner with target cells, Granzyme/perforin mediated apoptosis of target cells, or by secreting anti-inflammatory cytokines such as IL-10 or TGF-β [32].

Recently, the role of Aryl hydrocarbon receptor (AhR) in the induction of Foxp3 in Tregs has generated significant interest [33,34]. AhR was characterized as a ligand-activated transcription factor involved in xenobiotic metabolism but more recently, it has also been shown to play a critical role in the regulation of T cell differentiation, specifically induction of Tregs. 2,3,7,8-Tetrachlorodibenzo-p-dioxin (TCDD) is a ubiquitous environmental contaminant which causes immunosuppression and carcinogenesis [35]. TCDD is a potent ligand for AhR because of which it is widely used to study the effect of AhR activation in the regulation of immune response. Induction of

3

functional Tregs and immune-modulatory effect of TCDD in different disease models such as Experimental Autoimmune Encephalomyelitis (EAE) and Non-Obese Diabetic was well established [36,37]. Thus, AhR activation by TCDD-like ligands will provide a better understanding in underlying mechanism of Treg induction and their immunosuppressive function in immune system activation.

1.3 DIET-INDUCED OBESITY (DIO), CHRONIC INFLAMMATION

The growing incidence of obesity in the last 25 years defines it as an epidemic; with estimates upwards of 1.45 billion overweight adults in the world, of which approximately 500 million are obese [38]. Moreover, a maintenance of childhood obesity at 16% prevalence from 2006-2010 and a significant increase in obesity prevalence over a 12-year period in males aged 2-19 years was observed[39].

Chronic low-grade, systematic inflammation associated with obesity plays a major role in the development of various chronic disease states, including type 2 diabetes, metabolic syndrome and atherosclerotic cardiovascular disease, which contribute to high rates of mortality and morbidity [40].

Stromovascular fraction of adipose tissue is aggregated with immune cells during obesity[41]. In particular, with intense migration of Macrophages (Mϕ) in adipose tissue, Adipose Tissue Macrophages (ATMs) have been shown to be integral to the obesity-triggered inflammation in adipose tissue [42,43,44], and their recruitment to adipose tissue correlates with the production of pro-inflammatory molecules , including tumor necrosis factor-α (TNF-α) [45], interleukin-1β (IL-1β) and IL-6 [46,47] that potentiate insulin resistance [48]. Macrophages are phagocytic cells, which show incredible heterogeneity in phenotype

and function, as local milieu factors determine their activation state and subsequent properties. Mɸs are thought to be activated in two separate pathways becoming polarized to M1 or M2 states. With over-nutrition, M1 are said to be "classically activated" mɸs induced by LPS and IFNγ that secrete pro-inflammatory cytokines (TNF-α, IL-6, IL-12) and generate nitric oxide (NO, a reactive oxygen species) via iNOS activation [49,50]. However, "alternatively activated" mɸs or M2 that populate lean adipose tissue are activated by IL-4 and IL-13, secrete anti-inflammatory cytokines, and have upregulated arginase which opposes NO production [51]. However, studies have shown that the M1 and M2 macrophage phenotypes are not clearly defined, the key signaling molecules such as DNA methyltransferase 3b (DNMT3b) and peroxisome proliferator activated receptor-γ(PPAR-γ) deregulate ATMs polarization, inflammation and insulin insensitivity [50,51] .

In the current study, we utilized diet-induced obese (DIO) mice as the chronic inflammatory disease model. In order to have a better understanding in underlying chronic inflammatory mechanism of DIO phenotype and its associated metabolic dysfunction, we mainly focused on adipose tissue macrophages (ATMs). For the first time we uncovered the regulatory mechanism in induction of anti-inflammatory state in adipose tissue by triggering adipose tissue macrophages. The current study may represent a novel avenue in treatment of obesity-associated inflammation and metabolic syndrome. Outstandingly, our findings can be considered in therapeutic approaches for macrophage-related inflammatory disease models such as atherosclerotic cardiovascular disease and cancer, which contribute to high rates of mortality and morbidity.

5

1.4 THE ENDOCANNABINOID (EC) SYSTEM AND IMMUNE REGULATION

The onset of medical application of *Canabbis sativa* or marijuana plant is evident from Far Eastern folklore medicine. The Endocannabinoid (EC) system consists of classical (CB1, CB2) and non-classical (TRPV1, GPR55, etc) receptors and their endogenous and exogenous ligands. In the early 1900's, British scientists initiated the scientific approaches towards *cannabis,* and made efforts for extracting the principal active ingredient of the plant that exert psychoactive effects [54]. The preliminary experiments of *cannabis*, in a range of illnesses including cholera, rheumatic diseases, delirium tremens and infantile convulsions was conducted to test the possible therapeutic properties of the plant.

Eventually, the natural compounds of *cannabis* including (−)-Δ9-tetrahydrocannabinol (THC), with psychotropic activity, and cannabidiol (CBD), non-psychotropic, were extracted from the plant [55,56]. The extraction of the fundamental and active ingredient of the plant conveyed attentions to their endogenous binding sites in human body. Cannbinoid CB1 receptor was discovered by cloning rhodopsin class G-protein-coupled receptors (GPCRs) and experimenting THC for finding its potential binding site. Later on, Cannabinoid CB2 receptor was uncovered at Cambridge Medical Research Council in UK [54,57]. GPCRs are the largest membrane receptors, comprising of 7 transmembrane helices, and intervening loop N-terminus (an extracellular) and C-terminus (an intracellular) [58].

Ligands for non-classical receptors of Endocannabinoid system such as vanilloid (TRPV1) receptor and orphan GPR55 receptors, are comprised of cannabinoid and non-

cannabinoind (capsaicin) compounds. Vanilloid receptor can also be stimulated by voltage, heat, and proton [59,60,61].Therefore, non-classical receptors are not exclusively considered part of endocannabinoid system. Various organs in human body express classical EC receptors (CB1and CB2) with different patterns of intensity. For example, central nervous system (CNS) is rich in CB1 receptors. However, CB2 receptors are more abundant in periphery and immune system-related cells [62,63]. Meanwhile, CB2 receptors can also be found in CNS with lesser intensity [63]. Macrophages and activated T cells can express CB1 receptors as well [64]. Besides CB1/CB2 classical receptors and GPR55, non-classical receptors of EC, the structures and properties of new EC receptors which express on hippocampus and GPR119, remain elusive [65,66].

The rhodopsin x-ray crystal structure of CB1 receptors demonstrated the existence of hydrophobic binding pocket which requires carbon fatty acid chain with 20-22 length, saturation of the last five carbons in acyl chain, and the least three double bonded carbons (C=C) [67] . Alteration in binding affinity of different ligands and cannabinoid receptors is due to the polymorphism in single nucleotide binding site. Peptide sequence of CB1 and CB2 receptors revealed 44% similarities between them [68,69,70,71].

Investigations for detection of the potential endocannabinoid ligands (endogenous ligands), initiated in Raphael Mechoulam's lab led to the discovery of lipid based N-Arachidonoyl ethanol amine (Anandamide or AEA) in porcine brain in 1992 [72,73]. The plant source of Anadamide was reported in chocolate beans [74]. Anadamide is present in nearly all tissue and possess anti-inflammatory and orexigenic (appetite stimulant) properties [75,76] . 2-Arachidonoylglycerol (2-AG), the second lipid based endogenous

7

ligand of EC system, with the equal binding affinity to both CB1 and CB2 receptors is more concentrated in brain than Anadamide [77,78]. 2-AG is known as the strong GPCR stimulant based on in vitro findings, but the in vivo properties of 2-AG is yet elusive because of physiological complexity [79]. Fatty acid amide hydrolysis (FAAH) and monoacylglyceride lipase (MAGL), maintain EC levels of AEA and 2-AG respectively [80,81,82]. N-Arachidonoyl dopamine (NADA), Virodhamine (OAE), and 2-Arachidonyl glyceryl ether (noladin ether) are the other endogenous ligands in EC systems [79,83,84,85].

Discovery of EC system was followed by laboratory synthesis of different cannabinoids based on the herbal cannabinoid structure. The pioneers in synthetic cannabinoid were Roger Adams (1941) and Raphael Mechoulam's group. The findings of the endogenous ligand of EC systems led to the synthesis of new ligands for endocannabinoid receptors [86]. The synthetic ligands were structured in agonist or antagonist (inverse agonist) modes for specific endocannabinoid receptors [87].

SR141716A also known as Rimonabant, Acomplia , and Zimulti was the first selective CB1 receptor blocker (inverse agonist) to be approved for use as an anti-obesity drug [88]. The therapeutic effect of Rimonabant is not restricted to its anorectic properties, secession of smoking and addiction behaviors, improvement of short term memory, improvement of human sperms motility and viability, as well as inversing the psychoactive and cardiovascular effect of THC are considered as Rimonabant therapeutic applications [89,90,91,92,93].

Endocannabinoid system possess Neuro-protective and immune-modulatory effects. Immuno-modulatory effect of endocannabinoid and cannabinoid systems, is reliant on the intensities of cannabinoid receptor expression in blood immune cells (with

8

the following rank order: B cells > NK cells > monocytes/macrophages > polymorphonuclear neutrophils > CD8 lymphocytes > CD4 lymphocytes) [94] . Activation of endocannabinoid system in experimental autoimmune encephalomyelitis (EAE), an animal model of multiple sclerosis and MS patient (High level of Anandamide) was recognized. The intervention treatment with anandamide uptake inhibitor UCM707 can significantly ameliorates the pathological score of the disease [95,96,97] . Anti-tumor activity of Anadamide on Molt-4 human tumor cells, and murine EL-4 tumor T cells, was established by demonstrating its ability to trigger significant level of apoptosis [98]. Thus, management of endocannabinoids system may establish an innovative treatment modality against inflammatory disorders.

1.5 MICROBIOTA AND IMMUNE SYSTEM

Microbial community of gut is consisting of symbionts (beneficial), neutral (commensals) as well as detrimental (pathobionts) microorganisms. The homeostasis of these essential allies can modulate the host health and function.

Age, genetic, physiology, diet, environment are the main factors impacting gut microbiota [99]. Gut community becomes more stable, diverse, and highly complex by age [100]. Diet is the most potent manipulator of the gut microbial compositions. Previous studies have shown that both long term diet habit as well as short term changes in diet can lead to shift in gut microbiota [101,102]. Dietary pattern of more protein consumption is associated with more prevalence of Bacteroides versus more carbohydrates in diet is correlated with remarked gut Prevotella entrotype. Short term changes in diet also can

9

introduce rapid changes in the abundancee of gut microbiome [103]. Previous studies demonstrate that antibiotic treatment leads to disturbance of gut community and the repeated administration of antibiotic leads to profound and more permanent alteration in gut community [104]. The presence, absence and variations in particular genes also correlate with abundances of specific genera of gut microorganism. Break-down of tolerance to intestinal microbial community in IL-10 deficient mice, resulted in impulsive enterocolitis, adenocarcinoma, and subsequently spontaneous development of inflammatory bowel syndrome [105].

Hormone level, metabolism, immune system function and other physiological factors can also alter intestinal microbiota [106,107,108,109,110]. Dysbiosis of gut microbial community is associated with chronic inflammatory diseases including ulcerative colitis, diet-induced obesity and metabolic syndrome. Gut immune system determines colonization of microbial community in gut and contributes to the interaction of host-microbiome [111]. Dysregulation in innate (antibacterial peptide of Paneth cells and enterocytes) and adoptive (IgA production in mucosal associated lymphoid tissue) immune system function of gut also caused by the damage in gut barrier, leads to collapse in homeostatic state of intestinal host-microorganisms [112,113,114].

Thus, the potential therapeutic approaches to alter microbiota to treat a wide range of diseases, ranging from metabolic disorders (e.g. obesity and type 2 diabetes) to autoimmune diseases (such as inflammatory bowel disease and colitis), cancer, neurodevelopmental disorders (e.g. autism), and even allergies (Food poising, asthma), remains an exciting possibility that remains to be further explored. Taken together,

10

studies on gut microbiota, its manipulation, and fecal transplantation is considered as a potential therapeutic strategy for many disorders.

1.6 <u>MICRORNA (MIR)</u>

MicroRNAs (miRNAs) are a class of small non-coding RNAs (~18-22 nucleotides) with highly conserved RNA sequences [115]. miRNAs are capable of regulating gene expression at post-transcriptional and post-translational level. The first miRNA discovered in C.elegans in 1993, was named lin4 [116]. Several miRNAs have been involved in regulating innate and adoptive immune systems. Dysregulated miRNA profile in several disorders including cancer, inflammatory disease, and autoimmune illness has been reported [115]. For instance, two different miRNA (miR-155 and miR-182) were implicated in SEB-induced Acute Lung Injury (ALI) [117,118].

miRNAs which are known as the negative regulator of gene expression, can bind to the complementary sequences of the 3′ untranslated region (3′ UTR) of their target genes, and lead to mRNA degradation or translational cessation [119,120].

Different algorithms (miRmap, TargetScan, and miRwalk, etc) for target prediction are available. Ingenuity systems such as Ingenuity Pathway Analysis (Qiagen, Valencia, CA) tools and its modules, are a powerful system in prediction of differentially altered miRNA, their down-stream and up-stream effects, and top affected canonical pathways. Importing the differentially expressed genes into Cytoscape (ClueGo module) or other gene ontology software help predict the most implicated pathways.

In the current study, we investigated the role of the miRNA in amelioration of acute (SEB-primed mice) or chronic (Diet-Induced Obesity, DIO) disease models. We

11

identified the unique miRNAs which are the key regulators in modulating the immune responses and maintaining the immune homeostasis during the inflammatory disorders.

1.7 STATEMENT OF HYPOTHESIS AND AIMS

Because of the growing rise in autoimmunity and inflammatory disorders that are causing public health crisis, further investigation is critically needed to understand the mechanisms of pathogenesis as well as finding novel therapeutic approaches such as new non-toxic immunosuppressive drugs and other biologicals. Furthermore, chronic inflammation is implicated in a large number of immuno-pathological disorders including cardiovascular, neurodegenerative, cancer, diabetes, and metabolic disorders. Thus, understanding the underlying basic mechanisms of acute and chronic inflammation will open up new avenues for better targeted therapeutics for inflammatory disorders and their complications.

In the current study, we tested the central hypothesis that inflammation is regulated by complex interactions between epigenome and microbiome. Thus, agents that alter microRNA in immune cells and gut microbiota, can be used effectively to attenuate acute and chronic inflammation.

To test this hypothesis, in the first part of this study, we investigated the molecular mechanism of induction of immunosuppressive regulatory T cells(Tregs), after AhR activation with TCDD. Our data uncovered novel regulatory pathways mediated by microRNA that are induced following AhR activation that trigger inducible regulatory T cells, and attenuate acute inflammation.

12

In the second part of our study, we developed diet-induced obesity (DIO) phenotype as the model to study chronic inflammation. We targeted the endocannabinoid system in DIO by blocking the cannabinoid receptors and investigated its effect on miRNA profile and gut microbiota. Our data identified novel miRNA that targeted pro-inflammatory M1 macrophages and promoted their differentiation into anti-inflammatory M2 macrophages. Also, such a treatment to block cannabinoid receptors led to altered microbiota that promoted anti-inflammatory phenotype. Finally, we discovered a novel interaction of with neuroimmune guidance cue receptors and their related ligands which regulate macrophages chemotaxis, thereby attenuating inflammation and DIO phenotype. Together, the current study has identified how targeting AhR and Cannabinoid receptors leads to alterations in microRNA and microbiota profiles, which in turn attenuate inflammation. These studies form the basis for developing novel therapeutic regimen to treat inflammatory diseases.

CHAPTER II: ROLE OF MICRORNA IN EPIGENETIC REGULATION OF 2, 3, 7, 8-TETRACHLORODIBENZO-P-DIOXIN (TCDD)-MEDIATED INDUCTION OF FOXP3 IN T CELLS ACTIVATED BY STAPHYLOCOCCAL ENTEROTOXIN B

2.1 INTRODUCTION

Regulatory T cells (Tregs) are well characterized for their role in maintaining immunological tolerance and immune homeostasis [121,122]. The immunosuppressive function of T regulatory cells correlates with the expression of the forkhead transcription factor (Foxp3) in them [123,124], however, the precise regulatory mechanisms which govern the expression of Foxp3 remain unclear. Recently, the role of Aryl hydrocarbon receptor (AhR) in the induction of Foxp3 in Tregs has generated significant interest [125,126]. AhR was characterized as a ligand-activated transcription factor involved in xenobiotic metabolism but more recently, it has also been shown to play a critical role in the regulation of T cell differentiation, specifically induction of Tregs. 2,3,7,8-Tetrachlorodibenzo-p-dioxin (TCDD) is a ubiquitous environmental contaminant which causes immunosuppression and carcinogenesis [127]. TCDD is a potent ligand for AhR because of which it is widely used to study the effect of AhR activation in the regulation of immune response.

14

Epigenetic modifications such as DNA methylation of regulatory sequences, histone modifications and post-transcriptional and post-translational repression by microRNA are key players which direct the overall immune response [128,129]. Considering that AhR activation regulates Treg differentiation, and our previous studies demonstrating the ability of TCDD to modulate miR profile as well as cause epigenetic changes in immune cells, we were interested in knowing if there is any cross talk between these pathways that impact Treg differentiation during antigen exposure. It is known that the majority regulation of gene expression is mediated by various transcriptional factors via binding to their recognition sequences in the upstream of enhancer region of gene. Regulation of methylation of CpG dinucleotides in the gene regulatory region and acetylation of histones in nucleosome structure modifies the transcription pattern of genes by modulating the access of the transcription factors to their recognition sequences. Previously, it has been shown that TCR activation leads to the accumulation of Methyl-binding proteins MBD, MeCP1, MeCP2, and DNA methyltransferases (DNMTs) in Foxp3 promoter region, which results in repression of Foxp3 transcription [130,131]. Treatment of activated T cells with DNA methyltransferase (DNMT) and/or histone deacetylase (HDAC) inhibitors leads to the reactivation of transcription of Foxp3 mRNA and induction of Tregs [132,133]. Suppression of DNA methyltransferases at the regulatory regions of the gene is followed by less recruitment of histone deacetylases (HDACs)22 . HDACs enzymes catalyze the removal of the acetyl groups from the lysine residue in histones and thus results in closed chromatin configuration, which limits the access of the transcription factors to their recognition sequences [134,135].

In order to have a broader view of epigenetic mechanism regulating gene expression with TCDD treatment, we performed high throughput analysis of microRNAs which identified several pathways, including DNA methylation, Histone acetylation, Aryl hydrocarbon receptor (AhR) signaling, and differentiation of Tregs. Furthermore, our data demonstrated that TCDD influences the accessibility of Foxp3 transcription factor binding sequences by triggering DNMTs and HDACs in T cells activated by SEB.

2.2 MATERIALS AND METHODS

Animals-

Female C57BL/6 mice (aged 6-8 weeks) were purchased from the Jackson laboratory (Bar Harbor, ME). Foxp3/GFP knock-in mice, encoding a GFP-Foxp3 fusion protein were purchased from Jackson laboratory (Bar Harbor, ME). All mice were housed at the (American Association for the Accreditation of Laboratory Animal Care (AAALAC)-accredited animal facility at the University of South Carolina, School of Medicine (Columbia, SC). All procedures were performed according to NIH guidelines under protocols approved by the Institutional Animal Care and Use Committee.

Effects of TCDD on mice primed with SEB in vivo-

To determine the effect of TCDD on T cell response to SEB, mice were injected with SEB, in sterile phosphate-buffered saline (PBS), or PBS alone as a vehicle, into hind footpads of mice (10ug/footpad) once, as previously described (24200994) SEB was obtained from Toxin Technologies (Sarasota, FL). TCDD, kindly provided by Dr. Steve

16

Safe (Texas A & M Health Science Center, Collage Station, Texas), was administered immediately after SEB, intraperitonally (ip) at 10µg/kg in a total volume of 100ul in vehicle (corn oil) as previously described [136] .The draining popliteal lymph nodes (PLN) were excised from mice and made into single-cell suspensions by a tissue homogenizer. Cells were subjected to red blood cell lysis, counted, and stained with antibodies purchased from Biolegend (San Diego, CA) against CD3, Vβ8, Foxp3 and CD4, and analyzed by Beckman Coulter FC500 flow cytometer (Indianapolis, IN)

Measurement of cytokines from collected serum-

Cytokines levels were analyzed in the serum using enzyme-linked immunosorbent assay (ELISA) kits for interferon-gamma (IFN-γ), tumor necrosis factor-alpha (TNF-α), transforming growth factor-β (TGF-β) interleukin-6 (IL-6), and IL-10 purchased from Biolegend (San Diego, CA), as described [137]. All ELISAs were performed as per the manufacturer's instructions.

Total RNA isolation-

Total RNA (including small RNAs) was isolated from selected CD4+ cells (EasySep ^{TM} PE Positive Selection kit, Stem Cell Signaling, Vancouver, BC) from PLNs using the miRNeasy kit from Qiagen (Valencia, CA) by following the manufacturer's instructions. The purity and concentration of the RNA was confirmed spectrophotometrically with Nanodrop (Thermo Scientific, Waltham, MA)

17

miRs expression profiling and analysis-

The expression profile of miRs was assessed in the PLN cells by Affymetrix GeneChip miRNA 1.0 array platform [138]. The array contains 609 murine-specific probes from Sanger miRBase . Total RNA was labeled with FlashTag biotin HSR hybridization (Genisphere, Hatfield, PA) as described in manufacturer's instructions (Affymetrix, Santa Clara, CA). Correlation of the hybridization signal intensities of all the expressed miRNAs were log transformed and visualized in the form of a heatmap. Ward's method was assessed for hierarchical clustering of differentially expressed miRs. miRNA QC Tool (Affymetrix Inc), a software for data summarization, Log2 transformation, normalization and quality control, was used as described previously [139] .

Purification and analysis of mouse T regulatory Cells (Tregs) and T cells-

Tregs were sorted from Foxp3/GFP knock-in mice. The LN cells were sorted for GFP using flow cytometry to isolate Foxp3$^+$ Tregs.   regulatory cells by sorting with. In some experiments, CD4$^+$ T cells were purified using EasySep ^{TM} PE Positive Selection kit (Stem Cell Signaling, Vancouver, BC) and CD4 PE antibody (BioLegend, San Diego, CA).

Chromatin immunoprecipitation (ChIP) assay-

ChIP assay was performed using the ChIP kit (Cell Signaling, Danvers, MA), as described [140]. The DNA which was immuno-precipitated was amplified by qRT-PCR. Antibodies against the molecules used were as follows: DNMT3a, DNMT3b, DNMT1 and MeCP1 from NovusBio (Littleton,CO); KLF10 and AcH3 from Active Motif

18

(Carlsbad, CA); Sp1 from Abcam (Cambridge, MA); H3K9 from Cell Signaling (Danvers, MA). The primers sequences used for the upstream Foxp3 enhancer CpG site and Foxp3 proximal promoter were the same as previously described [141].

UpstreamFoxp3 enhancer CpG site were 5#-GCGGAGAGGGATCGGGAAA-3# (forward) and 5#-ATGAGGAAGACGATGGCGAGGAT-3# (reverse), and the primers for the Foxp3 proximal promoter were 5#-CCTTGGCAACATGATGGTGGTGAT-3# (forward) and 5#-AAGAAGGGATCAGAAGCCTGCCAT-3# (reverse).

Bioinformatics analysis-

The differentially expressed miRNA target genes were assessed by three of the leading miRNA target prediction algorithms: miRwalk (http://www.umm.uni-heidelberg.de/apps/zmf/mirwalk/), microRNA.org (http://www.microrna.org/microrna/home.do) and TargetScan (http://www.targetscan.org/).

To carry out an enrichment analysis of predicted target genes of miRs in biological pathways, we used, Ingenuity Pathway analysis (IPA), (Mountain View, CA, USA.). IPA predicts the top affected Canonical Pathways, causal connections between differentially altered miRs and their target genes, downstream effect along with their upstream regulators. The Molecular Activity Predictor (MAP) feature of IPA was performed to predict the downstream effect of the differentially expressed miRs which were overlaid to the dataset including miRs probes, fold changes and the p Values.

19

qReal Time PCR(qRT-PCR)-

Expression of mature miRNAs and target genes was determined by quantitative qRT-PCR. Total RNA was converted to cDNA using the miScript cDNA synthesis kit (Qiagen, Valencia, CA) according to the manufacturer's instructions. For miRNA validation, the miScript SYBR green PCR kit (Qiagen, Valencia, CA) was used, and fold change of miRNA was determined by using the $2-\Delta\Delta CT$ method. Snord96a was used as small RNA endogenous control. For mRNA validation, an SSO advanced SYBR green PCR kit from Bio-Rad (Hercules, CA) was used according to the manufacturer's instructions, and GAPDH was used as an endogenous control. The following primers were used: GAPDH forward (F) (5′-AATGGATTTGGACGCATTGGT -3′) and reverse (R) (5′-TTTGCACTGGTACGTGTTGAT -3′); Foxp3 F (5′-CACCTATGCCACCCTTATCCG-3′) and R (5′-CATGCGAGTAAACCAATGGTAGA-3′) and CYP1A1 F (5′-CAATGAGTTTGGGGAGGTTACTG-3′) and R (5′-CCCTTCTCAAATGTCCTGTAGTG-3′), KLF10 F (5′-GTGACCGTCGGTTTATGAGGA-3′), and R (5′-AGCTTCTTGGCTGATAGGTGG-3′), Sp1 F (5′-ATCACTATGGTTGCGATGGACT-3′), and R (5′-GCCGATCCAGTTACGGGAG-3′), DNMT1 F (5′-AAGAATGGTGTTGTCTACCGAC-3′), and R (5′-CATCCAGGTTGCTCCCCTTG-3′), DNMT3A F (5′-GAGGGAACTGAGACCCCAC-3′), and R (5′-CTGGAAGGTGAGTCTTGGCA-3′), DNMT3B F (5′-AGCGGGTATGAGGAGTGCAT-3′), and R (5′-GGGAGCATCCTTCGTGTCTG-3′), Mecp2 F (5′- ATGGTAGCTGGGATGTTAGGG-3′), and R (5′-TGAGCTTTCTGATGTTTCTGCTT-3′)

20

Transfection with miR-31 mimic, inhibitor, Foxp3 target gene protector and

CYP1A1 target gene protector-

Lymph nodes from naive C57BL/6 mice were harvested and cultured in 10 ml of complete medium at 37°C and 5% CO2. Complete medium was comprised of RPMI 1640 medium (Gibco Laboratories, Grand Island, NY) supplemented with 10% fetal bovine serum (FBS), 10 mM L-glutamine, 10 mM HEPES, 50 μM β-mercaptoethanol, and10 U/mL Penicillin/streptomycin. Cells were seeded at 4×10^5 cells in 24-well plates and transfected with either 40 nM synthetic mmu-miR-31-5p miScript miRNA mimic (AGGCAAGAUGCUGGCAUAGCUG) or AllStar negative-control small interfering RNA (siRNA). For inhibiting the miR-31, cells were treated with 100 nM anti-mmu-miR-31-5p miScript miRNA inhibitor (AGGCAAGAUGCUGGCAUAGCUG) or miScript AllStar negative control for 24 h using HiperFect transfection reagent (Qiagen, Valencia, CA) according to the manufacturer's instructions. To assess a reliable verification of miRNA-targeted genes, the transfection of the cells with miScript target protector for Foxp3 gene and CYP1A1 genes was performed. Target Protectors was used provide evidence that a gene is regulated by a particular miRNA. Foxp3miScript target protector was designed as:

CTGCAATTCTGGAGACAGCA

AGAATACAAGGCTTGCACCT

This target protector was aimed to detect several transcripts of the same gene (Foxp3): NM_001199348, NM_001199347, NM_054039

CYP1A1 miScript target protector was designed as:

TTCTGGCACAGAGGTGCTCT

21

TGCCACCTGCTGAGGCTAAA

This target protector was aimed to detect several transcripts of the same gene (Cyp1a1):

NM_001136059, NM_009992.

In these experiments, All-star negative control and negative control miScript Target

protector were used.

Statistical Analysis-

For the in vivo mouse experiments, 5or 4 mice were used per experimental group,

unless otherwise specified. In vitro experiments were performed in triplicate. For

statistical differences, one-way ANOVA was calculated for each experiment. Tukey's

post-hoc test was performed to analyze differences between groups. A p value of ≤ 0.05

was considered statistically significant.

2.3 RESULTS

TCDD decreases induction of SEB-driven Vβ8+ T cells and pro-inflammatory cytokines.

SEB is known to selectively trigger a strong Vβ8+ T cell response and the

cytokines storm. We investigated the effect of TCDD on SEB-induced inflammatory

response *in vivo*. Our lab had previously shown that a single dose of 10μg/kg of TCDD

was able to markedly decrease lymphocyte infiltration into colon lumen in the mouse

model of colitis[127]. Thus, to investigate the efficacy of TCDD in amelioration of SEB-

induced inflammation, we used the same dose. We treated mice with ip injections of

22

TCDD at the same time as the administration of SEB into footpads. In order to determine if TCDD could suppress SEB-induced T cell proliferation in draining PLN, we analyzed the cells on day 3, the peak of the response [131]. Because SEB activates Vβ8 TCR+ T cells [142], we examined their percentage and absolute cell numbers by staining the cells for CD3 and Vβ8 and analyzing them by flow cytometry. The data showed that in SEB+TCDD treated mice, there was marked decrease in the percentages of Vβ8+ T cells (8.3%) when compared SEB+Vehicle treated mice (14.1%) (Fig 2.1A). TCDD treatment also caused a significant decrease in the total cell numbers (Fig 2.1B).

Because SEB triggers cytokine storm[143], we next investigate the effect of TCDD on pro-inflammatory cytokine production both in the serum and in the draining lymph node (LN) following SEB administration. The data showed that TCDD treatment caused significant decrease in inflammatory cytokines, including IFN-γ, TNF-α, and IL-6 both in the serum (Fig 2.1C) as well as in the PLN culture supernatants (Fig 2.1 D), when compared to controls.

TCDD induces T regulatory cells and anti-inflammatory cytokines.

We next determined whether TCDD induces, Tregs in popliteal LNs of SEB primed mice. We noted a significant increase in the frequency of Tregs in the popliteal lymph node in SEB+TCDD group when compared to SEB+vehicle group (Fig 2.2A). Also, TCDD treatment induced significant increase in anti-inflammatory cytokines, including IL-10, TGF-β (Fig 2.2B).

Next, we determined if TCDD would enhance the induction of Tregs that were antigen (SEB)-specific. To test this, we used Foxp3/GFP knock-in mice, which were

23

immunized with SEB and treated with vehicle or TCDD. Three days later, the level of expression of Foxp3 within Vβ8+ T cells was analyzed by flow cytometry. Interestingly, TCDD caused significant induction of Foxp3 + Vβ8+ T cells, thereby suggesting that TCDD does induce antigen-specific T cells (Fig 2.2C)

To confirm that the TCDD-treated Tregs were indeed able to suppress SEB-activated T cell proliferation and cytokine production, we performed cell-mixing experiments. Tregs were isolated from the Foxp3/GFP knock-in mice and treated with 100 nM TCDD as previously described [127]. Cell-mixing experiments were performed by co-culturing Tregs and SEB-activated LN cells. Our results demonstrated that TCDD-derived Tregs suppressed the SEB-activated T cell proliferation in a dose-related manner (Fig 2.2D). In these co-culture supernatants, when we measured cytokines, we observed significant suppression of the pro-inflammatory cytokines (TNF-α, IFNγ, and IL-6) and induction of anti-inflammatory cytokines (Fig 2.2E)

TCDD administration profoundly changes the miR profile.

To investigate the role of miRs in TCDD-mediated decrease in anti-SEB T cell response differential expression of miRs was assessed using Affymetrix GeneChip® array of SEB-activated T cells, following vehicle or TCDD treatment. Cluster analysis of 609 miRs was analyzed by unsupervised hierarchical clustering and visualized in the form of dendrogram (Fig 2.3A). SEB+TCDD group showed distinct miR expression profile when compared to SEB+vehicle treated group.   We performed further analysis and identified 37 miRs that were significantly upregulated and 51 miRs that were significantly downregulated in SEB+TCDD groups when compared to SEB+vehicle

treatment group (Fig 2.3B). Next, we used Ingenuity Pathway (IPA) software application to identify the candidate targets for filtered miRs, which are shown in (Table 1), along with their seed sequence and respective fold change. A comprehensive network showing the interaction of the miRs and their target genes was generated by IPA (Fig 2.3C). TCDD-mediated alterations in the expression of miRs were linked to many pathways including AhR signaling (ARNT), apoptosis (Fas, FasL, caspases, BCL2), epigenetic (DNMTs and HDACs), and Tregs (Foxp3).

Over-expression of miR-148a and miR-491 upon TCDD administration, ameliorates demethylation of Foxp3 promoter regions.

The critical role of DNA Methyltransferases (DNMTs) within regulatory regions of Foxp3 was stressed by studies showing that conditional deletion of DNMT1in mice resulted in lethal autoimmunity, which can be reversed by the exogenous transfer of Tregs [144]. Interestingly, in the affymetrix microarray, we noticed that miR-148a and miR-491 were up-regulated upon TCDD exposure. We validated these findings with qRT-PCR, in which we showed that miR-148a and miR-491 were up-regulated in SEB+TCDD treated groups when compared to SEB+vehicle controls (Fig 2.4 A, and 2.4 B). We determined by Ingenuity Pathway Analysis that miR 148a and miR-491 target DNA methyltransferase, DNMT1, DNMT3a, and DNMT3b by binding to their 3'UTRs with significant mirSVR scores. Our results demonstrated the inverse correlation between miR-148a, miR-491 with DNMTs, in which over expression of miR-148a, miR-491 following TCDD treatment in activated T cells resulted in significant reduction in DNMT3a, DNMT3b and DNMT1 (Fig 2.4C, 2.4D, and 2.4E).

25

In order to investigate the interaction of DNMTs with Foxp3 promoter region, which contains the recognition binding sequences for transcription factors, we performed CHIP assays for DNMTs. We used purified Tregs from Foxp3/GFP knock-in mice as described in Methods. Our results demonstrated that Tregs from SEB+TCDD mice exhibited significant decrease in DNMT1 and DNMT3b binding to Foxp3 promoter CpG island when compared with SEB+Vehicle group (Fig 2.4 F, 2.4G). Whereas, there was no significant difference in DNMT3a and MeCP2 binding to Foxp3 promoter (Fig 2.4 H, 2.4 I). These data suggested that TCDD may inhibit DNA methyltransferase (DNMTs) in activated T cells, which may result from up-regulation of miR-491 and miR-148a.

miR-34a regulates Histone H3 acetylation in Tregs via HDAC1.

Previous studies from our laboratory demonstrated the involvement of HDAC-I family in SEB-activated T cells, in which HDAC-I was highly up-regulated in T cells upon SEB activation when compared to naïve T cells [131]. Data obtained from high throughput analysis, showed significant over expression of miR-34a (> 2.2) in TCDD+SEB group compared with Vehicle+SEB. Furthermore, we validated these findings with qRT-PCR, in which miR-34a was markedly up-regulated in TCDD+SEB group compared to Vehicle+SEB (Fig 2.5A). HDAC1, a target gene of miR-34a was significantly suppressed upon TCDD administration in SEB-activated T cells (Fig 2.5B). Next, we tested whether the decreased HDAC-1 triggers acetylation of H3. As before, we isolated Tregs, from Foxp3/GFP knock-in mice using the two groups: SEB+TCDD and SEB+vehicle. Chip assay was conducted for acetylation of histone 3 (AcH3) upstream of Foxp3 enhancer region. Our data demonstrated that Foxp3 regulatory region was significantly more acetylated in TCDD+SEB group compared with Vehicle+SEB

26

group (Fig 2.5C). Chip assay was performed for acetylation of H3K9 in Foxp3 promoter region and our data showed higher acetylation of H3K9 in Foxp3 regulatory region (Fig 2.5D). Taken together, our data suggested that decreased HDAC expression in SEB activated T cells which were treated with TCDD, correlated with increased acetylation of H3K9. The promoter region of actively transcribed gene is often acetylated at histone H3 lysine 9. Therefore; TCDD causes Tregs induction through the important epigenetic modification (HDAC/H3K9).

TCDD regulates the active binding of Sp1/KLF10 in Treg promoter via epigenetic mechanism.

Active role of the transcription factor Sp1 (specificity protein 1) in protection of CpG islands from de novo methylation is well established [145,146,147]. KLF10, a member of the Krüppel-like family of transcription factors, binds to Sp-1-GC rich DNA sequences and regulates the transcription of a number of genes [148]. In the present study, we therefore evaluated the expression level of KLF10 and Sp1 following TCDD administration in SEB-activated T cell with real time qRT-PCR, and the data showed that they were markedly up-regulated compared with SEB-activated T cell (Fig 2.6A, 2.6B). We then studied the predicted miRs regulators of Sp1 and KLF10 by Ingenuity Pathway Analysis (IPA) software. miR-31 is predicted to target Sp1 expression with mirSVR score: -0.1127 , and PhastCons score: 0.5983, while miR-26b is predicted to regulate KLF10 expression with mirSVR score: -0.6935, and PhastCons score:0.6217.

Furthermore, we noticed that in affymetrix microarray, miR-31 (Fold change: -1.60) and miR-26b (Fold change: -1.80) were down-regulated in SEB+TCDD group compared with SEB+vehicle group. We confirmed these findings by conducting qRT-

27

PCR, in which miR-31 was found to be down-regulated ~10 times and miR-26b was down-regulated ~3 times compared to vehicle treated group (Fig 2.6C, 2.6D). Next, Chip assay was used to show interaction of KLF10/Sp1 with upstream of Foxp3 enhancer region, using Tregs isolated from Foxp3/GFP knock-in mice, as before. Our data demonstrated that upon TCDD treatment in SEB-activated T cells there was more interaction of KLF10/Sp1 with Foxp3 promoter region compared to SEB+vehicle-activated T cells (Fig 2.6E. 2.6F), which led to the higher induction of Foxp3.

Dual role of miR-31 in TCDD-mediated upregulation of CYP1A1 and Foxp3 in activated T cells.

We we explored the putative target genes of miR-31 by using the comprehensive pipeline of ten different reliable algorithms miRWalk 2.0 [149,150], interestingly, we noted that Foxp3 was also identified as the highly predicted target gene for miR-31 ($p < 0.05$) using at least 5 different databases (miRwalk2.0, miRTarBase, miRecords, and TarBase 7.0, and PICTAR 2.0) We next utilized the miR functional analysis to investigate the effect of decreased expression of miR-31 in induction of functional and suppressive Tregs. Efficient inhibition of miR-31 activity in T cells was achieved by transfecting the SEB-activated T cells with customized inhibitor for miR-31. The data showed that the expression level of Foxp3 was significantly higher in transfected T cells with miR-31 inhibitor when compared to the mock (Fig 2.7A). Finally, we tested whether miR-31 regulates the expression of Foxp3 by directly targeting its 3' untranslated region or targets any negative or positive intermediate regulator of Foxp3 gene. For this purpose, we transfected SEB-activated T cells with miR-31 mimic and specific custom-designed

28

Foxp3 target protector. Our results demonstrated that while miR-31 mimic suppressed the expression level of Foxp3, co-transfection with miR-31mimic and Foxp3 target protector, resulted in higher expression of Foxp3 when compared to the mimic (Fig 2.7B, 2.7 C). Taken together, these data suggested Foxp3 as the direct target gene for miR-31.

Interestingly, using 4 different databases (miRWalk 2.0, microrna.org,miRBase, and Target Scan), we also identified CYP1A1 as the highly predicted target gene for miR-31. Transcription of CYP1A1 was markedly suppressed in transfected SEB-activated T cells with synthetic mimic for miR-31 , while co-transfection of SEB-activated T cells with mimic-31 and CYP1A1 target protector, rescued CYP1A1 from suppressive function of mir-31 mimic (Fig 2.7D). These data demonstrated that miR-31 can also directly regulate the transcription of CYP1A1.

TCDD induces AhR signaling by altering miR profile in SEB-activated T cells.

In the data assessed from affymetrix microarray, we also distinguished a group of 18 miRs, that were implicated in AhR signaling pathway. Using IPA software, we overlaid the AhR signaling canonical pathway with differentially expressed miRs and explored for meaningful paths by applying the Molecular Activity Predictor (MAP) feature to have an overview of the downstream effect of the differentially expressed miRs (Fig 2.8A). Among these miRs, we focused on the differential expression of miR-455, and miR-351 using qRT-PCR, and found that both miRs were significantly down-regulated in SEB+TCDD group compared with SEB+vehicle (Fig 2.8A, 2.8B). Also, ARNT, the target gene for miR-455, along with the CYP-1A1, the target gene for miR-351, were significantly up-regulated in SEB activated T cells upon TCDD treatment (Fig

29

2.8C, 2.8D), when compared to controls. These data demonstrated that TCDD–mediated differential expression of miRs can also play a critical role in AhR-signaling pathway.

2.4 <u>DISCUSSION</u>

In the current study we investigated the effect of 2,3,7,8-Tetrachlorodibenzo-p-dioxin (TCDD), an environmental contaminant, on T cell response to Staphylococcal Enterotoxin B (SEB), which is classified as the super antigen. In the mouse, SEB activates T cells that express the TCR, Vβ8. Thus, by studying Vβ8+T cells, one can investigate the direct effect of TCDD on antigen-specific T cells. In the current study we observed that TCDD suppressed pro-inflammatory (IFN-γ, TNF-α, and IL-6) and induced anti-inflammatory (IL-10, and TGF-β) cytokines. Moreover, TCDD also induced to Tregs that were antigen-specific (Vβ8+Foxp3+) and immunosuppressive.

Interestingly, miR analysis in TCDD- treated T cells revealed significant alterations in the expression of miRs that were directed towards induction of Foxp3+ Tregs. Our data suggested that TCDD-induced over-expression of miR-491 and miR-148a may cause demethylation within Foxp3 promoter region by targeting DNMT3a and DNMT3b, and consequent acetylation of histone H3. Increase in acetylated histone H3 may lead to the interaction of KLF10/SP-1 and potential induction of Foxp3. Interestingly, miR-31, which was down regulated following TCDD treatment, was found to be complementary to the 3'-UTR of Foxp3, CYP1A1 and SP-1. Importantly, miR-31 directly targeted Foxp3 as shown using transfection experiments. Moreover, miR-26b, which targets KLF10, was also down regulated in TCDD treated groups. Together, our

30

studies identified TCDD-mediated alterations in the expression of several miRs that either directly or through epigenetic pathways, induce the expression of Foxp3 in antigen-activated T cells.

In the current study, we used SEB, an enterotoxin produced by a ubiquitous Gram-positive coccus, *Staphylococcus aureus (S. aureus)*, which has been classified as a super antigen [151] to study the effect of TCDD on Tregs. SEB is listed as a category B priority agent by Center for Disease Control and Prevention due to its potential usage in a bioterrorist attack [152]. SEB is the main cause of nosocomial infections, acute and fatal respiratory distress and toxic shock syndrome[153,154,155]. SEB can activate ~ 20% of T cells by binding both to the non-polymorphic regions of the Major Histocompatibility Molecules (MHC) class-II on Antigen Presenting Cells (APC), and to the variable region of the β chain of the T cell receptor (TCR) such as Vβ8 TCR [156]. Thus, in addition to studying the effect of AhR activation on the enterotoxin, use of SEB provided us an opportunity to directly study antigen-specific Tregs that were Foxp3+ and Vβ8 TCR+.

We also used Foxp3/GFP knock-in mice so that we could sort the Foxp3+ Tregs there by giving us a tool to study the epigenetic changes in purified Treg population. Numerous chemicals can activate AhR including environmental contaminants such as TCDD, and other compounds such as tryptophan derivatives, flavonoids and biphenyls [1-4]. AhR ligands can be divided into nonbiological/synthetic or biological compounds resulting from natural processes [157]. FICZ is a tryptophan photoproduct, with structural similarity to a high affinity natural AhR ligand, FICZ. While AhR was identified in the context of xenobiotic metabolism and toxicity, its role in immune system regulation is beginning to unravel [158]. The ability of TCDD to induces suppressor T cells was

31

demonstrated as early as 1984, using mouse chimeras [159]. However, further studies were limited because no specific marker was identified on such suppressor T cells until the discovery of Foxp3, on CD4+ T cells, which were then designated as Tregs [160].

There have been conflicting reports on the nature of TCDD-induced Tregs. One group suggested that the Tregs induced by TCDD are CD4+CD25+ but may not express Foxp3 [161]. Studies from our own lab also showed that TCDD triggers Tregs that are Foxp3+ [162]. The differences in these studies can be explained by the nature of disease models studied. For example, in the study that found TCDD to not induce Tregs that were Foxp3+, the authors used graft-vs-host response [161] whereas in the study where TCDD was shown to induce Foxp3+ Tregs, EAE was used as a model [162]. In EAE, it is well established that the clinical disease primarily rests on the balance between Tregs and Th17 cells. In the current study, we clearly demonstrated the induction of Foxp3 on SEB antigen-activated Vβ8+ T cells following TCDD treatment.

miRs have emerged as important regulators of gene expression. In the current study, we explored the differential expression of miRs in the presence of TCDD during super-antigen-induced activation of T cells. We first carried out an affymetrix analysis of miR expression followed by Molecular Activity Predictor (MAP) feature in Ingenuity Pathway Analysis (IPA) software to identify the down-stream effect of differential of miR expression. Such an approach provided a global analysis of differentially regulated miRs in TCDD induced immunosuppression. Specifically, we also identified two miRs—miR-184a, and miR-491— as the important regulators of TCDD-induced Tregs in super-antigen- activated T cells because of their ability to modulate DNMT expression and modification of chromatin configuration. The connection between miR-148a and

32

DNMT1 expression has been studied in cancer models. For example, a recent study reported the dramatic suppression of miR-148a in pancreatic cancer tissues and that there was an increase seen in DNMT1 expression [163]. Over-expression of miR-148a in ASPC-1 cancer cells led to a decreased level of DNMT1 and suppression of metastasis. Also, over-expression of miR-148a was seen in CD4+ T cells in both patients with lupus and lupus-prone MRL/lpr mice characterized with demethylation of promoter of autoimmune-associated methylation-sensitive genes, such as CD70 and LFA-1. In the current study, we found that up-regulation of miR-148a upon TCDD administration contributed to hypo-methylation at Foxp3 regulatory region by potentially targeting DNMTs, which may lead to increased Foxp3 induction. We also noted that over-expression of miR-34a following TCDD treatment in SEB-activated T cell, led to suppression of HDAC1 and subsequently resulted in H3 acetylation at Foxp3 regulatory region. Another study elucidated the therapeutic manipulation of miR-34a in breast cancer cases, by demonstrating HDAC1 as the potent target for miR-34a, which led to deacetylation of HSP70/K246 and subsequently resulted in inhibiting autophagic cell death and cancer cell survival [164]. In agreement with the previous findings, we uncovered the HDAC-1 inhibitory function of TCDD at Foxp3 promoter region via miR-34a differential regulation.

Several epigenetic markers, such as histone methylation and acetylation, cytosine residue methylation in CpG dinucleotides of the promoter regions, have been identified as gene transcriptional regulators [165,166,167]. We investigated the methylation status of conserved CpG dinucleotides in the upstream of FoxP3 enhancer regions of TCDD-exposed SEB-activated Tregs and found it to be hypomethylated when compared to

33

vehicle controls. In a recent report, Kim et al identified the differential methylation state at Foxp3 regulatory region, and demonstrated that inhibiting the methylation with 5-azacytidine or using a lentiviral vector and siRNA to knock down DNMT1 in CD4+CD25− cells, resulted in demethylation of Foxp3 promoter and subsequently led to elevated Foxp3 expression [168]. Furthermore, when they examined the methylation status of Foxp3 promoter under Treg differentiation condition by addition of TGF-β, they found demethylation at both the mouse promoter and the cAMP response element binding protein (CREB) binding region [168]. In contrast, Janson et al. reported that human TGF-β induced-Tregs did not exhibit demethylation of human Foxp3 promoter region [169].

Previous studies from our laboratory demonstrated that TCDD induces demethylation of Foxp3 promoter region which leads to Foxp3 upregulation and enhanced Treg differentiation [162]. In the current study, we uncovered additional mechanistic effect of TCDD on methylation profile of Foxp3 regulatory region of activated-Tcells and introduced TCDD as the potent DNMT inhibitor in SEB-activated T cells. Our data revealed that DNMT inhibitory function of TCDD leads to hypo-methylation of Foxp3 regulatory region in SEB-activated T cells and increased Foxp3 induction. Busbee et al. reported that HDAC inhibitors were able to suppress SEB-induced inflammation and that HDAC1 was one the most significantly modified HDACs [131]. Interestingly, we also found HDAC-1 to be highly suppressed upon TCDD treatment in SEB-activated T cells.

In the current study, we found hypo-methylation and H3 acetylation of Foxp3 regulatory region. We believe that this opens the chromatin configuration and enables KLF10/Sp1 transcription factors to bind to their recognition sequences and subsequently

34

cause stable expression of Foxp3. The active role of the transcription factor Sp1 is protection of CpG islands from de novo methylation, which is well established in earlier studies [145,146,147]. Previous study demonstrated that deletion of Sp1binding site in mouse adenine phosphoribosyhransferase (aprt) gene resulted in hyper-methylation of CpG islands in transgenic mice [170]. Thus, Sp1 involved in many cellular processes including cell differentiation, cell growth and development, immune function and inflammation, by triggering chromatin remodeling. KLF10, a member of the Krüppel-like family of transcription factors, binds to Sp-1-GC rich DNA sequences and regulates the transcription of a number of genes [148]. Other studies revealed the critical role of KLF10 in regulation of Foxp3 expression in Tregs by interacting with transcription factor Sp1 [171]. Deletion of KLF10 in Tregs fosters atherosclerosis in ApoE(-/-) mice with increased peripheral inflammation.

We also validated the miRs regulating the expression of these transcriptional factors. We demonstrated down-regulation of miR-26b and miR-31 following TCDD exposure in SEB-activated T cells which led to re-expression of KLF10/Sp1 and Foxp3 induction. Interestingly, for the first time we identified the specific dual role of miR-31 in TCDD-mediated upregulation of CYP1A1 and Foxp3. Furthermore, we conducted transfection studies with synthetic miR mimic and particular customized target gene protector to validate the direct targeting of CYP1A1 and Foxp3 with miR-31. To our knowledge, this study is the first to report the functional role of miR-31 in regulation of inducible Tregs with TCDD. The comprehensive report of differential expression of miRs, which influences different canonical pathways, following TCDD administration in SEB-activated T cells, has been provided in supplementary data.

Collectively, this study has identified several complex epigenetic regulatory pathways of Foxp3 induction by TCDD, which also helps in the better understanding of mechanisms employed by epigenetic markers to promote differentiation of immunosuppressive Tregs.
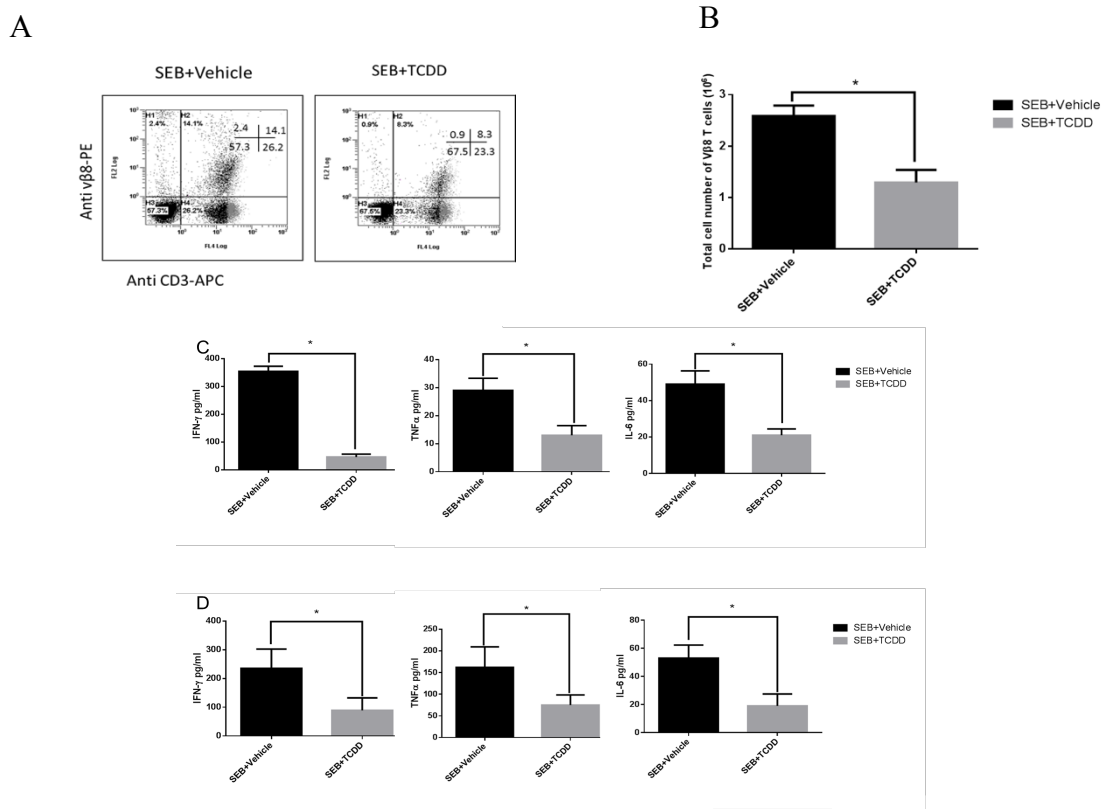
Figure2.1

FIGURE 2.1 Treatment with TCDD in vivo reduces percentage and number of SEB-specific Vβ8 T cells. (A) Groups of 5 C57BL/6 mice were given injections of 10ug of SEB in each hind footpad only once. Mice were given ip injection of TCDD (10μg/kg) simultaneously with SEB injection. On the peak response day 3, PLN were analyzed. The ratio (A) and total cell number (B) of Vβ8+ CD3+T cells is depicted as mean+/- SEM. Cytokines were measured in the serum (C) of mice or in the supernatants (D) of the cultured-popliteal lymphocytes using ELISA. Data represent mean+/- SEM. SEB+TCDD vs SEB+Vehicle, *p< 0.05 by Student's t-test.

A

SEB+Vehicle — SEB+TCDD (flow cytometry plots: Anti-CD4 FITC vs Anti-FoxP3 PE)

T1 87.0% T2 13.0% | 87 | 13
T3 0.0%   T4 0.0%

T1 78.2% T2 21.8% | 78.2 | 21.8
T3 0.0%   T4 0.0%

B

C

SEB+Vehicle B 4.4%   SEB+TCDD B 13.9%

D
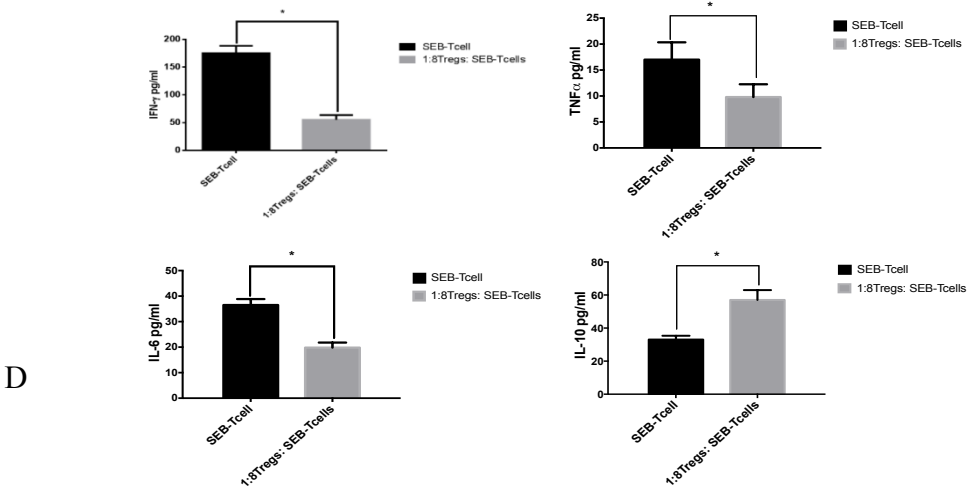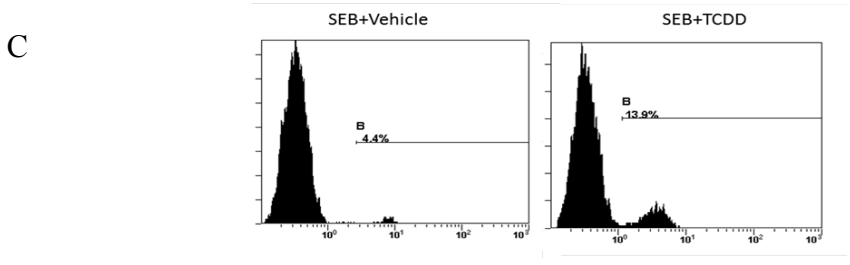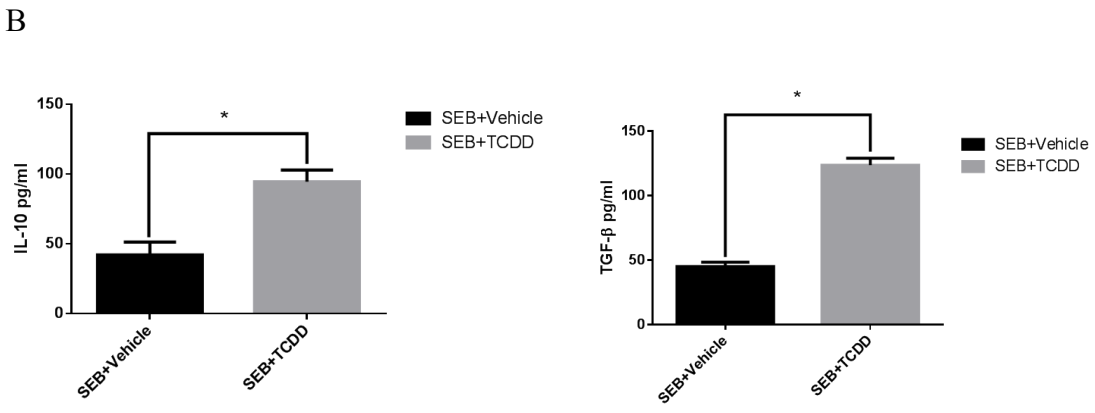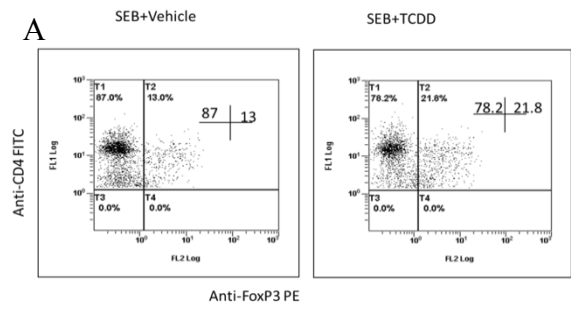
E
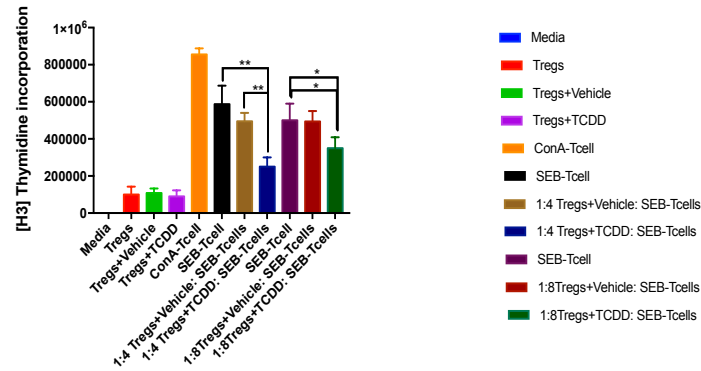
Figure2.2

FIGURE 2.2 TCDD induces Tregs and anti-inflammatory cytokines against SEB
C57BL/6 mice were treated with SEB and TCDD, as described in Figure 1 legend.(A)
flow cytometric analysis CD4+Foxp3+ Tregs in PLN. (B) Cytokines were measured in
the supernatants of the cultured-popliteal lymphocytes using ELISA. (C)Regulatory T
cells were isolated by sorting from the Foxp3/GFP knock-in mice, treated with 100 nM
TCDD and added to co-cultures of LN cells activated with SEB at two different ratios of
Tregs: SEB-activated T cells (1:4, and 1:8). Cell proliferation was measured by 3H-
thymidine uptake assay (D) Cytokines were measured in the supernatants of the co-
cultures as described above. (E) PLN cells stained for Vβ8 in Foxp3/GPF gated
population. SEB+TCDD vs SEB+Vehicle, *p< 0.05 by Student's t-test.

A

SEB+Vehicle   **SEB+TCDD**

B

Down-regulated

37   521   51

Up-regulated

C
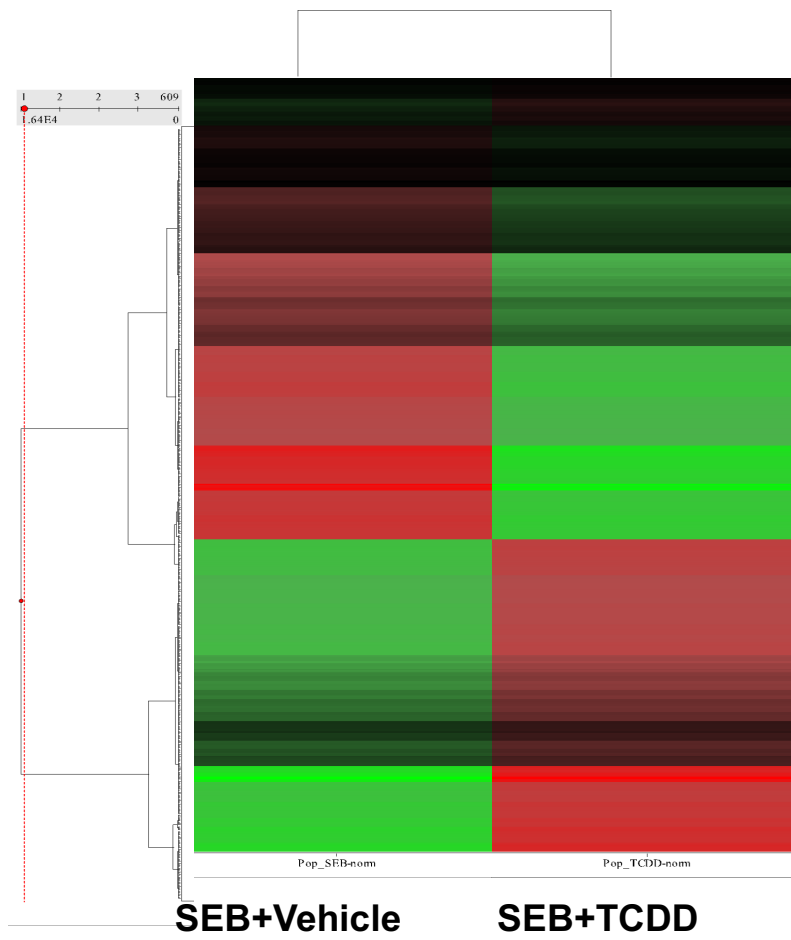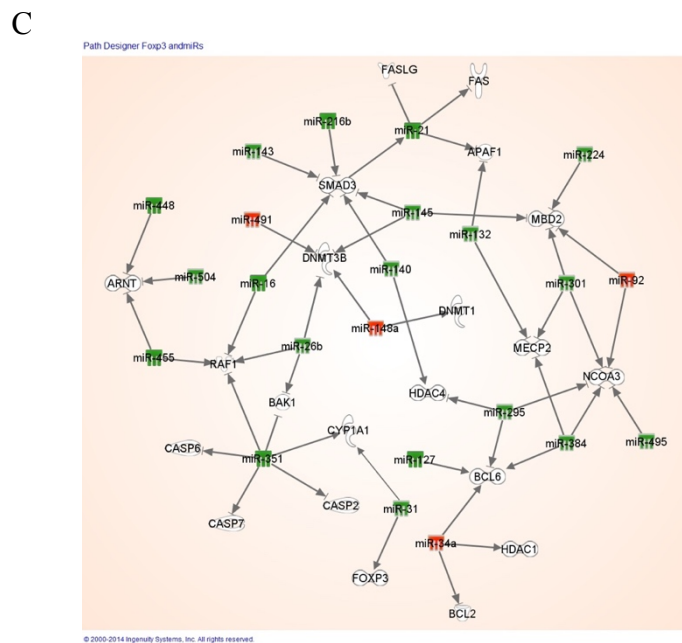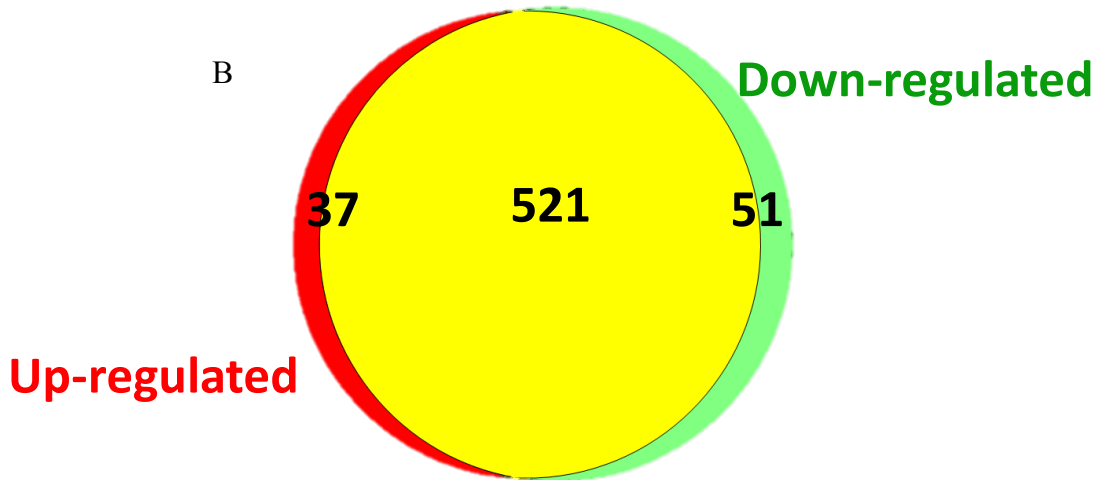
Figure 2.3

FIGURE 2.3. miR expression profile in SEB-injected mice treated with TCDD
miRs was isolated from CD4+ PLN cells from mice exposed to Vehicle+SEB or
TCDD+SEB (A) Differential expression heat map of 609 miRNAs between SEB+TCDD
or SEB+Vehicle groups. (B) Cluster analysis of microRNAs shows that 37 miRs were up
regulated while 51 were down-regulated in SEB+TCDD mice compared to SEB+vehicle
group. (C) Interaction between the microRNAs and their target genes was assessed by
ingenuity pathway analysis (IPA) software. Fig Several pathways are affected with target
genes and microRNA differentially regulated upon TCDD exposure.

Figure 2.4

41

www.manaraa.com
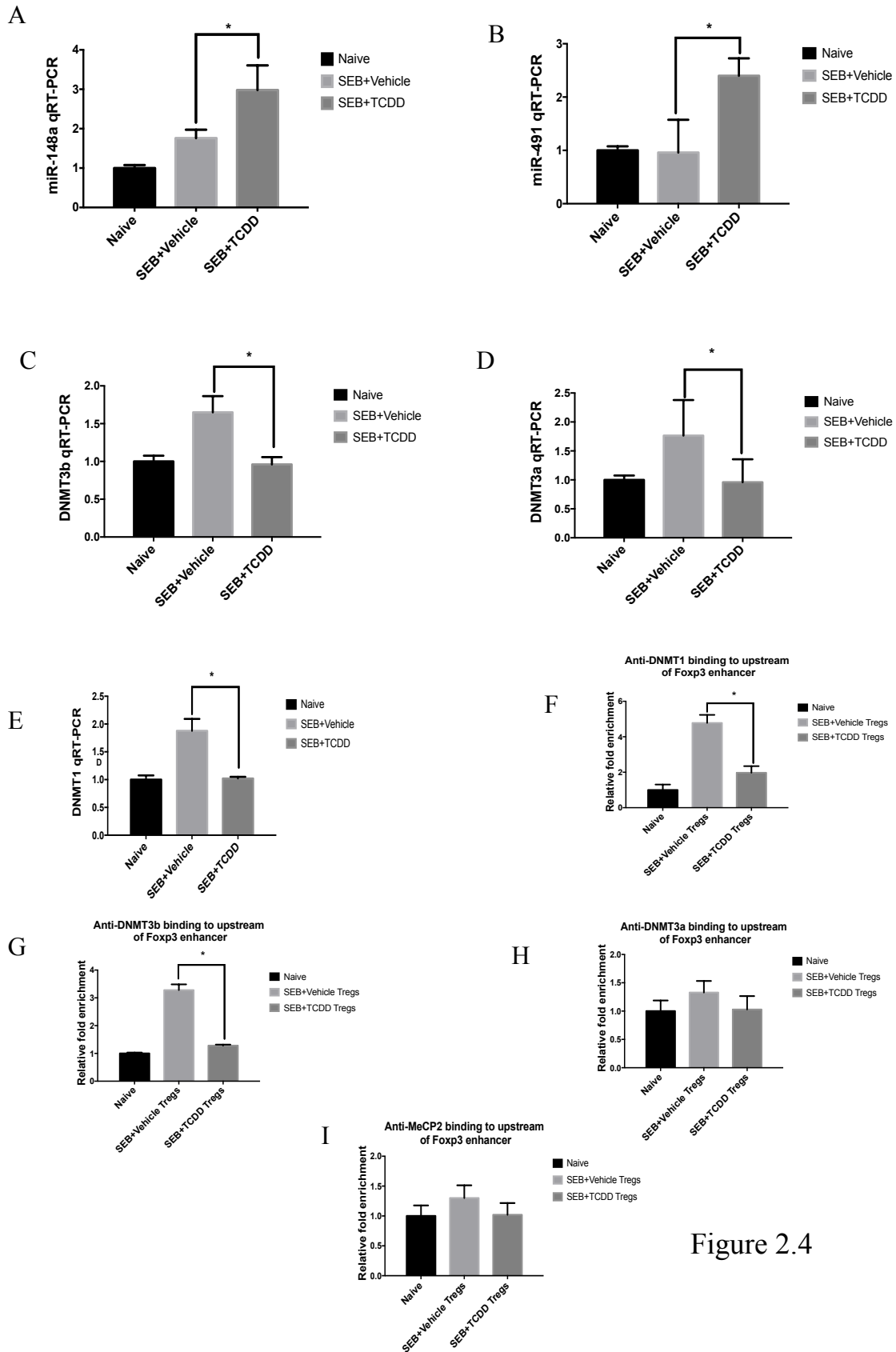
FIGURE 2.4 In vivo miR expression and target gene expression for miR-148a and miR-491. Mice were exposed to SEB+TCDD or SEB+Vehicle as described in Fig 1 legend. Total RNA was isolated from popliteal CD4+ T cells and expression levels were measured by qRT-PCR. (A) miR-148a (B) miR-491 (C) DNMT3b (D) DNMT3a (E) DNMT1. ChIP assay on Foxp3 enhancer elements using GFP+ cells from Foxp3/GFP knock in mice with (F) anti-DNMT1, (G) anti-DNMT3b, (H) anti-DNMT3a, and (I) anti-MeCP2. Data shown are representative of 2-3 independent experiments for each panel (Mean+/- SEM, Student's t-test *, $p < 0.05$)
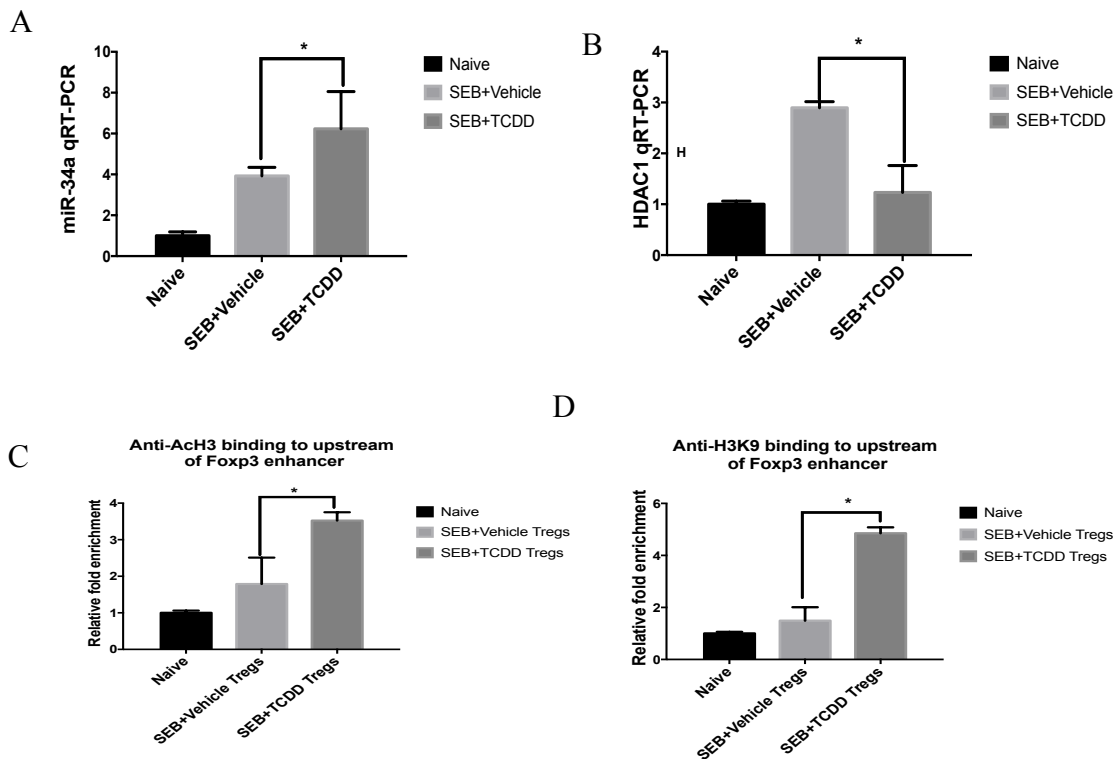
Figure 2.5

FIGURE 2.5 miR-34a regulates Histone H3 acetylation in Tregs via HDAC1
Mice were exposed to SEB+TCDD or SEB+Vehicle as described in Fig 1 legend. Total RNA was isolated from popliteal CD4+ T cells and expression levels were measured by qRT-PCR. (A) miR-34a (B) HDAC1. ChIP assay on upstream of Foxp3 enhancer using the isolated GFP+ cells from Foxp3/GFP knock in mice with (C) anti-AcH3 and (D) anti-H3K9. Data shown are representative of 2-3 independent experiments for each panel.(Mean+/- SEM, Student t-test *, $p < 0.05$)

42
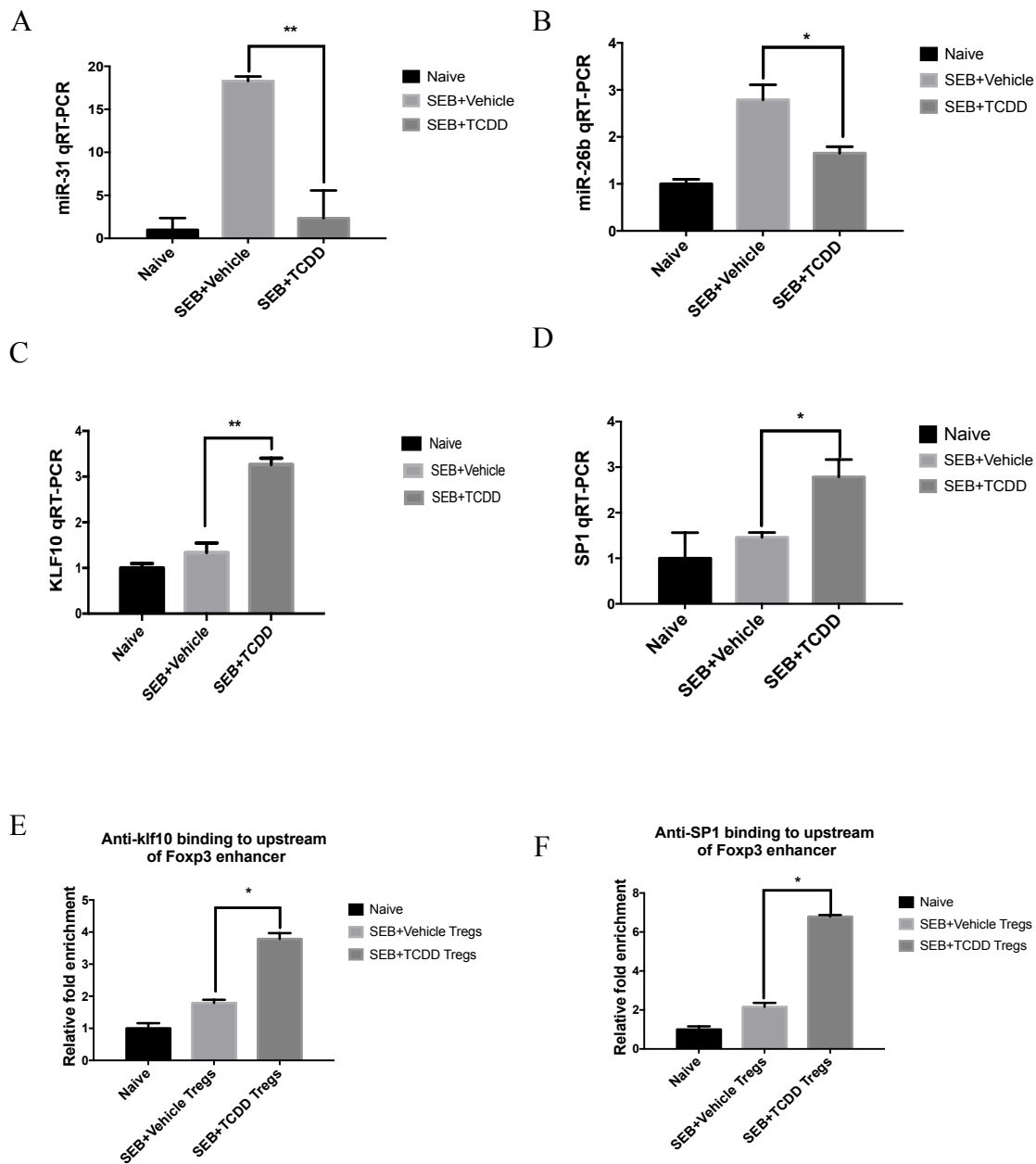
Figure 2.6

FIGURE 2.6 Foxp3 promoter of TCDD-induced Tregs is transcriptionally active.
Mice were exposed to SEB+TCDD or SEB+Vehicle as described in Fig 1 legend. Total
RNA was isolated from popliteal CD4+ T cells and expression levels were assayed using
qRT-PCR. (A) miR-31 (B) miR-26b (C) KLF10 (D) Sp1. ChIP assay upstream of Foxp3
enhancer using the GFP+ cells isolated from Foxp3/GFP knock in mice with (E) anti-
KLF10 (F) anti-Sp1. Data shown are representative of 2-3 independent experiments for
each panel. (Mean+/- SEM, Student t-test *, $p < 0.05$)

43

A

SEB+Mock
SEB+AllStars Negative control
SEB+miR-31 inhibitor

B

SEB+Negative control
SEB+miR-31 mimic/Foxp3 Protector
SEB+miR-31 mimic

44

Figure 2.7

FIGURE 2.7 miR-31 inhibition leads to induction of Foxp3P3 and CYP1A1
SEB-activated cells were transfected with customized inhibitor for miR-31 or were mock transfected. The expression levels of Foxp3 were quantified by (A) qRT- PCR. SEB-activated cells were transfected with miR-31 mimic and specific custom-designed Foxp3 target protector. The expression levels of Foxp3 were quantified by (B) qRT- PCR and (C) Western blot analysis. Co-transfection of SEB-activated lymphocytes with mimic-miR-31 and CYP1A1 target protector was conducted in vitro. The expression levels of CYP1A1 were quantified by (D) qRT- PCR analysis. (Mean+/- SEM, Student t-test $*p< 0.05$, $**p< 0.01$). miR-31/Foxp3 alignment with the mirSVR score: -0.6807 (down-regulation score) miR31/CYP-1A1 alignment with mirSVR score:-0.1340 (down-regulation score)has been depicted.

45

A Path Designer ahr radial pathway
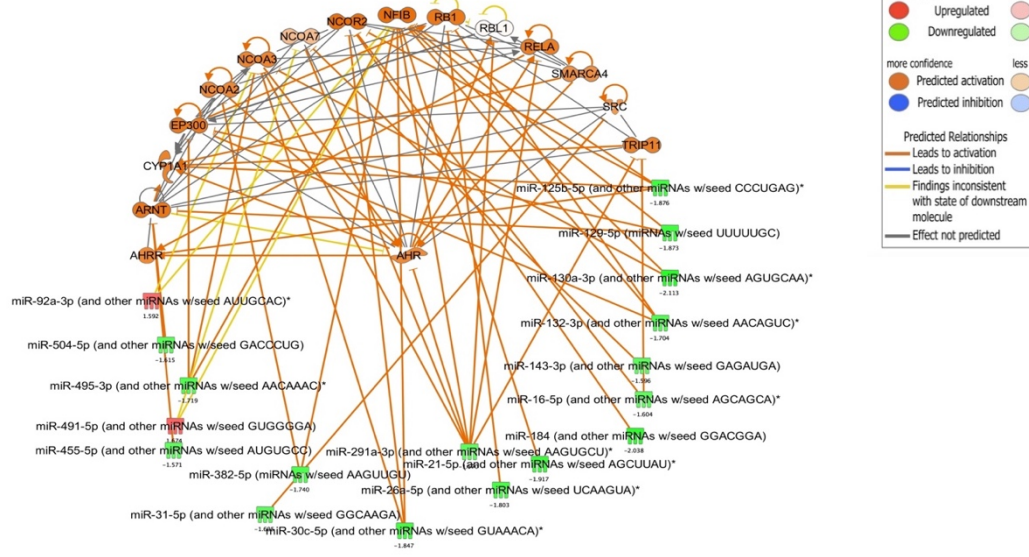
Supplementary Figure 2.1

46
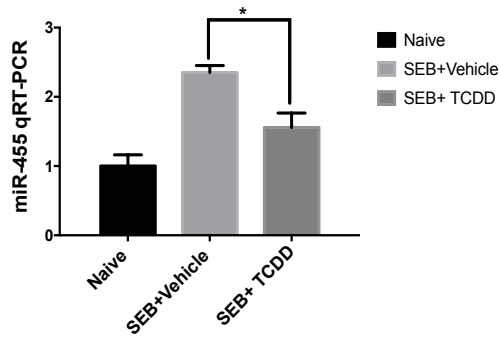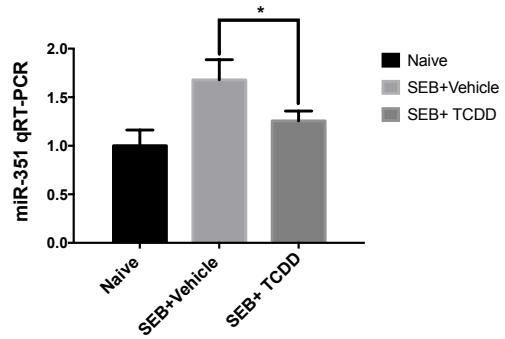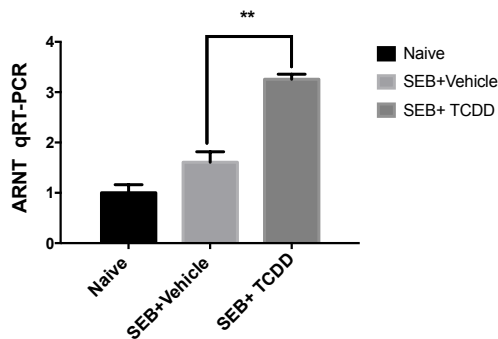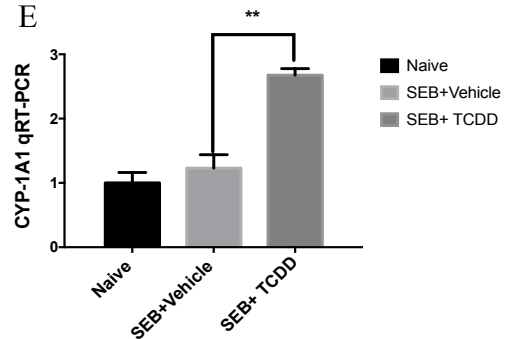
Supplementary figure 2.1 TCDD induces AhR signaling by altering miR profile in SEB-activated T cells. Mice were exposed to SEB+TCDD or SEB+Vehicle as described in Fig 1 legend. (A) Overlay of AhR signaling canonical pathway with miRs that were significantly changed upon TCDD administration in SEB-activated T cells. Predicted downstream effect of differentially expressed miRs using Molecular Activity Predictor (MAP). qRT- PCR analysis was carried out for (B) miR-455 (C) miR-351(D) ARNT(E) CYP1A1. (Mean+/- SEM, Student t-test *p< 0.05 , **p< 0.01).
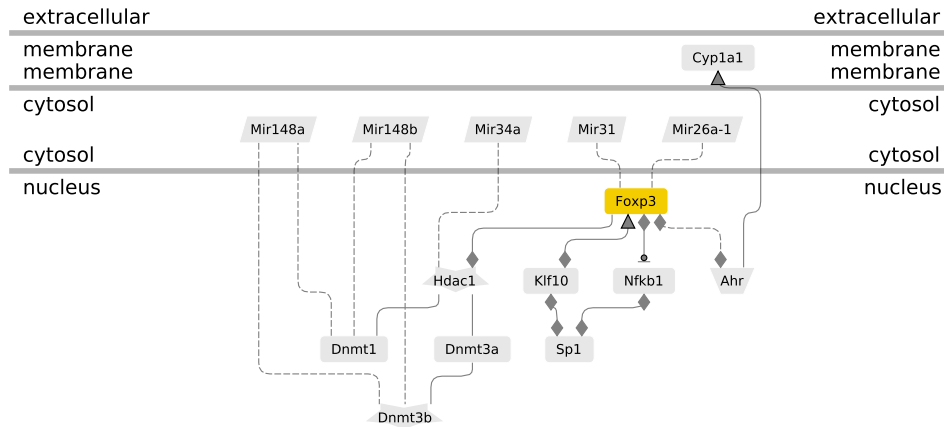
Supplementary Figure 2.2

Supplementary figure 2.2. Schematic of the role microRNA and epigenetic regulators play in TCDD induced Foxp3 expression in Tregs

Table2.1: candidate targets for filtered miRs, along with their seed sequence and respective fold change. The highly predicted and experimentally observed targets has been listed. 7 mer seed sequence are in bold red.

miRNA	MiRBase #	Chr.	Sequences	Experimentally observed/highly predicted targets	FC
miR-148a	NIMAT0000516	Chr6	U**CAGUGC**ACUACAGAACUUUGU	DNMT1,DNMT3B,DNMT3A	1.737
miR-491	NIMAT0003486	Chr4	A**GUGGGGA**ACCCUUCCAUGAGG	DNMT3B,STAT3,STAT5B,GSK3B,Foxo1,Foxo3,TGFβR2	1.674
miR-34a	NIMAT0000542	Chr4	U**GGCAGUG**UCUUAGCUGGUUGU	HDAC1,SOCS4,SOCS7,SIRT1,P53	2.267
miR-31	NIMAT0000538	Chr4	A**GGCAAGA**UGCUGGCAUAGCUG	Foxp3,CYP1A1,Sp1,STAT5A,Kpna1,TGFβR2,GSK3B,STAT5B	-1.605
miR-26b	NIMAT0000534	Chr1	UU**CAAGUA**AUUCAGGAUAGGU	KLF10,PTGS2,PTEN,CTGF,GSK3B,MAP3K1,RB1	-1.83
miR-351	NIMAT0000609	ChrX	U**CCCUGAG**GAGCCCUUUGAGCCUG	CYP-1A1,BAK-1,CASPASE6,CASPASE7,MAP2K7,CDK6	-1.876
miR-455	NIMAT0003485	Chr4	U**AUGUGCC**UUUGGACUACAUCG	ARNT,ARNT2,CYP-20A1,CYP-4F3,MYD88	-1.571

47

CHAPTER III: BLOCKADE OF CB1 CANNABINOID RECEPTOR ALTERS GUT MICROBIOTA AND ATTENUATES INFLAMMATION AND DIET-INDUCED OBESITY.

3.1 <u>INTRODUCTION</u>

Gut microbiome is the key feature in maintaining the whole body energy balance by affecting the glucose metabolism and low-grade chronic inflammation associated with obesity. Previous studies have shown that obese mice had broad phylum level changes in their microbial community and fecal transfer from obese mice into gnotobiotic lean mice conferred many inflammatory features of diet- induced obesity to the recipients [172,173]. Correlation between progression of metabolic syndrome and alteration in gut microbial community has been reported in mice with deletion of Toll-Like Receptor 5(TLR5) gene [174]. Fecal transfer from the TLR5 deficient mice to wild type germ-free mice mimic multiple symptoms of metabolic disease in the recipient mice.

Microbial community of the gut consists of symbionts (beneficial), neutral (commensals) as well as detrimental (pathobionts) microorganisms. The homeostasis of these essential allies can modulate the host health and function [175]. The mutual interaction of gut microbiota and host immune system is necessary in maintaining their symbiotic relationship[176,177,178,179,180]. Gut immune system determines colonization of microbial community in gut and contributes to the interaction of host-microbiome [181].

Metabolic endotoxemia and inflammation in obese mice may result from the chronically higher levels of lipopolysaccharide (LPS) and pro-inflammatory cytokines[182]. Higher intake of saturated fat leads to the disruption of multi-layered mucus structures and tight junctions in gut, leading to permeability of gut barrier and consequent leakage of LPS in circulation [183]. LPS absorption by gut enterocyte chylomicrons results in robust release of systematic LPS, which is believed to contribute to inflammatory and metabolic disorders [184]. Macrophages are the first-line of target of LPS and their retention in adipose tissue is implicated in pathophysiology of diet-induced obesity and metabolic syndrome [185,186].

Numerous studies have demonstrated that diet-induced obesity and associated-inflammatory disorders may result from dysregulation of endocannabinoid (eCB) system. Augmentation in eCB levels in plasma and adipose tissue as well as modulation of CB1 receptors has been reported in obese individuals [187,188,189,190,191]. Alterations in gut eCB system is implicated in the dysregulation of LPS level, gut integrity disruption, chronic inflammatory state of gut, and dysbiosis of gut micro-flora [192]. Previous study has shown that LPS leads to dysregulation of eCB system in macrophages [193]. LPS causes robust production of endogenous ligands of cannabinoid receptors, specifically Anandamide (arachidonylethanolamide, AEA) in adipose tissue macrophages, which contributes to exacerbation of chronic inflammation in visceral fat, hyperglycemia and insulin resistance [194].

Numerous pharmacological, preclinical and clinical studies indicate that blockade of cannabinoid CB1 receptor can significantly improve obesity complications and multiple risk factors of metabolic syndrome [195,196,197,198,199,200,201]. However, the direct

implications and precise physiological role of CB1 receptor antagonist in the modulation of gut microbial communities in diet-induced obesity has not yet been fully determined. Herein, for the first time, we uncovered the changes in gut microbial community in a mouse model of diet-induced obesity treated with CB1 antagonist, SR41716A. In order to demonstrate the effect of SR141716A on gut microbiota beyond its effect on diet intake and weight loss, we included pair-feeding controls as well as body weight-matched controls. The current study provides compelling evidence that targeting the eCB system in diet induced obesity model by utilizing SR141716A as the CB1 receptor blocker, remodels the gut microbial colonization and subsequently leads to amelioration of pro-inflammatory macrophages and metabolic parameters.

3.2 MATERIALS AND METHODS

Animals and SR141716A treatment-

Diet-induced obesity was studied in male C57BL/6J mice (Jackson Laboratory, Bar Harbor, ME) by feeding high fat diet of 60 kcal% fat (Research Diets Incs, New Brunswick, NJ). Lean age-matched controls were fed with low fat diet of 10 kcal% fat, and match 17% sucrose in HFD (Research Diets Incs, New Brunswick, NJ). Intervention treatment with SR141716A was performed after 12 weeks of high fat diet. Pair-fed and body weight-matched controls were included in the study in order to investigate the effect of SR141716A treatment beyond its effect on diet intake and body weight loss. Pair-fed and body weight matched controls were included as previously described [198]. SR141716A was administered to the DIO mice in 0.1% tween 80 for four weeks, (10mg/kg/daily).

50

Controls lean (LFD), DIO (HFD), pair-fed to SR141716A(PFSR) and body weight-matched (BWM) controls were treated with vehicle. Body composition was assessed by using a Dual-Energy X-ray Absorptiometry (DEXA, LUNAR, Madison, WI) at the baseline of the study; mice were normalized to the different groups based on the fat mass. Food intake was monitored daily and changes in body weight was recorded daily after starting the intervention treatment. Mice were sacrificed under anesthesia and different tissues were dissected. Metabolic parameters were collected at both baseline and prior to the sacrifice day. All mice were housed at the (American Association for the Accreditation of Laboratory Animal Care-accredited (AAALAC) animal facility at the University of South Carolina, School of Medicine (Columbia, SC). All procedures were performed according to NIH guidelines under protocols approved by the Institutional Animal Care and Use Committee.

Assessment inflammatory profile- locally and systematically-

Cytokines levels were measured in plasma and quantified using Bio-Plex multiplex immunoassay system (Bio-Rad, Hercules, CA), as described by us previously [202]. RNA was isolated from epididymial fat pad using the E.Z.N.A.® Total RNA Kit (Omega Bio-tek, Norcross, GA). The purity and concentration of the RNA was confirmed spectrophotometrically with Nanodrop (Thermo Scientific, Waltham, MA). Total RNA was converted to cDNA using the miScript cDNA synthesis kit (Qiagen, Valencia, CA) according to the manufacturer's instructions. SsoAdvanced™ Universal SYBR® Green Supermix kit (Bio-Rad,Hercules, CA) was used to analyze gene expression , and GAPDH was used as the housekeeping gene. List of all the primers have

51

been provided in supplementary Table 4. Complete Blood Cell count (CBC) was performed using hematological analyzer VetScan HM5 (ABAXIS, Union City, CA). Circulating LPS level was quantified as previously described [203]. Colonic myeloperoxidase was assessed according to the manufacturer's instruction (Abcam, Cambridge, MA) [204].

Free fatty acid was quantified in serum according to the manufacturer's instruction (Zen-Bio Inc, Research Triangle Park, NC)

Isolation of adipocytes and infiltrated cells in adipose tissue-

Fat pads of mice were excised and placed in gentleMACS C Tubes (MACS Miltenyi Biotec, San Diego, CA) containing digestion medium (HBSS, 2mg/ml collagenase (Sigma-Aldrich, St. Louis, MO) and 2% BSA, and homogenized by utilizing gentleMACS Dissociator (MACS Miltenyi Biotec, San Diego, CA). After incubation at 37 °C for 30 min with shaking, the cell suspension was filtered through a 100-μm filter and then spun at 1200 rpm for 10 min to separate floating adipocytes from the Stromal Vascular Fraction (SVF) pellet. Supernatant was aspirated completely and cells were re-suspended in FACS buffer for flow cytometry. Samples were digested until the majority of the SVF population were separated from the adipose tissue.

Glucose and Insulin tolerance test-

Glucose tolerance test was carried out as previously described [205]. After determining fasting blood glucose, each animal received a glucose gavage 1.5g/KG body mass of glucose (25% D-glucose, Sigma, St.Louis, MO) . Blood glucose levels were

determined after 15, 30, 60 and 120 minutes. Insulin-tolerance tests were performed on

un-fasted animals by injecting i.p 1.5 U/Kg body mass of insulin (HumilinR 100U/ml).

Blood glucose levels were assessed after 15, 30, 60 and 120 minutes. Total cholesterol

(TC), HDL-C, LDL-C, and triglycerides at the baseline and after intervention were

quantified as previously described [206,207] .Homeostatic model assessment (HOMA) index

was calculated as follow: insulin resistance index =fasting insulin (μU/ml) x fasting

glucose (mmol/l)/22.5 [208] .

Measurement of adiposity and macrophage retention in adipose tissue-

The mean adipocyte size in epididymal adipose tissue was quantified with imageJ

analysis software (National Institution of Health,NIH) as previously described [206].

Macrophage retention in adipose tissue was quantified per 100 adipocytes by Spot Studio

v1.0 Analysis Software (Advanced Cell Diagnostics, Hayward, CA).

Mucosal layer staining and thickness-

Mouse colon fixation and mounting was performed as previously described [209].

Periodic acid Schiff was conducted according to the manufacturer instruction (Abcam,

Cambridge, MA) . The thickness of mucosal layer was assessed by analysis software

package Gene 5(Cytation5, BioTek, Winooski, VT) and MetaMorph (Molecular Devices,

Wokingham, UK).

Gut permeability in vivo-

Mice were deprived of food and water for 4 hours. Intestinal permeability was measured after they received dextran-4kDa-FITC (Sigma, St. Louis, Missouri) by oral-gavage (500 mg/kg body weight, 125 mg/ml). Measurements were taken as described earlier [183]. Serial dilution of FITC–dextran in the serum were performed to generate the standard curve.

Measurement of AEA and 2-AG in serum and tissue-

Tissue lipids were extracted as described earlier [193]. Extracted lipid from serum and adipose tissue was processed as previously described [210]. The levels of endocannabinoid from tissue and serum was quantified by triple quadrupole mass spectrometer with electrospray ionization at the Mass Spectrometry Center at the Department of Chemistry and Biochemistry, University of South Carolina. Samples were introduced into Micromass Quattro-LC through a liquid chromatograph. It used in tandem Mass spectrometry (MS/MS) mode for qualitative and quantitative analyses.

Microbial analysis after SR141716A intervention treatment of obese mice-

16S rRNA gene sequencing was performed on 25 fecal samples from Diet-Induced obese (HFD), SR141716A treated-DIO (HFD+SR) mice, Pair-fed to SR141716A (PFSR) mice, body-weight matched to SR141716A (BWM) and age matched low fat diet (LFD) controls (n=5 mice per group). DNA was extracted from frozen extruded feces using the QIAamp DNA Stool Mini Kit (Qiagen, Valencia, CA) according to the manufacturer's instructions. Purified DNA was indexed with TrueSeq

54

DNA PCR-free LT Library preparation kit for low-throughput studies (Illumina, San Diego, CA) according to the manufacturer's instructions. DNA was PCR-amplified using primers for paired-end 16s community sequencing on the Illumina MiSeq platform using bacteria/archaeal primer sense 319F/ anti-sense 806R targeting hyper-variable regions V3-V4 of the 16S rRNA gene. Each primer is followed by a barcode identifier generated specifically for the set of primers. Phix V3 (25%) was used as a control for Illumina sequencing runs. The library was sequenced on 300 paired-end MiSeq run as previously described at John's Hopkins Deep Sequencing and Microarray Core facility [211].

16S rRNA gene sequence analysis-

The sequences were preprocessed and demultiplexed with CASAVA 1.8.2 during conversion of bcl to Fastq [212]. The demultiplexed sequences were quality filtered for chimeras, using the Quantitative Insights In to Microbial Ecology (QIIME, version1.9.0) software package to avoid false diversity. Forward and reverse Illumina reads were joined using the SepPrep method (https://github.com/jstjohn/SeqPrep). We used QIIME default parameters for quality filtering as described previously [209]. Sequences were assigned to Operational Taxonomical Units (OTUs) using the closed reference OTU picking protocol against the Greengenes database with a 97% threshold of pairwise identity.

Beta-diversity of the gut microbiome was evaluated by weighted UniFrac-based principle co-ordinates algorithm. The analysis was performed using the abundance matrix of genus-level OTUs in different samples, rarefaction was performed (10,000 sequences per sample) and used to compare abundances of OTUs across samples. Exceptions from

55

study groups were observed, confounded by variations in other environmental exposure and genetics factors on these microbiomes. Chao1 index was calculated to estimate the species richness of present organisms in the community.

Specific quantitative PCR (qPCR) targeting the employed fecal samples in 16S rRNA gene sequencing was performed using Quantifast SYBER Green PCR Kit (Bio-Rad, Hercules, CA). Abundance of Akkermansia muciniphila (A. muciniphila), Lanchnospiraceae and Erysipelotrichaceae were quantified by specific primers (Supplementary Table 4). Total microbial DNA was quantified and addressed as the endogenous control, we used universal bacterial primers 319F and 806R— the same used for 16S sequencing.

Short-chain fatty acids quantification by Gas chromatography with flame Ionization Detector (GC-FID)-

Cecal content (100 mg) were homogenized in in 400 μl of deionized water, followed by acidification with 25% metaphosphoric acid (Sigma-Aldrich, St. Louis, MO) at a 1:5 ratios (1 volume of acid for 5 volumes of sample) for 30 min on ice as previously described [213]. Fatty acid was then isolated from the samples followed by centrifugation at 12,000g for 15 minutes at 4 °C. Supernatants were filtered over Ultrafree MC column with .22 μm pore size (EMD Millipore, Billerica, MA), and elute was stored at -80 until it was analyzed by GC-FID.

SCFA concentrations in specimens were quantified according to a modified method as described earlier [214] . Calibration standards were prepared as aqueous stock solutions using the following fatty acids at the given concentration; acetic, propionic, and

56

n-butyric at 400 mM, isovaleric and valeric 200 mM, isobutyric 100 mM, caproic and *n*-heptanoic 50 mM. Each standard was injected to identify their retention times. Standard mixture was prepared at several concentrations suitable for the samples. Internal standard (IS) 2-ethylbutyric acid was added at 0.30 mM to the standard mixtures as well as to each sample before injection. Standard mixture with the IS was used to determine the response factors. Samples were prepared by first thawing at room temperature, taking 100 μL of the samples in to a vial and adding 40 μL of acetone and 60 μL of 0.10 mM IS solution. Then the mixture was vortexed and centrifuged. The clear solution was transferred to a glass GC vial and used for analysis. A HP 5890 gas chromatograph configured with flame-ionization detectors (GC-FID) for analysis of volatile organic compounds was used for this assay. Stabilwax®-DA Column (fused silica) of 30 m × 0.32 mm i.d. coated with 0.50 μm film thickness was used. Helium was supplied as the carrier gas at a flow rate of 15 mL/min. The temperature was programmed to achieve the following run parameters: initial temperature 100 ^{o}C, hold for 0.5 min, ramp 20 ^{o}C/min, final temperature 250 ^{o}C maintain for 5 min. The injected sample volume for GC analysis was 1 μL splitless and the total run time was 18.0 min.

Response factors (RF) were calculated via dividing the peak areas of the responses by the respective concentrations of the standards. To quantify the peak area in terms of concentration, the relative response factor (RRF) was used. The RRF was calculated using the formula RRF = $RF_{Standard}/RF_{IS}$. The concentration of the samples was calculated using the following equation, Conc. $_{samples}$ = Peak Area$_{Sample}$ x (Conc. $_{IS}$/ Peak Area$_{IS}$)(1/RRF)

57

Statistical Analysis-

Data were presented as mean ± SD. Differences between two groups were assessed using the unpaired two-tailed Student's t-test. ANOVA followed by Newman-Keuls post hoc tests was performed to analyze differences between data sets that involved more than two groups. Generalized Estimating Equation (GEE) and Generalized Linear Mixed Model (GLMM) was performed to fit a repeated measurement logistic regression. Trapezoidal Rule in R was used to assess Area Under the Curve (AUC) from the replicated experiments. Pearson correlation was performed in R with the cor () function in ggplot2. In the figures, data with different superscript letters were used to indicate statistical significant differences in groups ($p < 0.05$). Data were analyzed using GraphPad Prism version 7.00 for Windows (San Diego, CA), Excel, R a language and environment for statistic computing (R Development Core Team, 2010), and IBM SPSS Statistics for Windows, Version 22.0. (Armonk, NY).

3.3 RESULTS

Effect of SR141716A on diet intake, body weight and body composition

Consistent with previous research studies, treatment of DIO mice with SR141716A (HFD+SR) transiently reduced calorie intake and induced weight loss as compared with vehicle-treated DIO mice (HFD) (Fig 3.1B,3.1C) [215,216]. To assess the effect of SR141716A beyond its effect on weight loss and calorie intake, pair-feeding was conducted in diet-intake matched controls (PFSR), and diet intake was adjusted in body-weight- matched (BWM) controls (Fig 3.1 A). The transient reduction of calorie intake in HFD+SR mice during the first week, was diminished by day 9 of treatment, and

58

reaching even to the same intake as HFD group (Fig 3.1B). However, we noted

continuous weight loss in HFD+SR group through the end of treatment (Fig 3.1C). In

order to maintain the same body weight in BWM group as HFD+SR group, the diet

intake was restricted to even lower intake than HFD+SR group (Fig 3.1B).

In order to examine the effect of SR141716A beyond its effect on calorie intake,

the pair-fed DIO control (PFSR) mice were fed with the same amount of high fat diet as

consumed by the SR141716A-treated DIO mice(HFD+SR). The weight loss pattern in

PFSR group was similar with HFD+SR during the first two weeks of treatment, but then

PFSR group started to gain weight and reaching a close body weight to HFD group by

end of the treatment (Fig 3.1C).

Correlation between changes in body weight and caloric intake within different

groups, demonstrated consistent weight loss in HFD+SR group regardless of its high

level of calorie intake close to HFD group (Fig 3.1D).

Assessing body composition after 4 weeks of SR141716A intervention in DIO

mice (HFD+SR) showed significant reduction in fat gain as compared with vehicle-

treated DIO mice (HFD), while there was no difference in lean mass (Fig 3.1E).

Inasmuch as SR141716A-treated DIO mice (HFD+SR) demonstrated less fat mass when

compared to body weight-matched control (BWM) , the data suggested that other factors

are associated with use of SR141716A besides its effect on calorie intake and weight loss

(Fig 3.1E). Lower fat mass within SR141716A-treated group (HFD+SR) has been

characterized with less adiposity. Assessing the area of the adipocytes demonstrated

significant shrinkage in adipocytes of the SR141716A-treated DIO mice (HFD+SR)

59

when compared to vehicle-treated DIO mice(HFD), pair-fed control(PFSR) as well as body weight-matched control (BWM) (Fig 3.1F).

Adipose tissue fibrosis, in obese phenotype is associated with an increase in local inflammation. The Picrosirius red fibrillar collagens were interspersed among the adipocytes in HFD group. SR141716A treatment in DIO mice (HFD+SR) resulted in a significant suppression of adipose tissue fibrosis and consequently further reduction in local adipose tissue inflammation and dysfunction (Supplementary Fig 3.1A, 3.1B).

Lighter fat pad (mainly in epididymal fat pad) in SR141716A-treated DIO mice (HFD+SR) was associated with smaller liver when compared with vehicle-treated DIO (HFD), Pair-fed DIO control(PFSR), and body weight-matched control(BWM) (Fig 3.1G)

Effect of SR141716A on systematic and local inflammation

Based on the active role of macrophages in initiation of inflammation in adipose tissue, we examined the changes in macrophage population in adipose tissue. Intervention treatment of DIO mice with SR141716A (HFD+SR) demonstrated significant reduction in the ratio of macrophages/adipocytes as compared with vehicle-treated DIO (HFD), pair-fed control(PFSR) and body weight matched-control(BWM) (Fig 3.2A). Flow cytometric analysis for the subset of macrophages showed significant reduction in both frequency and absolute number of pro-inflammatory M1 macrophages with SR141716A treatment (HFD+SR) when compared to vehicle-treated DIO controls (HFD) (Fig 3.2B, 3.2 C). Inflammatory profile has been assessed by examining chemokines and cytokines in the serum for the systemic inflammation. Treatment of DIO mice with SR141716A

60

(HFD+SR) led to lower level of IL-17, MCP-1, Eotaxin and MIP-1α when compared to vehicle-treated DIO mice (HFD) (Fig 3.2 D-3.2G). The same trend was seen with TNF-α, IL-6 ,RANTES, MIP-1β and MIP-2 but the differences were not significant . Changes in LPS as the major simulator of macrophages has been assessed [217]. The data showed there was significant reduction in LPS level in the serum of SR141716A-treated DIO mice (HFD+SR) as compared with vehicle-treated DIO (HFD), pair-fed DIO control(PFSR) and body weight matched-control (BWM) (Fig 3.2 H).

We also investigated the inflammation profile of adipose tissue and colon locally and to that end, the mRNA level of RORγ, TNF-α, iNOS, and IL-6 were quantified in adipose tissue (Fig 3.2I-3.2L). Overall, intervention treatment of DIO mice with SR141716A (HFD+SR) led to improvement of inflammatory state of adipose tissue beyond its effect on diet restriction.

Local inflammation in colonic tissue was also determined by assessing the level of myeloperoxidase. SR141716A-treated DIO mice (HFD+SR) showed significant improvement in colonic inflammation, independent of its effect on weight loss and diet intake (Fig 3.2M).

We also observed a significant increase in both the percentage and numbers of CD4+GATA3+ Th2 cells (anti-inflammatory T cell subset) following treatment with SR141716A of DIO mice (HFD+SR) (Supplementary Fig 3.2 A,3.2B).

Myeloid Derived-Suppressor Cells (MDSC) that are GR-1+CD11b+ have been identified as potent anti-inflammatory cells. In the current study, we noted that MDSCs were induced with SR141716A treatment in DIO mice (HFD+SR) when compared to vehicle-treated DIO (HFD) (Supplementary Fig 3.2C, 3.2D). We also assessed the

61

changes in blood MDSCs. The data showed a significant decrease in MDSC with SR141716A treatment in the blood (Supplementary Fig 3.2E) thereby suggesting that they may be migrating to the site of inflammation (adipose tissue).

Differential analysis of Complete Blood Cell (CBC) revealed significant leukocytosis in DIO mice (HFD) when compared to SR141716A-treated DIO (HFD+SR) and lean (LFD) mice. Leukocytosis in DIO mice was more pronounced in neutrophils subpopulation, which are the first responder to inflammation. Our data suggested that treating DIO mice with SR141716A reduces neutrophilic leukocytosis. Furthermore, SR141716A treatment balanced the increased level of hemoglobin and HCT% in DIO mice. (Supplementary Table 3.1). Taken together, our data suggested that intervention treatment of DIO mice with SR141716A (HFD+SR) attenuates systematic inflammation and metabolic endotoxemia.

Effect of SR141716A on metabolic parameters

Glucose Tolerance Test (GTT) and Insulin Tolerance Test (ITT) showed remarkable improvement in metabolic parameters in DIO mice when treated with SR141716A (HFD+SR) as compared with vehicle-treated DIO (HFD) and pair-fed (PFSR) controls (Fig 3.3A, 3.3B). Improvement in other serum metabolic parameters such as Fasting Blood Glucose (FBG), TGs, HDL, LDL, HOMA index as well as free fatty acid was also observed following SR141716A treatment in DIO (HFD+SR) when compared to vehicle-treated DIO (HFD) and pair-fed to SR141716A (PFSR) (supplementary Table 3.2, Fig 3.3)

62

Effect of SR141716A on gut barrier integrity

SR141716A counteracted diet-induced colon mucosal barrier dysfunction during high fat diet feeding by modulating the mucosal thickness (Fig 3.4A, 3.4B). Mucus-related genes expression, Mucin2 (Muc2) and Kruppel-Like Factor 4 (KLF4) were improved with SR141716A treatment in DIO mice (HFD+SR) as compared with vehicle-treated DIO mice (HFD), pair-fed to SR141716A (PFSR) control and body weight-matched (BWM) controls (Fig 3.4C, 3.4D). SR141716A didn't show any effect on the Trefoil Factor 3 (Tff3) gene expression (Figure 3.4 E).

In addition, we performed in vivo intestinal permeability assay using an FITC-labelled dextran method. Less leakage in the gut of SR141716A-treated DIO mice (HFD+SR) was observed when compared to vehicle-treated DIO (HFD) and pair-fed to SR14716A (PFSR) controls (Figure 3.4 F) Taken together these data indicated that SR141716A intervention treatment in DIO mice (HFD+SR) ameliorates the compromised mucosal layer and gut leakage in DIO phenotype.

Effect of SR141716A on Endocannabinoid system

Obesity has been characterized with over activation of eCB system[187]. In the current study, we found that CB1 receptor expression was down-regulated with SR141716A treatment of DIO mice (HFD+SR) when compared to vehicle-treated DIO mice (HFD) (Fig 3.5A) . Level of endogenous ligand of cannabionoid receptors in adipocytes and serum was assessed by LC/MS/MS. We observed significant reduction in adipose tissue anandamide (AEA) in DIO mice treated with SR141716A (HFD+SR)

when compared to the control DIO mice (HFD) (Fig 3.5B, 3.5C). We were unable to detect significant levels of 2-AG in all samples.

Effect of SR141716A on adipogenic related-genes

Next, we investigated the effect of SR141716A on adipose tissue metabolism, which was assessed by RT-PCR for lipogenesis, oxidation and differentiation genes. We observed that SR141716A treatment of DIO mice (HFD+SR) increased the mRNA expression of markers of lipid oxidation (carnitine palmitoyltransferase-1 (CPT1), acyl-CoA oxidase (Acox1), peroxisome proliferator-activated receptor gamma coactivator-1 alpha (PGC-1α), and peroxisome proliferator-activated receptor alpha (PPARα) (Fig 3.6A), and adipocyte differentiation (CCAAT/enhancer–binding protein-α (C/EBPα) and peroxisome proliferator-activated receptor γ (PPARγ)(Fig 3.6B). Changes in lipogenic properties of adipose tissue was examined with (acetyl-CoA carboxylase (Acc1) and fatty acid synthase (FASN) quantification (Fig 3.6C). Together, our data suggested that the shrinkage in fat mass in SR141716-treated DIO mice (HFD+SR) was associated with an increase in lipid oxidation differentiation and lipogenesis.

Effect of SR141716A on dysbiosis of gut microbiota in diet-induced obesity

To test that role of gut microbiota, we performed 16S rRNA metagenomics sequencing against both variable regions (V3+V4) of fecal samples in different groups of our study (n = 5 per group), and rarefied to a depth of 10,000 reads per sample. We grouped microorganisms in Operational Taxonomic Units (OTUs) in order to standardize grouping based on 97% similarities in DNA sequence (Supplementary Table 3.3). The obtained data demonstrated that overall, microbial communities were strongly structured

64

by diet.   We observed significant separation between lean mice and DIO mice. Interestingly, principal coordinate analysis performed based on distance matrix demonstrated that microbial community structure was more sensitive to SR141716A treatment than dietary fat intake (Fig 3.7A). In order to estimate the diversity of micro-organisms in regard to their numbers and their similarities in abundance, Alpha diversity was calculated based on Chao1 index (Fig 3.7B). Relative taxa abundance area plots at the genus taxonomical level for individuals from the five populations was assessed by taking the OTU table at genus level as an input . Individuals were represented along the horizontal axis, and relative taxa frequency at the genus level was denoted by the vertical axis (Fig 3.7 C). Taken together, our data suggested that OTUs were differentially enriched within the different groups in our study. In order to investigate the exclusive effect of SR141716A in the gut-flora of DIO mice (HFD+SR), we conducted pair-fed to SR141716A (PFSR) and body-weight matched control to HFD+SR. Our data indicated significant enrichment of Akkermansia OTUs in DIO-treated mice with SR141716A (HFD+SR) as compared with both pair-fed obese (PFSR) and body-weight matched (BWM) controls. Interestingly, the significant reduction in immunogenic Lanchnospiraceae and Erysipelotrichaceae seen with SR141716A treatment was beyond the effect of SR141716A on the weight loss and diet intake restriction. Because the disruption in gut mucosal layer was improved in DIO mice with SR141716A treatment (HFD+SR), we investigated the effect of treatment on residential bacteria of mucosal layer, specifically Akkermansia muciniphila [218,219,220,221,222,223].

Numerous studies have shown the inverse correlation between the abundance of A.muciniphila and metabolic syndrome. RT-PCR from the isolated fecal DNA

65

demonstrated significant enrichment in A.muciniphila colonization in SR141716A-treated DIO mice (HFD+SR) as compared with vehicle-treated DIO (HFD), pair-fed to SR141716A (PFSR), and body weight matched to SR141716A (BWM) (Fig 3.7D). Previous studies have demonstrated that Lanchnospiraceae and Erysipelotrichaceae, within firmicutes phylum are implicated in gaining weight and induction of metabolic syndrome [224,225,226,227,228]. Our studies demonstrated that Lanchnospiraceae and Erysipelotrichaceae were significantly decreased in SR141716A-treated DIO mice (HFD+SR) as compared with vehicle-treated DIO (HFD) control. In addition, the RT-PCR from the fecal content validated the 16s rRNA sequenced data (Fig 3.7E, 3.7F).

Effect of SR141716A on Short Chain Fatty Acid (SCFA) in Diet-Induced Obesity

In order to investigate the effect of SR141716 intervention treatment in DIO mice (HFD+SR), on Short Chain Fatty Acid (SCFA), we quantified the level of SCFA in serum, cecal and fecal content of mice. Interestingly, we found a significant increase in concentration of propionic acid, I-butyric as well as n-butyric acid, in cecal and fecal content of SR141716A treated DIO (HFD+SR) mice when compared with vehicle-treated DIO (HFD) mice (Fig 3.8A, 3.8B). The same trend was observed in concentration of acetic acid as well as valeric acid, but the changes weren't significant. In order to evaluate the alteration in SCFA systemically, we assessed the concentration of SCFA in serum. Because the SCAFs are mostly abundant in colon and stool, the same trend but at the lower concentration than SCFAs in fecal and cecal content was observed in SCFAs of serum. (Supplementary figure 3.4) .

3.4 <u>DISCUSSION</u>

There is growing evidence to suggest that blockade of cannabinoid CB1 receptor possesses anorectic anti-obesity properties and modulates metabolic parameters in diet-induced obesity [216,229,230,231] . However, most of the previous studies did not fully investigate the effect of cannabinoid CB1 antagonist on chronic inflammation in DIO model. Our study investigated both systematic and local inflammatory profiles in DIO model and demonstrated that intervention treatment of DIO mice with SR141716A, can ameliorate the obese phenotype and associated metabolic complications. Because there is a clear association between adipose tissue macrophage accumulation and metabolic dysfunction in DIO model, we investigated the effect of CB1 antagonism on macrophages and it was remarkable to note that SR141716A treatment could suppress pro-inflammatory macrophages (M1) in adipose tissue and their associated cytokines (MIP-1α, MCP-1, and plasma LPS). Indeed, blockade of cannabinoid CB1 receptors in mice fed a high fat diet reduced macrophage retention in adipose tissue, suppression of local and systematic inflammation as well as insulin resistance. In the current study, we also observed improvement in colonic inflammation (MPO) in DIO model following SR141716A treatment.

It is of the interest that blockade of cannabinoid CB1 receptor with SR141716A in obese mice resulted in attenuation of neutrophilic leukocytosis associated with obesity. One of the possible mechanistic effect of SR141716A on the neutrophilic leukocytosis can be attributed to the inhibition of the neutrophil elastase activity. Recent study identified that the neutrophilic leukocytosis in DIO mice exacerbate the chronic

67

inflammation in adipose tissue [232]. Increase in neutrophil population is associated with more release of, a serine proteinase, elastase, which results in activation of Toll-Like Receptor 4 (TLR4) pathway, and massive release of chemo-attractants from the immune cells and adipocytes. Consistent with our findings, the neutrophilic knockout mice were protected from insulin resistance associated with obesity phenotype [232]. The direct effect of blockade of cannabinoid CB1 receptor on neutrophils and their elastase activity warrant further investigation.

In order to evaluate the effect of SR141716A treatment beyond its effect on calorie intake and weight loss, we conducted pair-fed to SR141716A (PFSR) and body weight-matched (BWM) to SR141716A-treated obese (HFD+SR) mice as controls [198]. Pair-fed to SR141716A (PFSR) consumed the same amount of high fat diet as the SR141716A-treated obese mice (HFD+SR). Diet intake was adjusted in body weight-matched (BWM) controls to perpetuate the same weight loss pattern as in SR141716A-treated obese mice (HFD+SR). Our study demonstrated that transient reduction in calories intake and sustained weight loss in SR141716A-treated obese mice (HFD+SR), was associated with less adiposity and smaller fat mass. The smaller adipocytes in SR141716A-treated obese mice (HFD+SR) was associated with the significant reduction in fat storage. Previous studies have shown that SR141716A may trigger futile calcium cycling, which results in enhanced whole body energy expenditure [216,233]. Therefore, one potential explanation for SR141716A-induced reduction in fat mass independent of calorie intake, is enhanced lipolysis and lipid oxidation to maintain ATP for futile cycle (calcium and substrate).

In contrast to the previous studies, our data demonstrate that blockade of cannabinoid CB1 receptor with SR141716A in obese mice contribute to increased lipogenesis [198,234,235]. Interestingly, a previous study uncovered the regulatory role of LPS in mediating inhibitory effect on lipogenesis, on cultured adipose tissue via PPAR-γ blockade [192]. In conjunction with our data, several studies have shown that over-activity of endocannabinoid system in DIO model, is associated with increased LPS levels and inflammation [192] .Furthermore, we found that SR141716A-treated obese (HFD+SR) mice demonstrated improvement in gut permeability as compared to vehicle-treated obese (HFD) mice. Consistent with our study, earlier reports demonstrated improvement in gut permeability in SR141716A-treated ob/ob obese mice by induction of two tight junction proteins, occludin and ZO-1 [183,224]. Thus, increase in lipogenesis with SR141716A treatment may result from less gut permeability which prevents the LPS-inhibitory effect on lipogenesis. These data also suggest that cross-talk between endocannabinoid system and LPS may modulate adiposity.

It is exciting to note that the protective effect of SR141716A against obesity and metabolic disruption observed in our study, could be explained by the potential link between gut microbial community and endocannabinoid system. Enhanced endocannabinoid (eCB) system activity including higher level of endocannabinoids in plasma and adipose tissue as well as changes in cannabinoid CB1 receptor expression has been defined in diet induced-obesity and metabolic syndrome models [187,189,190,236]. The CB1 receptor knockout mice are resistant to diet-induced-obesity [237,238]. Selective reduction in CB1 receptor expression in the colon of germ free mice, Myd88(-/-) mice, TRIF (-/-) mice, probiotic and antibiotic treated-obese mice, can attributed to altered gut

69

microbial composition [183,239,240,241]. Myd88 and TRIF are the integral adaptor molecules of toll-like receptor (TLR) signaling pathway which mediates the microbial community-host interactions [242]. Alteration in gut microbial community following blockade of cannabinoid CB1 receptor in DIO model has not been previously studied. Thus, the current study, demonstrated for the first time that the protective effect of a CB1 receptor antagonist in diet induced-obesity may result from dysbiosis of gut microbiota.

Previous studies demonstrated significant reduction in Akkermansia muciniphila in both genetically ob/ob and diet-induced-obese mice [243,244]. Protective properties of dietary polyphenols and probiotics in obese and diabetic phenotypes has been attributed to the restoration of the abundance of this strain in gut [245,246,247]. Recent study identified the protective effect of orally transferred A.muciniphila in dextran sulfate sodium (DSS)-induced colitis model [248]. Furthermore, adoptive transfer of live A.muciniphila but not the heat-killed cells was shown to ameliorate obese and diabetic phenotypes, reduce metabolic endotoxemia, host adiposity, and improve glucose metabolism [218,222,249]. In the present study, we demonstrated that the resorted abundance of A.muciniphila in DIO mice following blockade of CB1 receptor was independent of calorie restriction and weight loss. To further confirm the therapeutic effect of CB1 receptor antagonist in DIO model, we investigated the direct effect of SR141716A treatment on the colon physiology in the host. We demonstrated significant improvement in MUC2 and KLF4 genes in colon of the SR141716A-treated obese mice when compared to the vehicle-treated obese mice. The transcription factors KLF4 and MUC2 regulate differentiation of goblet cells which is associated with mucin formation in colon [250]. Our data suggested that A.muciniphila is responding to increased host mucin production following blockade of

70

cannabinoid CB1 receptor in DIO mice, and mucin serves as the main of carbon, nitrogen, and sulfur for A.muciniphila growth.

Furthermore, we conducted gas chromatography to address the changes in short chain fatty acid of cecal material. Blockade of cannabinoid CB1 receptor caused more production of propionate and butyric acid in cecal material. Previous studies identified the regulatory mechanism of propionate and butyrate in glucose homeostasis, lipid and cholesterol metabolism, and improvement of gut barrier function, supporting the beneficial regulatory effect of SR141716A on the metabolic parameters in obese individuals [251]. The anti-inflammatory properties of propionate (suppression of pro-inflammatory M1 macrophages), and butyrate (inhibition of inflammation via NF-κB pathway) has been established earlier [252,253]). Consistent with our data, earlier research defined propionate as the A.muciniphila metabolite [244,254]. Recent study elucidated the protective effect of propionate and butyrate against diet-induced obesity complications and metabolic syndrome. Propionate and butyrate SCFA have been identified to suppress appetite actively by modulating the gut hormones such as Peptide YY (PYY), and Glucagon-Like Peptide-1 (GLP-1) [222,255]. The excessive release of GLP-1 and PYY into portal vein was identified following propionate infusion into the murine colon. Additionally, higher activity of entroendocrine L-cells (GLP-1, and GLP-2 secretion) was identified with the growth of Akkermansia muciniphila, and further investigation is needed to uncover the mechanism underlying this connection [183,218]. However, whether the primary beneficial effect of SR141716A can be attributed to the gut abundance of A.muciniphila or higher activity of L-cells in DIO remains an interesting question that warrants further investigations.

71

In conclusion, the current study suggests that the underlying mechanisms through which SR141716A, a CB1 antagonist, exerts its protective effect against diet induced-metabolic dysfunction may involve changes in the gut microbial community with an increase in A. muciniphila and a decrease in immunogenic Lanchnospiraceae and Erysipelotrichaceae. Indeed, the direct application of A.muciniphila as the therapeutic intervention remains elusive because of its anaerobic growth condition. Therefore, therapeutic intervention strategies aimed at growth of A.muciniphila, will likely be an interesting tool for combating the global burden of obesity and metabolic syndrome.

A

Fed *ad-libitum*			Restricted Diet	
LFD+Vehicle	HFD+Vehicle	HFD+SR	PFSR	BWM
Low-fat diet	High-fat diet			

B

C

D

E

F

LFD+Vehicle

HFD+Vehicle

HFD+SR

PFSR

BWM

G
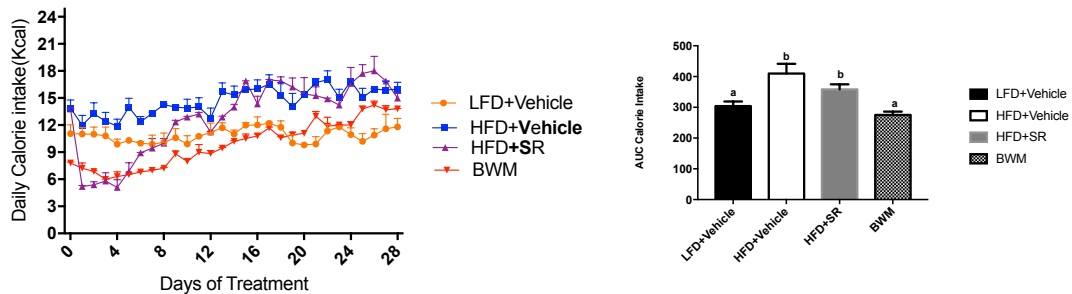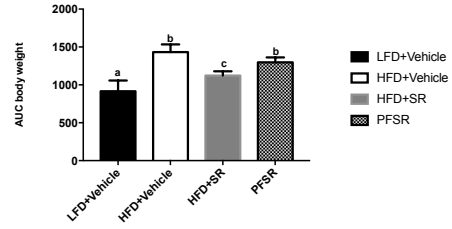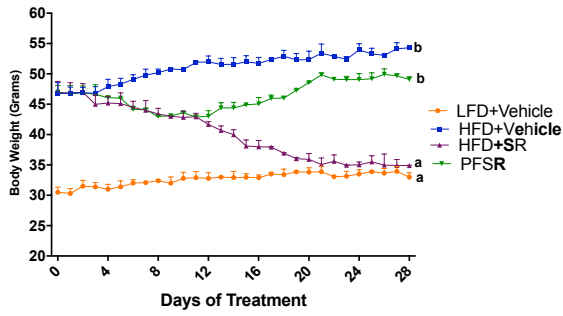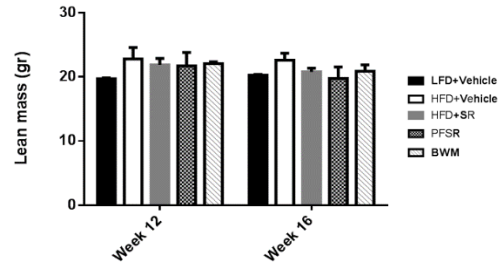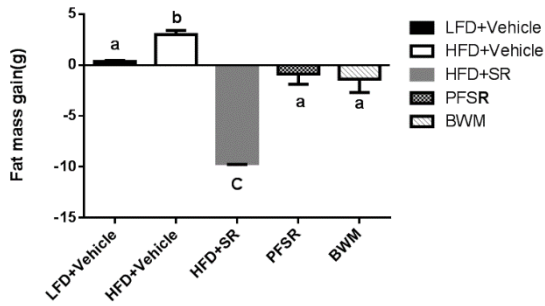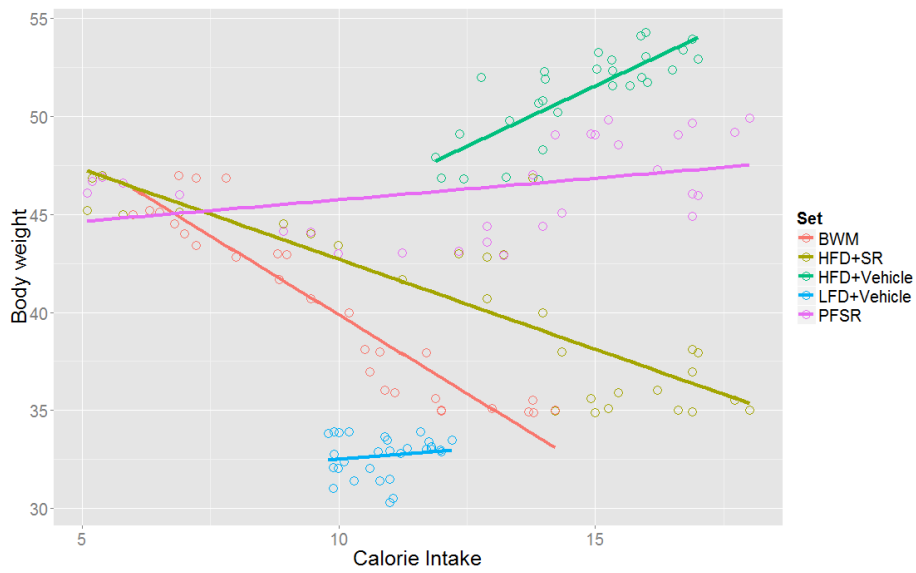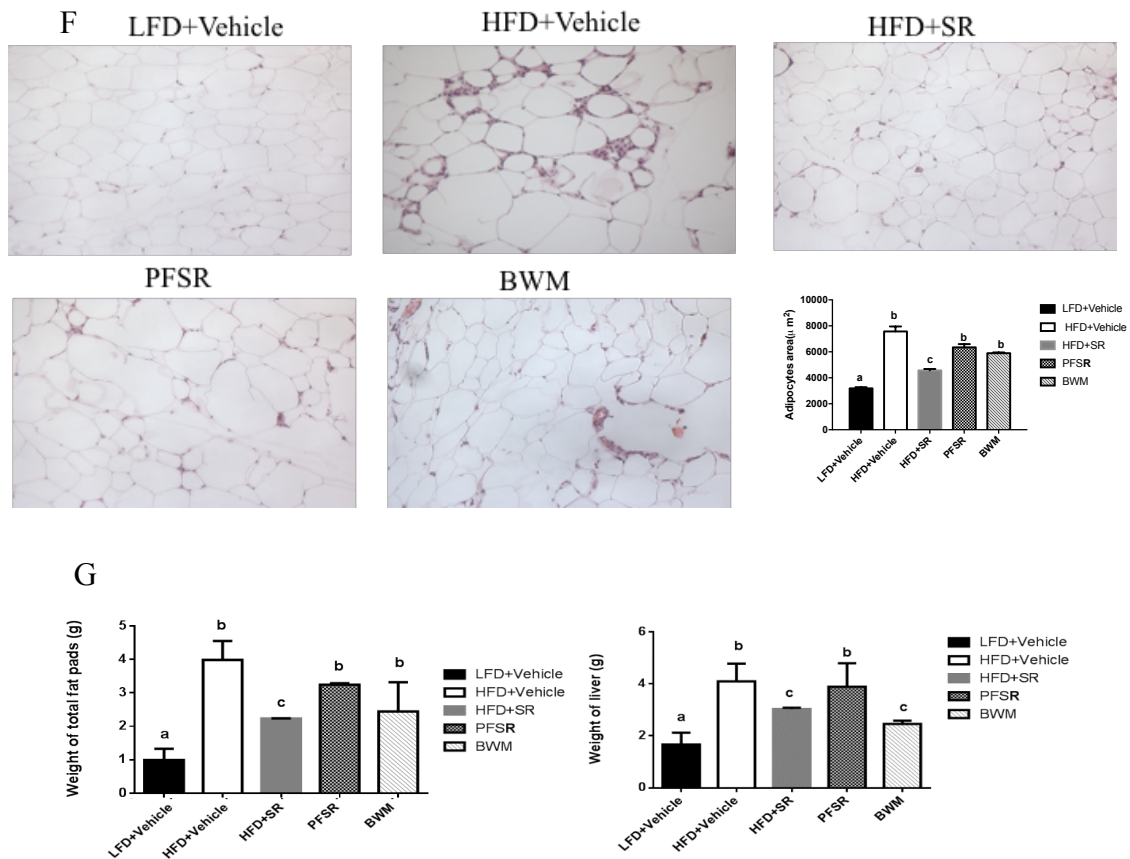
Figure 3.1

Figure 3.1 SR141716A causes transient reduction in diet intake and persistent weight loss as compared with Vehicle-treated DIO control. (A) DIO model was generated by feeding C57BL/6J male mice with high-fat diet (HFD+Vehicle) whereas their lean, age-matched controls were fed low-fat diet (LFD+Vehicle). HFD-fed mice were treated with either SR141716A (10mg/kg/day) (HFD+SR) or vehicle (0.1% Tween 80) (HFD+Vehicle) by daily oral gavage for 4 weeks starting at week 12. In order to assess the anti-inflammatory effect of SR141716A beyond its effect on calorie intake inhibition and weight loss in DIO phenotype, pair-feeding was conducted in diet-intake matched controls (PFSR) and diet intake was adjusted in body-weight-matched controls (BWM).; n=8-10 mice/group. (B) Daily energy intake during 4 weeks' treatment with SR141716A in DIO mice was recorded, Area Under the Curve (AUC) was calculated

74

from the 5 replicated experiments (C) Daily body weight of each group of mice is shown during the whole period of treatment, Area Under the Curve (AUC) was calculated from the 5 replicated experiments which were identical to the replicates in Figure 1b. AUC was calculated with Trapezoidal rule in R software. Generalized Estimating Equation (GEE) was performed to fit a repeated measurement logistic regression in SPSS. Data are shown as as means ± SD. Data with different superscript letters are significantly different ($P < 0.05$). (D)Pearson correlation between changes in body weight and caloric intake within different groups was assessed in R software. (E)Total fat mass gain and changes in lean mass was assessed at the baseline and after 4 weeks of treatment with Dual Energy X-ray absorptiometry (DEXA).Data are shown as as means ± SD. Data with different superscript letters are significantly different ($P < 0.05$).(F) The surface area of 100 adipocytes was determined and then averaged to represent mean adipocyte size for each mouse using ImageJ software,NIH. Data are shown as means ± SD. Data with different superscript letters are significantly different ($P<0.05$) according to post hoc ANOVA one-way statistical analysis. (n=10) (G) Weights of fat pads and livers were assessed at the end of the treatment. After treatment for 4 weeks, HFD+SR group had lower body weight, smaller fat pads and livers than HFD+Vihcle group. Smaller fat pads and lower body weight was recorded in HFD+SR group than HFD Pair-fed to SR141716A(PFSR), although both groups had the same quantity of high fat diet intake. The HFD+SR group has a smaller fat pad than Body weight Matched (BWM) group. Overall data is suggesting the effect of SR141716A treatment is beyond its effect on weight loss and diet intake
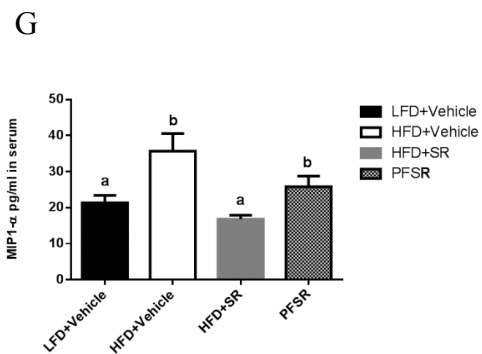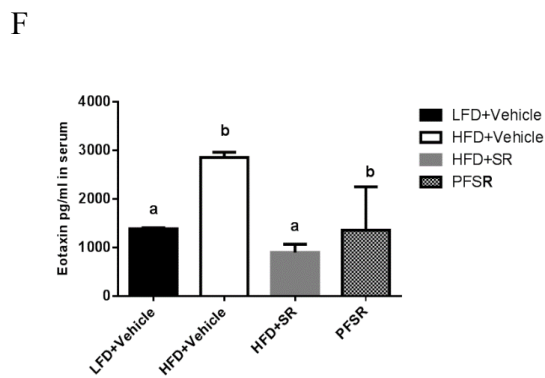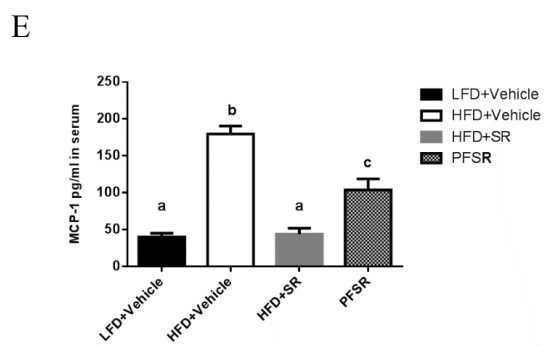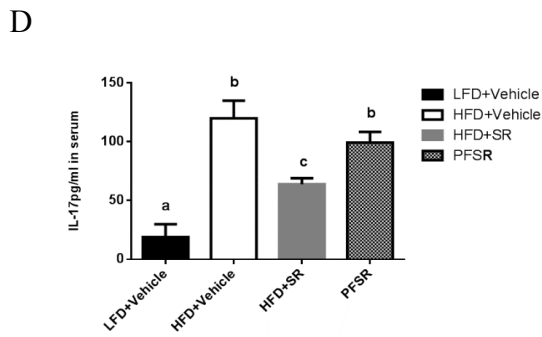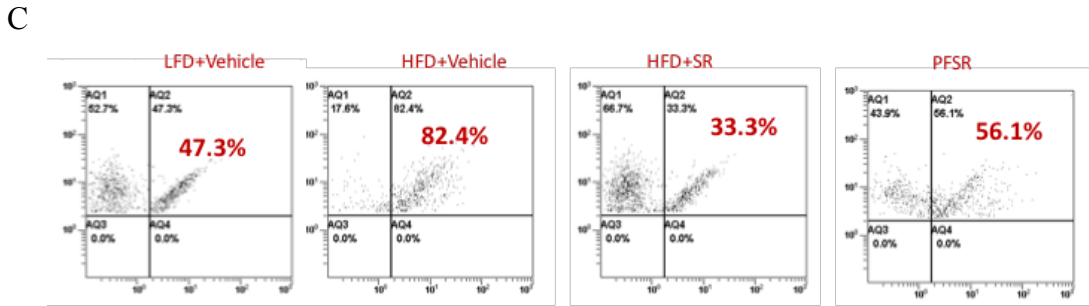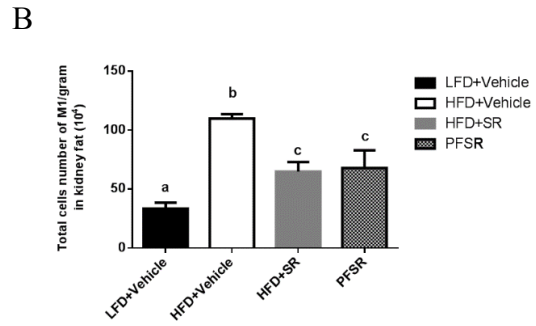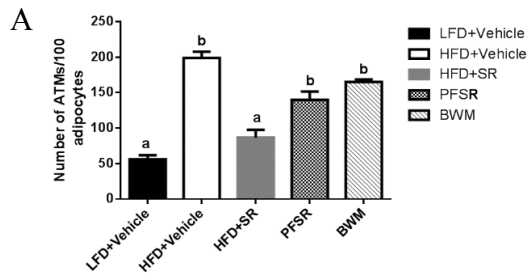
H
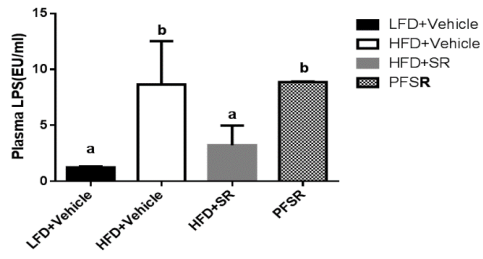
I
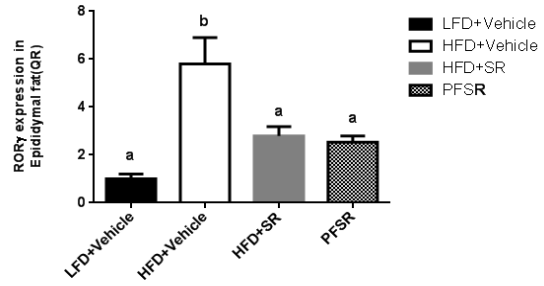
J
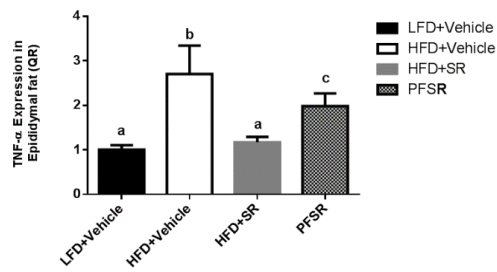
K
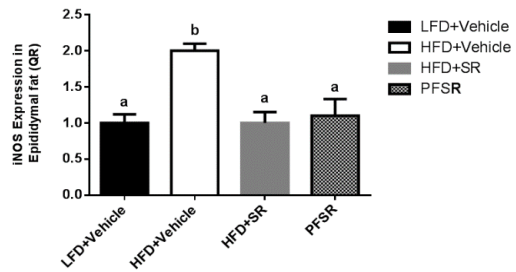
L
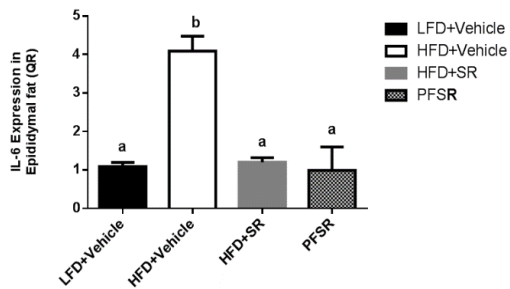
M
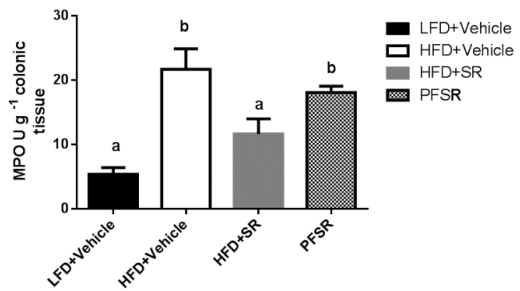
Figure 3.2

Figure 3.2 SR141716A attenuates local and systematic inflammation in diet-induced obesity phenotype. (A)Adipose Tissue Macrophages (ATMS) were quantified per 100 adipocytes by Spot Studio v1.0 Analysis Software. (B,C)Kidney fat were isolated from 10 mice in each group. The ratio and total cell number of kidney fat F4/80 and CD11c cells was decreased with SR141716A treatment (33.3%) when compared to HFD+Vehicle (82.4%) (D) Effect of SR141716A on the plasma IL-17 levels, (E) monocyte chemoattractant protein-1(MCP-1) levels, (F) Eotaxin plasma levels, and (G) macrophage inflammatory protien-1α (MIP-1α) level in plasma was quantified with multiplex detection immunoassays. SR141716A-treated DIO mice(HFD+SR) have significantly lower systematic inflammation (as compared to vehicle-treated DIO mice(HFD+Vehicle), and Pair-fed to SR141716A controls(PFSR). (H) Plasma LPS level in DIO mice treated with SR141716A for four weeks and controls was quantified (I) Effect of SR141716A treatment on the mRNA level of ROR$_\gamma$ (J)TNF-α (K) iNOS (l) IL-6 in the epididymal adipose tissue was examined. (M) Myeloperoxidase (MPO) level in colonic tissue was measured. Data are shown as means $\pm$ SD. Data with different superscript letters are significantly different (P<0.05) according to post hoc ANOVA one-way statistical analysis. (n=5 except LFD+Vehicle n=4)

A

B
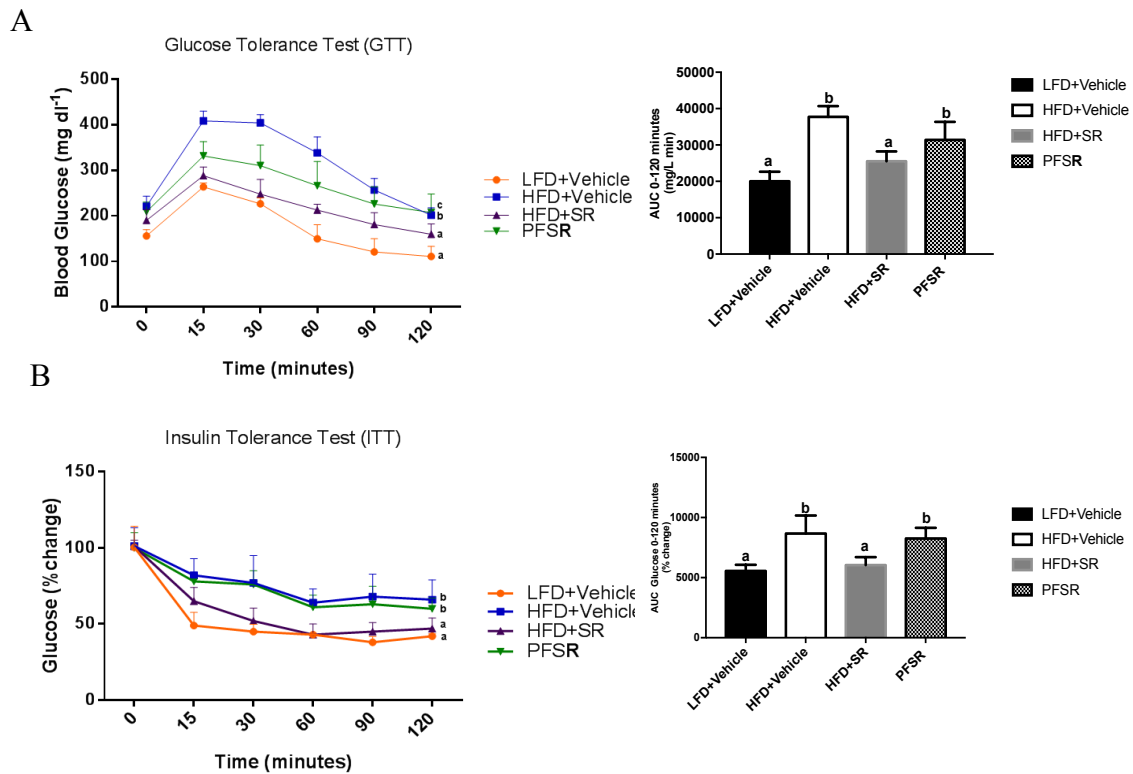
Figure 3.3

Figure 3.3 SR141716A ameliorates metabolic dysfunction in diet-induced obesity phenotype. (A) Glucose tolerance test(GTT) and (B)Insulin tolerance test (ITT) of mice fed LFD+Vehicle (n=10), HFD+Vehicle (n=10), HFD+SR (n=9) and Pair-fed to SR141716A (PFSR) (n=10). Each animal received a glucose gavage 1.5g/KG body mass of glucose (25% D glucose) Blood glucose levels were determined after 15,30,60 and 120 minutes. Insulin-tolerance tests were carried out on un-fasted animals by injecting an i.p injection of 1.5 U/Kg body mass of insulin. Blood glucose levels were detected after 15, 30,60 and 120 minutes. Generalized Linear Mixed Model (GLMM) was performed to calculate p values for the repeated measures in SPSS. Mean area under the curve (AUC) from triplicate experiments measured between 0-120 minutes after glucose (GTT) and insulin (ITT) load. AUC was assessed with Trapezoidal rule in R software. Data with different superscript letters are significantly different. GTT ($P<0.01$), ITT ($P<0.05$).
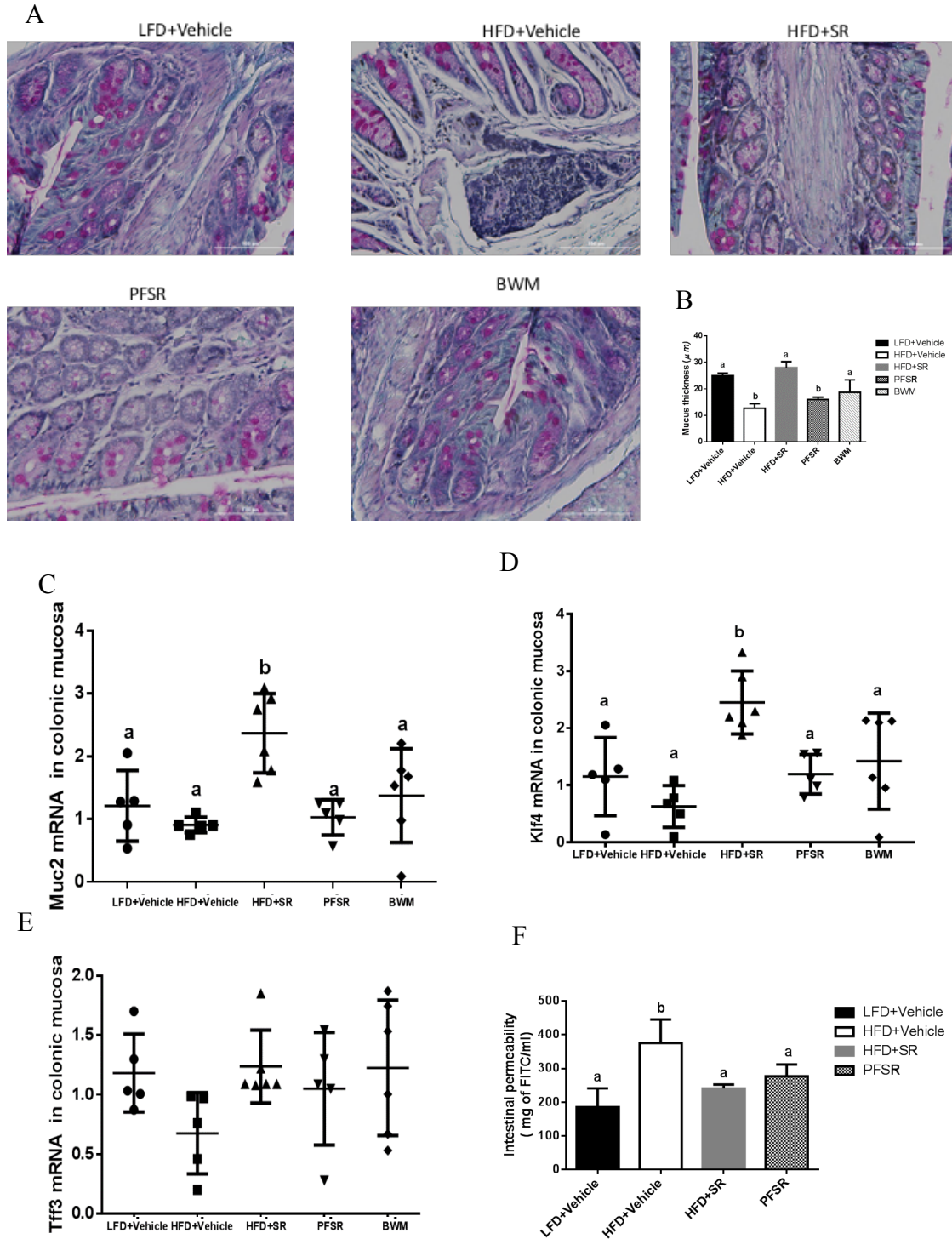
Figure 3.4

Figure 3.4 SR141716A restores gut barrier function in diet-induced obesity phenotype. (A) Representative Periodic Acid Schiff images that were used for in situ mucus layer staining, scale bar,100 μm. (B)Thickness of the mucus layer measured by histological image analysis software MetaMorph (LFD+Vehicle *n=5*, HFD+Vehicle *n=5*, SR *n=6*, PFSR *n=5*, and BWM *n=6*). (C-E) mRNA expression analysis by qRT-PCR of mucus-related genes in the colonic mucosa. (F)Intestinal permeability measured by levels of serum FITC-Dextran (4kDa) following oral gavage (*n*=5 except LFD+Vehicle *n*=4). Data are shown as means $\pm$ SD. Data with different superscript letters are significantly different (*P*<0.05) according to post hoc ANOVA one-way statistical analysis.

A

B

C
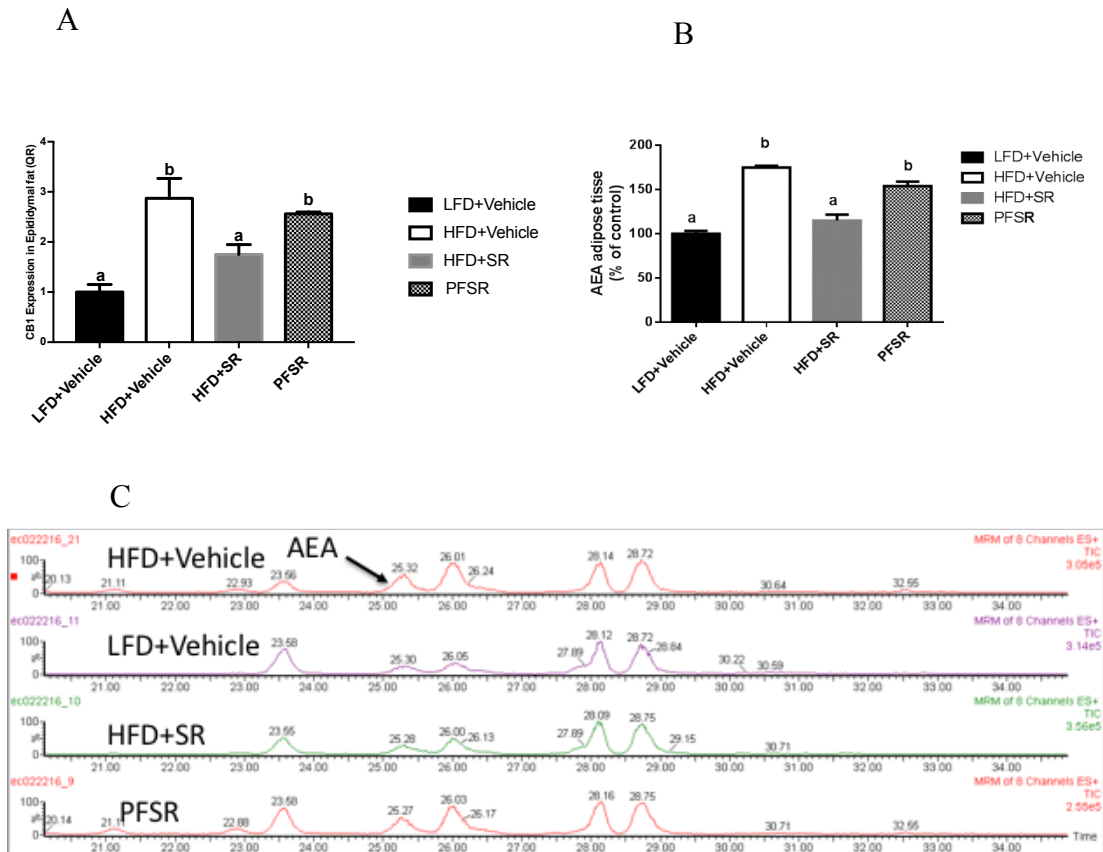
Figure 3.5

Figure 3.5 SR141716A attenuates over-activity of endocannabinoids system in diet-induced obesity phenotype. (A)Adipose tissue CB1 mRNA levels in SR141716A-treated DIO, (HFD+SR), vehicle-treated DIO (HFD+Vehicle), lean mice (LFD+Vehicle) and Pair-fed to SR141716A (PFSR) controls mice was assessed by RT-PCR. (B)White adipose tissue AEA level from the same mice (percent of control values) were measured with LC/MS/MS (*n*=3). AEA levels (percent of LFD+Vehicle) in the epididymal adipose tissue of HFD+SR, HFD+Vehicle and PFSR(*n*=3). Data are shown as means $\pm$ SD. Data with different superscript letters are significantly different (*P*<0.05) according to post hoc ANOVA one-way statistical analysis.

81

A
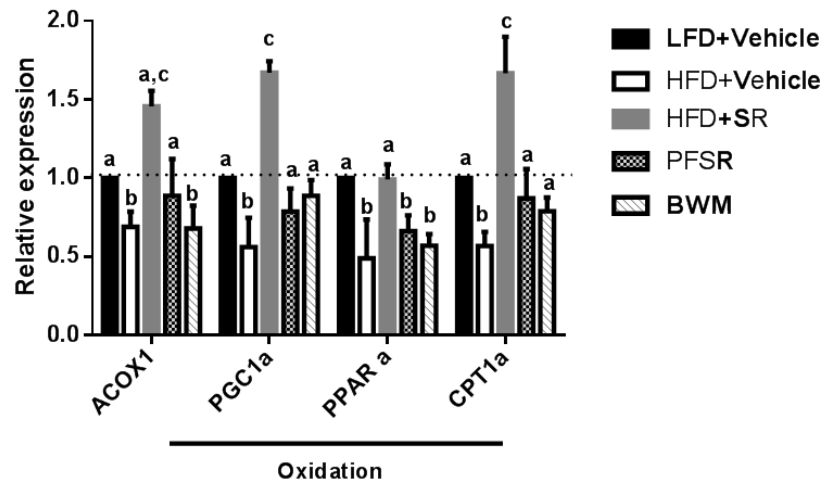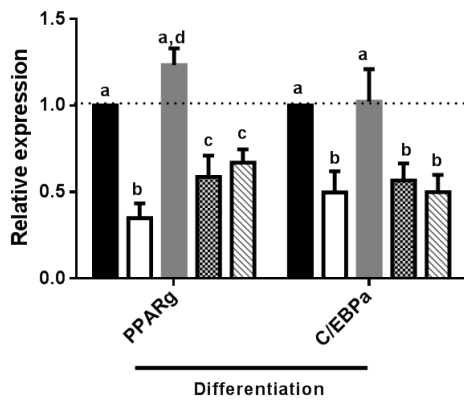
B   C
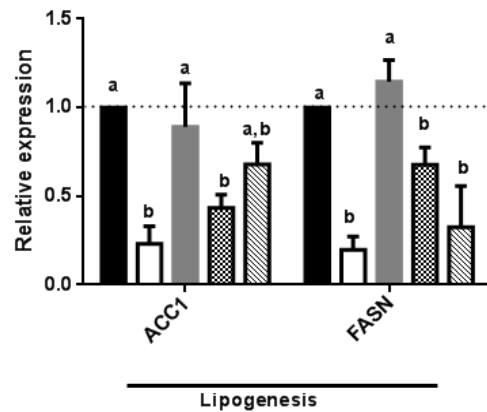
Figure 3.6

Figure 3.6 SR141716A improves adipose tissue metabolism   in diet-induced obesity phenotype. (A)mRNA expression of markers of adipocyte differentiation (C/EBPα,PPARγ), (B) lipogenesis (ACC1; FASN), (C) and lipid oxidation (CPT1; ACOX1; PGC-1α; and PPARα) was measured in epididymal fat depots (n = 5). Data are shown as means ± SD. Data with different superscript letters are significantly different (P < 0.05) according to post hoc ANOVA one-way statistical analysis.

82

A
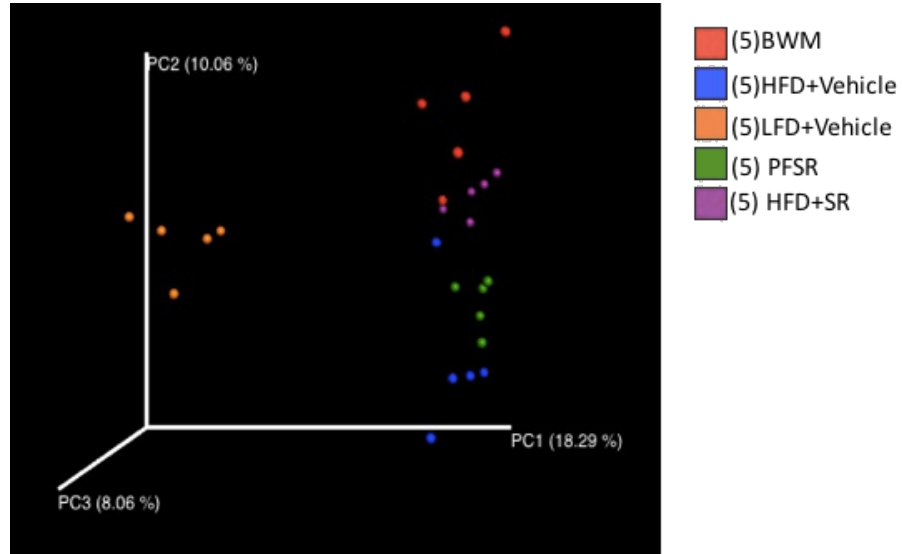
B
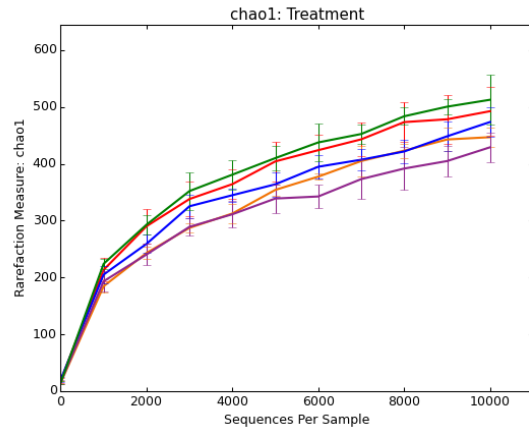
C
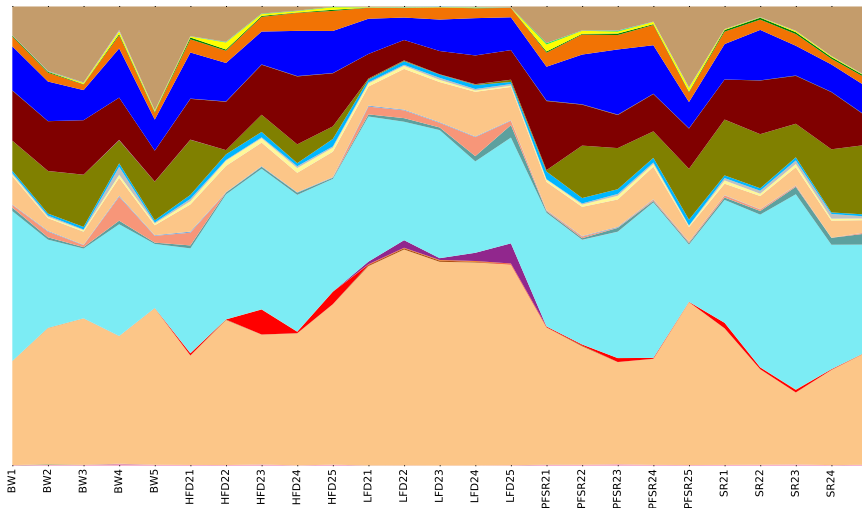
k__Bacteria;p__Acidobacteria;c__Solibacteres;o__Solibacterales;f__Solibacteraceae;g__
k__Bacteria;p__Actinobacteria;c__Actinobacteria;o__Actinomycetales;f__Actinomycetaceae;g__Actinomyces
k__Bacteria;p__Actinobacteria;c__Actinobacteria;o__Actinomycetales;f__Corynebacteriaceae;g__Corynebacterium
k__Bacteria;p__Actinobacteria;c__Actinobacteria;o__Actinomycetales;f__Microbacteriaceae;g__Microbacterium
k__Bacteria;p__Actinobacteria;c__Actinobacteria;o__Actinomycetales;f__Micrococcaceae;g__Rothia
k__Bacteria;p__Actinobacteria;c__Actinobacteria;o__Actinomycetales;f__Propionibacteriaceae;g__Propionibacterium
k__Bacteria;p__Actinobacteria;c__Actinobacteria;o__Actinomycetales;f__Tsukamurellaceae;g__Tsukamurella
k__Bacteria;p__Actinobacteria;c__Coriobacteriia;o__Coriobacteriales;f__Coriobacteriaceae;g__Adlercreutzia
k__Bacteria;p__Bacteroidetes;c__Bacteroidia;o__Bacteroidales;f__;g__
k__Bacteria;p__Bacteroidetes;c__Bacteroidia;o__Bacteroidales;f__Bacteroidaceae;g__Bacteroides
k__Bacteria;p__Bacteroidetes;c__Bacteroidia;o__Bacteroidales;f__Porphyromonadaceae;g__Parabacteroides
k__Bacteria;p__Bacteroidetes;c__Bacteroidia;o__Bacteroidales;f__Prevotellaceae;g__Prevotella
k__Bacteria;p__Bacteroidetes;c__Bacteroidia;o__Bacteroidales;f__Rikenellaceae;g__
k__Bacteria;p__Bacteroidetes;c__Bacteroidia;o__Bacteroidales;f__Rikenellaceae;g__AF12
k__Bacteria;p__Bacteroidetes;c__Bacteroidia;o__Bacteroidales;f__S24-7;g__
k__Bacteria;p__Bacteroidetes;c__Bacteroidia;o__Bacteroidales;f__[Odoribacteraceae];g__Odoribacter
k__Bacteria;p__Bacteroidetes;c__Flavobacteriia;o__Flavobacteriales;f__Flavobacteriaceae;g__Flavobacterium
k__Bacteria;p__Cyanobacteria;c__4C0d-2;o__YS2;f__;g__
k__Bacteria;p__Cyanobacteria;c__Chloroplast;o__Streptophyta;f__;g__
k__Bacteria;p__Deferribacteres;c__Deferribacteres;o__Deferribacterales;f__Deferribacteraceae;g__Mucispirillum
k__Bacteria;p__Firmicutes;c__Bacilli;o__Bacillales;f__Bacillaceae;g__Bacillus
k__Bacteria;p__Firmicutes;c__Bacilli;o__Bacillales;f__Planococcaceae;g__
k__Bacteria;p__Firmicutes;c__Bacilli;o__Bacillales;f__Staphylococcaceae;g__Staphylococcus
k__Bacteria;p__Firmicutes;c__Bacilli;o__Gemellales;f__;g__
k__Bacteria;p__Firmicutes;c__Bacilli;o__Lactobacillales;f__;g__
k__Bacteria;p__Firmicutes;c__Bacilli;o__Lactobacillales;f__Aerococcaceae;g__Aerococcus
k__Bacteria;p__Firmicutes;c__Bacilli;o__Lactobacillales;f__Carnobacteriaceae;g__Granulicatella
k__Bacteria;p__Firmicutes;c__Bacilli;o__Lactobacillales;f__Enterococcaceae;g__
k__Bacteria;p__Firmicutes;c__Bacilli;o__Lactobacillales;f__Enterococcaceae;g__Enterococcus
k__Bacteria;p__Firmicutes;c__Bacilli;o__Lactobacillales;f__Lactobacillaceae;g__Lactobacillus
k__Bacteria;p__Firmicutes;c__Bacilli;o__Lactobacillales;f__Leuconostocaceae;g__Weissella
k__Bacteria;p__Firmicutes;c__Bacilli;o__Lactobacillales;f__Streptococcaceae;g__Lactococcus
k__Bacteria;p__Firmicutes;c__Bacilli;o__Lactobacillales;f__Streptococcaceae;g__Streptococcus
k__Bacteria;p__Firmicutes;c__Bacilli;o__Turicibacterales;f__Turicibacteraceae;g__Turicibacter
k__Bacteria;p__Firmicutes;c__Clostridia;o__;f__;g__
k__Bacteria;p__Firmicutes;c__Clostridia;o__Clostridiales;f__;g__
k__Bacteria;p__Firmicutes;c__Clostridia;o__Clostridiales;f__Christensenellaceae;g__
k__Bacteria;p__Firmicutes;c__Clostridia;o__Clostridiales;f__Clostridiaceae;g__
k__Bacteria;p__Firmicutes;c__Clostridia;o__Clostridiales;f__Clostridiaceae;g__02d06
k__Bacteria;p__Firmicutes;c__Clostridia;o__Clostridiales;f__Clostridiaceae;g__Candidatus Arthromitus
k__Bacteria;p__Firmicutes;c__Clostridia;o__Clostridiales;f__Clostridiaceae;g__Clostridium
k__Bacteria;p__Firmicutes;c__Clostridia;o__Clostridiales;f__Clostridiaceae;g__SMB53
k__Bacteria;p__Firmicutes;c__Clostridia;o__Clostridiales;f__Dehalobacteriaceae;g__Dehalobacterium
k__Bacteria;p__Firmicutes;c__Clostridia;o__Clostridiales;f__Lachnospiraceae;g__
k__Bacteria;p__Firmicutes;c__Clostridia;o__Clostridiales;f__Lachnospiraceae;g__Anaerostipes
k__Bacteria;p__Firmicutes;c__Clostridia;o__Clostridiales;f__Lachnospiraceae;g__Blautia
k__Bacteria;p__Firmicutes;c__Clostridia;o__Clostridiales;f__Lachnospiraceae;g__Coprococcus
k__Bacteria;p__Firmicutes;c__Clostridia;o__Clostridiales;f__Lachnospiraceae;g__Dorea
k__Bacteria;p__Firmicutes;c__Clostridia;o__Clostridiales;f__Lachnospiraceae;g__Roseburia
k__Bacteria;p__Firmicutes;c__Clostridia;o__Clostridiales;f__Lachnospiraceae;g__[Ruminococcus]
k__Bacteria;p__Firmicutes;c__Clostridia;o__Clostridiales;f__Peptococcaceae;g__
k__Bacteria;p__Firmicutes;c__Clostridia;o__Clostridiales;f__Peptococcaceae;g__rc4-4
k__Bacteria;p__Firmicutes;c__Clostridia;o__Clostridiales;f__Peptostreptococcaceae;g__
k__Bacteria;p__Firmicutes;c__Clostridia;o__Clostridiales;f__Peptostreptococcaceae;g__Clostridium
k__Bacteria;p__Firmicutes;c__Clostridia;o__Clostridiales;f__Peptostreptococcaceae;g__[Clostridium]
k__Bacteria;p__Firmicutes;c__Clostridia;o__Clostridiales;f__Ruminococcaceae;g__
k__Bacteria;p__Firmicutes;c__Clostridia;o__Clostridiales;f__Ruminococcaceae;g__Anaerotruncus
k__Bacteria;p__Firmicutes;c__Clostridia;o__Clostridiales;f__Ruminococcaceae;g__Clostridium
k__Bacteria;p__Firmicutes;c__Clostridia;o__Clostridiales;f__Ruminococcaceae;g__Faecalibacterium
k__Bacteria;p__Firmicutes;c__Clostridia;o__Clostridiales;f__Ruminococcaceae;g__Oscillospira
k__Bacteria;p__Firmicutes;c__Clostridia;o__Clostridiales;f__Ruminococcaceae;g__Ruminococcus
k__Bacteria;p__Firmicutes;c__Clostridia;o__Clostridiales;f__[Mogibacteriaceae];g__
k__Bacteria;p__Firmicutes;c__Clostridia;o__Clostridiales;f__[Tissierellaceae];g__Anaerococcus
k__Bacteria;p__Firmicutes;c__Erysipelotrichi;o__Erysipelotrichales;f__Erysipelotrichaceae;g__
k__Bacteria;p__Firmicutes;c__Erysipelotrichi;o__Erysipelotrichales;f__Erysipelotrichaceae;g__Allobaculum
k__Bacteria;p__Firmicutes;c__Erysipelotrichi;o__Erysipelotrichales;f__Erysipelotrichaceae;g__Clostridium
k__Bacteria;p__Firmicutes;c__Erysipelotrichi;o__Erysipelotrichales;f__Erysipelotrichaceae;g__Coprobacillus
k__Bacteria;p__Firmicutes;c__Erysipelotrichi;o__Erysipelotrichales;f__Erysipelotrichaceae;g__[Eubacterium]
k__Bacteria;p__Fusobacteria;c__Fusobacteriia;o__Fusobacteriales;f__Fusobacteriaceae;g__Fusobacterium
k__Bacteria;p__Proteobacteria;c__Alphaproteobacteria;o__RF32;f__;g__
k__Bacteria;p__Proteobacteria;c__Alphaproteobacteria;o__Rhizobiales;f__;g__
k__Bacteria;p__Proteobacteria;c__Alphaproteobacteria;o__Rhizobiales;f__Bradyrhizobiaceae;g__
k__Bacteria;p__Proteobacteria;c__Alphaproteobacteria;o__Rhizobiales;f__Bradyrhizobiaceae;g__Bradyrhizobium
k__Bacteria;p__Proteobacteria;c__Alphaproteobacteria;o__Rhizobiales;f__Hyphomicrobiaceae;g__Rhodoplanes
k__Bacteria;p__Proteobacteria;c__Alphaproteobacteria;o__Rhizobiales;f__Methylobacteriaceae;g__
k__Bacteria;p__Proteobacteria;c__Alphaproteobacteria;o__Rhizobiales;f__Phyllobacteriaceae;g__
k__Bacteria;p__Proteobacteria;c__Alphaproteobacteria;o__Rhizobiales;f__Phyllobacteriaceae;g__Mesorhizobium
k__Bacteria;p__Proteobacteria;c__Alphaproteobacteria;o__Rhodospirillales;f__Acetobacteraceae;g__
k__Bacteria;p__Proteobacteria;c__Alphaproteobacteria;o__Rhodospirillales;f__Rhodospirillaceae;g__
k__Bacteria;p__Proteobacteria;c__Alphaproteobacteria;o__Rickettsiales;f__Rickettsiaceae;g__Wolbachia
k__Bacteria;p__Proteobacteria;c__Alphaproteobacteria;o__Rickettsiales;f__mitochondria;g__Victoria
k__Bacteria;p__Proteobacteria;c__Alphaproteobacteria;o__Sphingomonadales;f__Erythrobacteraceae;g__
k__Bacteria;p__Proteobacteria;c__Alphaproteobacteria;o__Sphingomonadales;f__Sphingomonadaceae;g__Sphingomonas
k__Bacteria;p__Proteobacteria;c__Betaproteobacteria;o__Burkholderiales;f__Alcaligenaceae;g__Sutterella
k__Bacteria;p__Proteobacteria;c__Betaproteobacteria;o__Burkholderiales;f__Burkholderiaceae;g__Burkholderia
k__Bacteria;p__Proteobacteria;c__Betaproteobacteria;o__Burkholderiales;f__Comamonadaceae;g__
k__Bacteria;p__Proteobacteria;c__Betaproteobacteria;o__Burkholderiales;f__Comamonadaceae;g__Variovorax
k__Bacteria;p__Proteobacteria;c__Betaproteobacteria;o__Burkholderiales;f__Oxalobacteraceae;g__Herbaspirillum
k__Bacteria;p__Proteobacteria;c__Betaproteobacteria;o__Burkholderiales;f__Oxalobacteraceae;g__Janthinobacterium
k__Bacteria;p__Proteobacteria;c__Betaproteobacteria;o__Neisseriales;f__Neisseriaceae;g__
k__Bacteria;p__Proteobacteria;c__Deltaproteobacteria;o__Desulfovibrionales;f__Desulfovibrionaceae;g__
k__Bacteria;p__Proteobacteria;c__Deltaproteobacteria;o__Desulfovibrionales;f__Desulfovibrionaceae;g__Bilophila
k__Bacteria;p__Proteobacteria;c__Deltaproteobacteria;o__Desulfovibrionales;f__Desulfovibrionaceae;g__Desulfovibrio
k__Bacteria;p__Proteobacteria;c__Deltaproteobacteria;o__Syntrophobacterales;f__Syntrophobacteraceae;g__
k__Bacteria;p__Proteobacteria;c__Epsilonproteobacteria;o__Campylobacterales;f__Helicobacteraceae;g__
k__Bacteria;p__Proteobacteria;c__Epsilonproteobacteria;o__Campylobacterales;f__Helicobacteraceae;g__Flexispira
k__Bacteria;p__Proteobacteria;c__Epsilonproteobacteria;o__Campylobacterales;f__Helicobacteraceae;g__Helicobacter
k__Bacteria;p__Proteobacteria;c__Gammaproteobacteria;o__Cardiobacteriales;f__Cardiobacteriaceae;g__Cardiobacterium
k__Bacteria;p__Proteobacteria;c__Gammaproteobacteria;o__Enterobacteriales;f__Enterobacteriaceae;g__
k__Bacteria;p__Proteobacteria;c__Gammaproteobacteria;o__Enterobacteriales;f__Enterobacteriaceae;g__Enterobacter
k__Bacteria;p__Proteobacteria;c__Gammaproteobacteria;o__Enterobacteriales;f__Enterobacteriaceae;g__Serratia
k__Bacteria;p__Proteobacteria;c__Gammaproteobacteria;o__Enterobacteriales;f__Enterobacteriaceae;g__Yersinia
k__Bacteria;p__Proteobacteria;c__Gammaproteobacteria;o__Pseudomonadales;f__Moraxellaceae;g__Acinetobacter
k__Bacteria;p__Proteobacteria;c__Gammaproteobacteria;o__Pseudomonadales;f__Pseudomonadaceae;g__Pseudomonas
k__Bacteria;p__Proteobacteria;c__Gammaproteobacteria;o__Xanthomonadales;f__Xanthomonadaceae;g__
k__Bacteria;p__TM7;c__TM7-3;o__CW040;f__F16;g__
k__Bacteria;p__Tenericutes;c__Mollicutes;o__Anaeroplasmatales;f__Anaeroplasmataceae;g__Anaeroplasma
k__Bacteria;p__Tenericutes;c__Mollicutes;o__RF39;f__;g__
k__Bacteria;p__Verrucomicrobia;c__Verrucomicrobiae;o__Verrucomicrobiales;f__Verrucomicrobiaceae;g__Akkermansia

84

www.manaraa.com
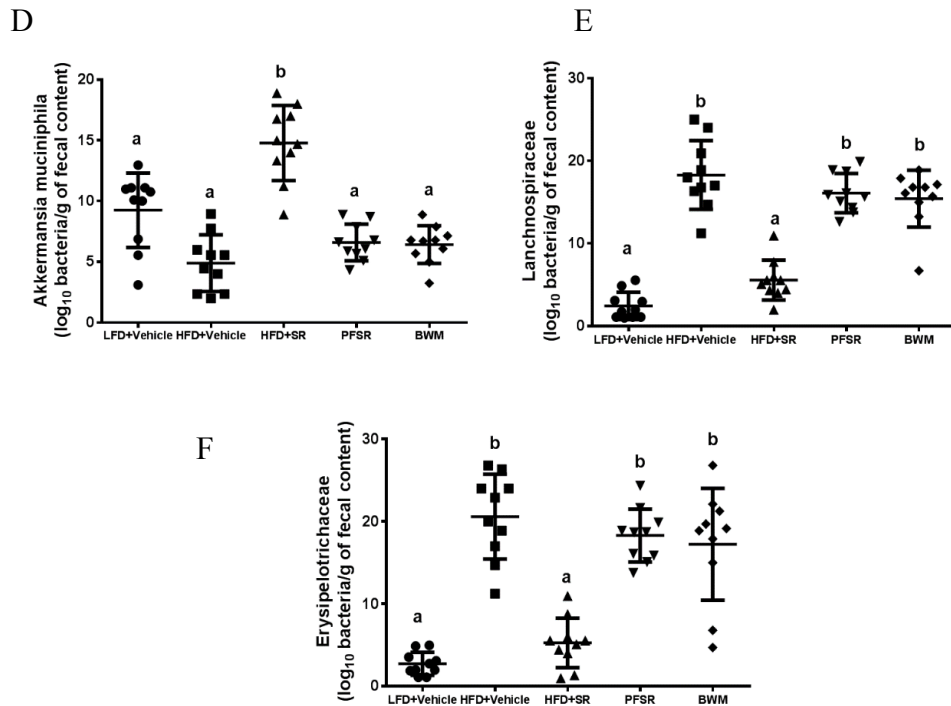
Figure 3.7

Figure 3.7 SR141716A alters gut microbiota in diet-induced obesity phenotype.
Metagenomics analysis were performed on 16S rRNA V3+V4region data, rarefied to a depth of 10,000 reads per sample. (A)Beta-diversity of the gut microbiome was evaluated by weighted UniFrac-based principle co-ordinates algorithim. The analysis was performed using the abundance matrix of genus-level OTUs in different samples, and pairwise community distances were determined with .97 similarity using the weighted UniFrac algorithm. Exceptions from study groups were observed. (B)Species richness metric based on Chao1 method was calculated. (C) Relative taxa abundance area plots for individuals from the five populations, summarized at the genus level. Individuals are represented along the horizontal axis, and relative taxa frequency is denoted by the vertical axis. (D)A. muciniphila (E) Lanchnospiraceae, (F) and Erysipelotrichaceae abundance (log10 of bacteria per g of fecal content) measured in the fecal content of mice (n = 10). Values with different superscript letters are significantly different, (P<0.01) according to post hoc ANOVA one-way statistical analysis.

85

A

	Acetic Acid	Propionic Acid	i-Butyric Acid	n-Butryic Acid	i-Valeric Acid	n-Valeric Acid	n-Caproic Acid	Heptanoic Acid
LFD+Vehicle	2.024	0.2595	0.089	0.098	0.049	0.115	0.014	0
HFD+Vehicle	1.731	0.158	0.035	0.079	0.076	0.122	0.013	0
HFD+SR	1.892	0.659	0.253	0.353	0.178	0.179	0.019	0
PFSR	1.438	0.1508	0.043	0.055	0.054	0.114	0.005	0
BWM	1.544	0.128	0.044	0.039	0.061	0.088	0	0

B

	Acetic Acid	Propionic Acid	i-Butyric Acid	n-Butryic Acid	i-Valeric Acid	n-Valeric Acid	n-Caproic Acid	Heptanoic Acid
LFD+Vehicle	1.465528698	0.142257724	0.023828076	0.13239027	0.030033823	0.064231342	0	0
HFD+Vehicle	0.611271599	0.073255029	0.012503673	0.052238371	0.020995438	0.073576893	0	0
HFD+SR	0.999584304	0.239428204	0.082373749	0.174153533	0.099785328	0.096772047	0	0
PFSR	0.995289106	0.105999612	0.022160348	0.117166004	0.028535283	0.069207669	0	0

Figure 3.8

Figure 3.8 SR141716A treatment changes gut microbiome and its SCFAs metabolites which mimics anti-inflammatory status in diet-induced obesity phenotype. (A-B) Gas chromatography with flame Ionization Detector(GC-FID) quantification of SCFA levels in the cecal and fecal contents. Representative data are from triplicate experiments. Vertical bars represent mean ± SD. ANOVA/Tukey *$p < 0.05$; **$p < 0.01$; ***$p < 0.001$

86

A

B
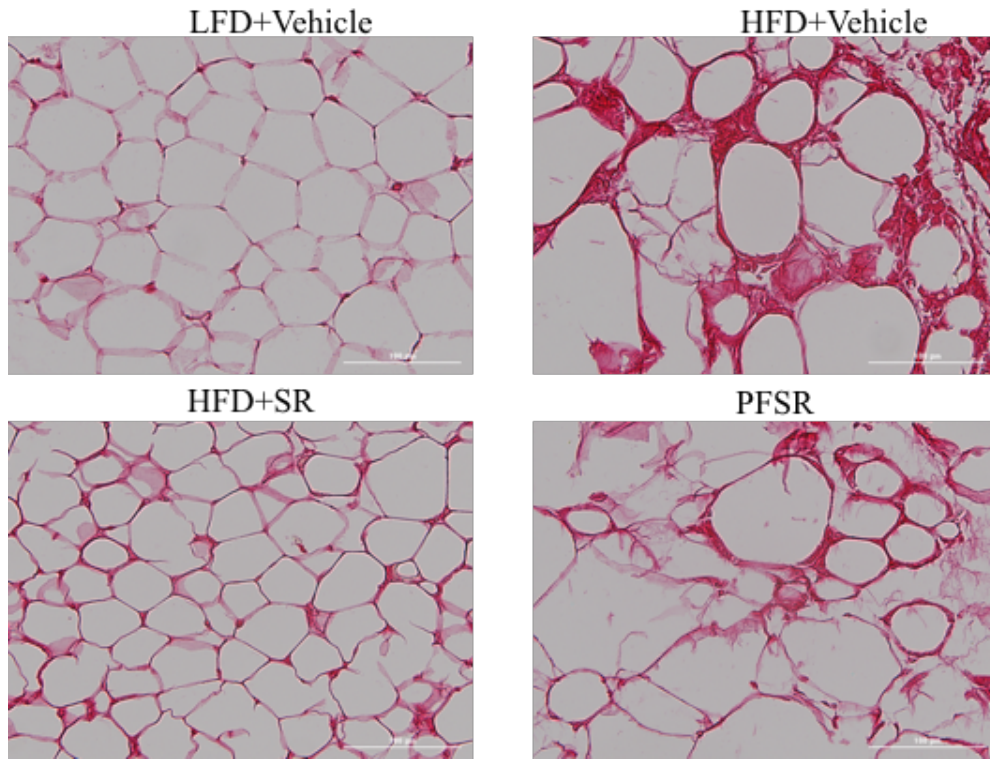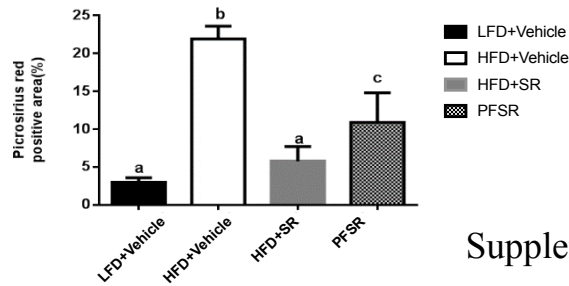
Supplementary Figure 3.1

Supplementary Figure 3.1 SR1417161A significantly reduced the interstitial fibrosis of adipose tissue in diet-induced obesity phenotype. (A)Representative picrosirius red images that were used for quantification of fibrosis area in adipose tissue of individuals (LFD+Vehicle *n=6*, HFD+Vehicle *n=10,* SR *n=9*, and PFSR *n=7*). (B)The percentage area for picrosirius red-positive was quantified by converting the image to RGB (Red, Green, Blue) stack image and setting the lower and upper threshold values into the feature of interest and background in Image J software, NIH. Data are shown as means $\pm$ SD. Data with different superscript letters are significantly different ($P<0.05$) according to post hoc ANOVA one-way statistical analysis.
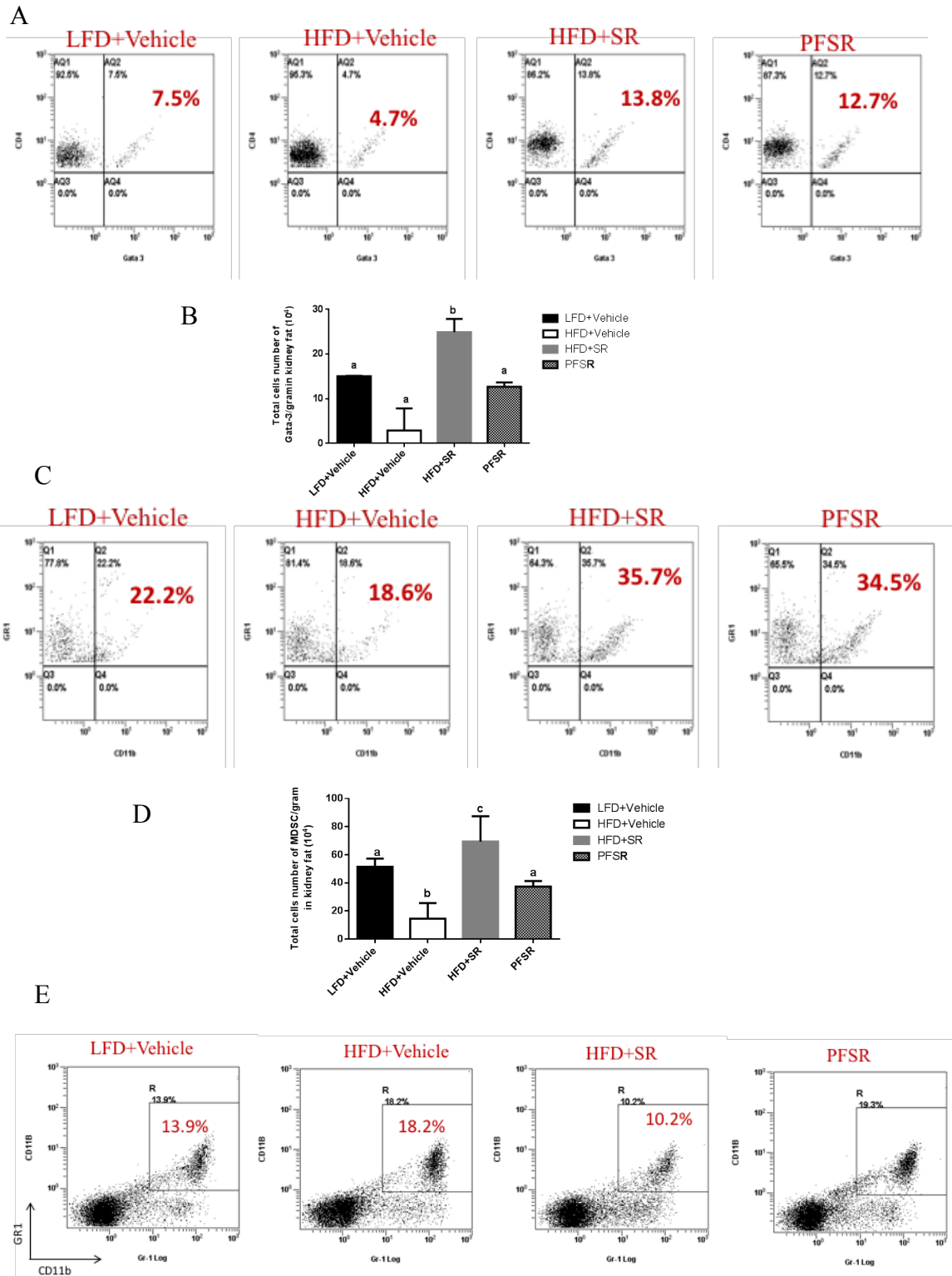
Supplementary Figure 3.2

Supplementary Figure 3.2 SR141716A improves anti-inflammatory Th2 subset and Myeloid Derived Suppressive Cells (MDSCs) in diet-induced obesity phenotype. (A,B)Kidney fat was isolated from 10 mice in each group. The ratio and total cell number of Gata-3+ CD4+ cells (Th2) in stromal vascular fraction of kidney fat was increased with SR141716A treatment in DIO mice (HFD+SR) (13.8%) when compared to vehicle-treated DIO mice HFD+Vehicle (4.7%). (C,D) The ratio and total cell number of GR-1+ and CD11b+ cells (MDSC) in stromal vascular fraction of kidney fat were increased with SR141716A treatment in DIO mice (HFD+SR) (35.7%) when compared to vehicle-treated DIO mice (HFD+Vehicle)(18.6%) Data are shown as means ± SD. Data with different superscript letters are significantly different ($P<0.05$) according to post hoc ANOVA one-way statistical analysis. (E) The ratio of MDSC was assessed by flow cytometry in blood from different groups. The percentage of circulating GR-1+ and CD11b+ cells (MDSC) were decreased with SR141716A treatment in DIO mice (10.2%) when compared to vehicle-treated DIO HFD+Vehicle mice (18.2%).

Table 3.1 SR141716A treatment improves the impaired CBC in diet-induced obesity phenotype. Whole blood was collected from posterior vena cava and subjected to the differential hematological analyzer. (LFD+Vehicle *n=8*, HFD+Vehicle *n=9,* HFD+SR *n=10*, and PFSR *n=6*). Data are shown as means ± SD. Unpaired- Ttest was performed between HFD+SR and HFD+Vehicle group. Statistical significance was set as value of *p* < 0.05.

Variable	LFD+Vehicle	HFD+Vehicle	HFD+SR	PFSR
WBC 10^9/l	10.195±5.84326	12.6044444±6.1765729	10.536±5.69566151*	8.45833333±1.86880086
LYM 10^9/l	5.795±4.732966	8.46333333±3.58347248	6.838±3.9607821	7.245±1.53385462
MON 10^9/l	0.48±.684377	0.48222222±.48625553	0.344±.46159626	0.17166667±.09495613
NEU 10^9/l	3.92±1.46659	5.6566667±3.1812576	3.357±2.14668763*	1.04666667±.34621766
RBC 10^12/l	10.06125±.95038996	10.9266666666667±.63517714	10.41±1.00162091	10.415±.4429334
HGB g/dl	14.775±.76298287	15.2666666666667±.61032778	14.24±.962886609*	14.6833333333333±.49564772
HCT %	41.3575±4.16817106	45.1033333333333±2.81388077	41.931±4.14813064*	42.735±1.56113741
MCV fl	41.125±.991031209	41.2222222222222±.833333333	40.3±1.059349905	41±.632455532
MCH pg	14.775±1.41698876	14±.70887234	13.78±1.55763353	14.1±.4
MCHC g/dl	36±3.91407716	33.9111111111111±1.70985704	34.25±3.87305507	34.3333333333333±.46332134
RDWs fl	30.9375±1.23512579	31.5111111111111±1.08448657	31.55±1.74626586	30.8666666666667±1.45418935
RDWc %	18.725±.68400084	19.0666666666667±.4	19.56±1.11773581	18.7333333333333±.69474216
PLT 10^9/l	594±385.49345	431.222222222222±293.1850004	764.857142857143±542.8159383	773.166666666667±206.110084
MPV fl	5.7875±2.35519942	6.72222222222222±.56075346	6.97142857142857±.62373682	6.38333333333333±.38166303
PDWs fl	8.8±1	8.63333333333333±1.25830574	9±1.99749844	6.55±.27386128

Table 3.2 SR141716A treatment improves the impaired metabolic parameters in diet-induced obesity phenotype. Plasma was assessed for fasting (5 hr) concentrations of glucose, insulin, total cholesterol (TC), HDL-C, LDL-C, and triglycerides prior to the SR141617A treatment at week 12 of diet and at the end of the SR141716A treatment course at week 16. Insulin resistance was estimated by HOMA index as follows: insulin resistance index = fasting insulin (μU/ml) x fasting glucose (mmol/l)/22.5

Plasma analyses after 4-weeks treatment with SR141716A(10mg.kg^{-1}.day-1) in dietary obese mice				
Variables	**Glucose(mmol/l)**		**Insulin (pmol/L)**	
Weeks of Diet	**Week12**	**Week 16**	**Week 12**	**Week 16**
LFD+Vehicle	12.2 ± 0.7$^{a\&}$	12.6 ± 0.2$^{a\&}$	188 ± 6 $^{a\&}$	190 ± 15 $^{a\&}$
HFD+Vehicle	14.2 ± 0.3$^{a\#}$	14.8 ± 0.2 $^{a\#}$	556 ± 25 $^{a\#}$	634± 26 $^{a\#}$
HFD+SR	14.0± 0.1$^{a\#}$	10.2 ± 0.4 $^{b\&}$	562 ± 75 $^{a\#}$	221± 46 $^{b\&}$
PFSR	13.8± 0.6$^{a\#}$	14.2 ± 0.1 $^{a\#}$	618 ± 16 $^{a\%}$	490± 18b $^{b\%}$
Variables	**HOMA (unit)**		**Total Cholesterol(mmol/l)**	
Weeks of Diet	**Week 12**	**Week 16**	**Week 12**	**Week 16**
LFD+Vehicle	10.19 ± 0.7 $^{a\&}$	10.64 ± 0.4 $^{a\&}$	4.01 ± 0.01 $^{a\&}$	3.99 ± 0.03 $^{a\&}$
HFD+Vehicle	35.08 ± 0.5 $^{a\#}$	41.7 ± 0.5 $^{b\#}$	5.41 ± 0.03 $^{a\#}$	6.09 ± 0.02 $^{b\#}$
HFD+SR	34.96 ± 0.8 $^{a\#}$	10.01 ± 0.9 $^{b\&}$	5.07± 0.01 $^{a\#}$	3.57 ± 0.01 $^{b\&}$
PFSR	37.9 ± 1.1 $^{a\#}$	30.92 ± 0.4 $^{b\#\%}$	5.98 ± 0.04 $^{a\#}$	5.88 ± 0.05 $^{a\#}$
Variables	**LDL-C (mmol/l)**		**HDL-C (mmol/l)**	
Weeks of Diet	**Week 12**	**Week 16**	**Week 12**	**Week 16**
LFD+Vehicle	0.96 ± 0.02 $^{a\&}$	0.98 ± 0.07 $^{a\#}$	1.45 ± 0.01 $^{a\&}$	1.52 ± 0.02 $^{a\&}$
HFD+Vehicle	1.83 ± 0.01 $^{a\#}$	1.92 ± 0.03 $^{a\&}$	1.28± 0.09 $^{a\#}$	1.27± 0.02 $^{a\#}$
HFD+SR	1.80 ± 0.06 $^{a\#}$	1.03 ± 0.02 $^{b\#}$	1.34 ± 0.01 $^{a\&\#}$	1.83± 0.09 $^{b\&\%}$
PFSR	1.90 ± 0.01 $^{a\#}$	1.73 ± 0.06 $^{a\&}$	1.25 ± 0.07 $^{a\#}$	1.27 ± 0.04 $^{a\#}$
Variables	**TC/HDL-C ratio (unit)**		**Triglycerides (mmol/l)**	
Weeks of Diet	**Week 12**	**Week 16**	**Week 12**	**Week 16**
LFD+Vehicle	2.6 ± 0.3 $^{a\&}$	2.6 ± 0.2 $^{a\&}$	0.8 ± 0.03 $^{a\&}$	0.8 ± 0.05 $^{a\&}$
HFD+Vehicle	4.2 ± 0.2 $^{a\#}$	4.7 ± 0.9 $^{a\#}$	0.9 ± 0.01 $^{a\#}$	1.02 ± 0.01 $^{b\#}$
HFD+SR	3.7 ± 0.8 $^{a\#}$	1.9 ± 0.5 $^{b\&}$	0.9 ± 0.05 $^{a\#}$	0.9 ± 0.09 $^{a\#\&}$
PFSR	4.7 ± 0.8 $^{a\#}$	4.6 ± 0.2 $^{a\#}$	0.8 ± 0.04 $^{a\&}$	0.9 ± 0.03 $^{b\&\#}$
Values are means ± SD (n=10, except HFD+SR n=9).values with different superscripted letter (a,b) differ significantly over time within the group ($P<0.05$) . Values with diffeerent supercripted symbol (&#%) differ significantly among groups within the given week ($P<0.05$)				
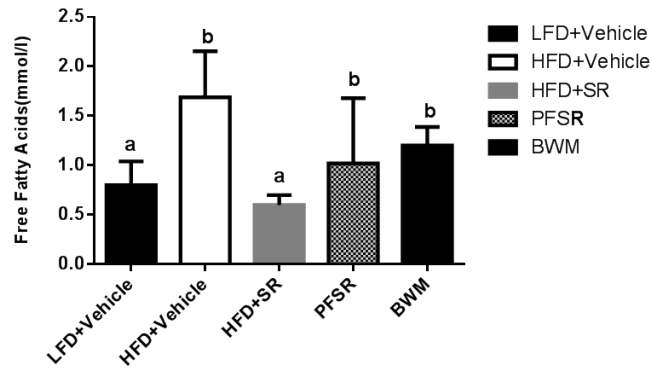
Supplementary Figure 3.3

Supplementary figure 3.3 SR141716A treatment reversed the increase in Free Fatty Acids in diet-induced obesity phenotype. FFA concentrations were measured in serum. Data represent means ± SD from (LFD+Vehicle *n=5*, HFD+Vehicle *n=5,* SR *n=6*, PFSR *n=5*, and BWM *n=6*). Data with different superscript letters are significantly different (*P*<0.05) according to post hoc ANOVA one-way statistical analysis.

91

Table 3.3 Composition of Chimeras and Operational Taxonomical Units (OTUs) in 16srRNA sequencing. The percentage of the chimeras in each fastq files of individual samples and total counts of OTUs was obtained from Qiime software. Number of samples: 25, Number of observations: 17245, Total count: 8220204, Table density (fraction of non-zero values): 0.219 ,Min counts: 220662.0, Max counts: 601577.0, Median of counts: 308574.000, Mean of counts: 328808.160 with Std. dev.:79010.459

Sample ID:	OUT Counts	Chimeras Count	Chimeras%
LFD21	338281	39130	10.13%
LFD22	308574	34101	9.77%
LFD23	397221	45346	10.04%
LFD24	330399	38243	10.20%
LFD25	296668	31517	9.45%
HFD21	283187	31372	9.84%
HFD22	282486	28988	9.18%
HFD23	313719	33506	9.52%
HFD24	601577	64986	9.60%
HFD25	350915	41863	10.52%
SR21	272991	28203	9.23%
SR22	401397	52916	11.44%
SR23	295770	30971	9.35%
SR24	443454	47524	9.54%
SR25	407996	39303	8.67%
PFSR21	235337	25512	9.61%
PFSR22	290634	34094	10.26%
PFSR23	220662	26089	10.33%
PFSR24	408989	47556	10.19%
PFSR25	280616	31358	9.91%
BW1	300380	34993	10.22%
BW2	322817	35825	9.84%
BW3	241940	27361	10.01%
BW4	314008	37185	10.44%
BW5	280186	31751	9.98%
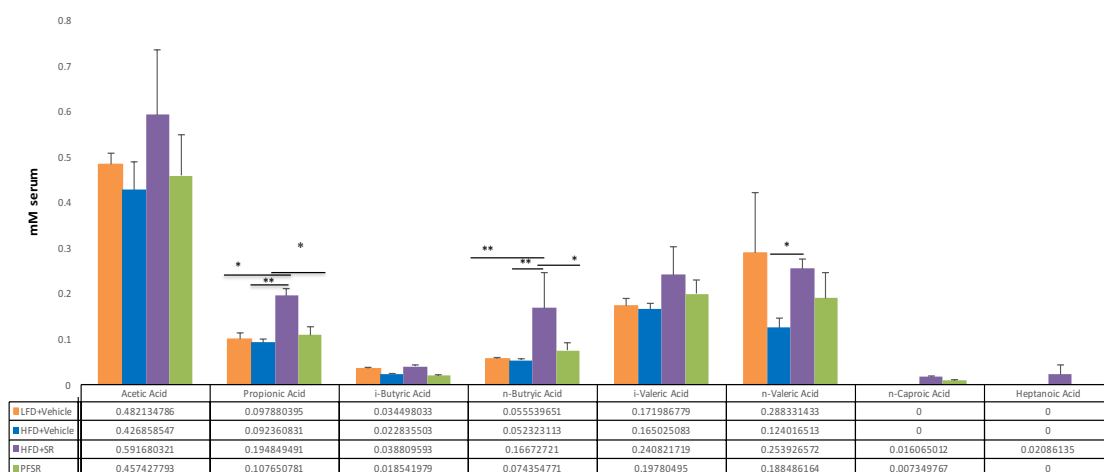
Supplementary Figure 3.4

Supplementary Figure3.4 SR141716A treatment alters Short Chain Fatty Acids (SCFAs) systematically. Gas chromatography with flame Ionization Detector(GC-FID) quantification of SCFA levels in serum. Representative data are from triplicate experiments. Vertical bars represent mean ± SD. ANOVA/Tukey $*p < 0.05$; $**p < 0.01$; $***p < 0.001$

Table 3.4 Primers sequences. The forward and reverse sequences of each primer in the current study is provided.

FASN	TTCCAAGACGAAAATGATGC	AATTGTGGGATCAGGAGAGC
CPT1a	AGACCGTGAGGAACTCAAACCTAT	TGAAGAGTCGCTCCCACT
Pgc1a	AGCCGTGACCACTGACAACGAG	GCTGCATGGTTCTGAGTGCTAAG
Ppara	CAACGGCGTCGAAGACAAA	TGACGGTCTCCACGGACAT
Acox1	CTATGGGATCAGCCAGAAAGG	AGTCAAAGGCATCCACCAAAG
Acc1	TGTTGAGACGCTGGTTTGTAGAA	GGTCCTTATTATTGTCCCAGACGTA
Cebpa	GAGCCGAGATAAAGCCAAACA	GCGCAGGCGGTCATTG
G6pc	AGGAAGGATGGAGGAAGGAA	TGGAACCAGATGGGAAAGAG
A.muciniphila	CAGCACGTGAAGGTGGGGAC	CCTTGCGGTTGGCTTCAGAT
Erysipelotrichaceae	TCACTT TGAACCCGGCCTAT	GCAGATCTTGAC ACGCTC AG
Lanchnospiraceae	CCGCATAAGCGCACAGC	TCGCTTCCCTTTGTT TACGC

CHAPTER IV: ROLE OF MICRORNA IN THE REGULATION OF NETRIN-1-MEDIATED MACROPHAGE MIGRATION AND POLARIZATION IN ADIPOSE TISSUE THROUGH AGAP-2 INTERACTION WITH UNC5B

4.1 INTRODUCTION

The growing incidence of obesity in the last 25 years defines it as an epidemic; with estimates upwards of 1.45 billion overweight adults in the world, of which approximately 500 million are obese[256]. Moreover, a maintenance of childhood obesity at 16% prevalence from 2006-2010 and a significant increase in obesity prevalence over a 12 year period in males aged 2-19 years was observed[257].

Chronic low-grade, systematic inflammation associated with obesity plays a major role in the development of various chronic disease states, including type 2 diabetes, metabolic syndrome and atherosclerotic cardiovascular disease which contribute to high rates of mortality and morbidity[258]. Stromovascular fraction of adipose tissue is aggregated with immune cells during obesity[259]. In particular, with intense migration of Macrophages (Mφ) in adipose tissue, Adipose Tissue Macrophages (ATMs) have been shown to be integral to the obesity-triggered inflammation in adipose tissue [260,261,262], and their recruitment to adipose tissue correlates with the production of pro-inflammatory

molecules , including tumor necrosis factor-α (TNF-α)[263], interleukin-1β (IL-1β) and IL-6 [264,265] that potentiate insulin resistance [266]. Macrophages are phagocytic cells which show incredible heterogeneity in phenotype and function, as local milieu factors determine their activation state and subsequent properties. Mϕs are thought to be activated in two separate pathways becoming polarized to M1 or M2 states. With over-nutrition, M1 are said to be "classically activated" mϕs induced by LPS and IFNγ that secrete pro-inflammatory cytokines (TNF-α, IL-6, IL-12) and generate nitric oxide (NO, a reactive oxygen species) via iNOS activation[267, 268]. However, "alternatively activated" mϕs or M2 that populate lean adipose tissue are activated by IL-4 and IL-13, secrete anti-inflammatory cytokines, and have upregulated arginase which opposes NO production[269.] However, studies have shown that the M1 and M2 macrophage phenotypes are not clearly defined, the key signaling molecules such as DNA methyltransferase 3b (DNMT3b) and peroxisome proliferator activated receptor-γ(PPAR-γ) deregulate ATMs polarization, inflammation and insulin insensitivity[270,271]. In addition, other studies have shown that besides the molecules which trigger the macrophages recruitment in adipose tissue, other signaling molecules such as neural guidance cue (semaphorin, ephrin and netrin families) modulate macrophages retention in adipose tissue and regulate immunometabolism[272, 273,274]. Indeed, a recent study showed inhibition of semaphorin 3E in the visceral adipose tissue of DIO mice resulted in a significant improvement in adipose tissue inflammation and subsequently insulin resistance in this model[275]. Collectively, studies on neuronal guidance cue in ATMs define them as key regulators for macrophages accumulation in adipose tissue in regard to chronic inflammation of VAT.

Weight loss is associated with beneficial effects on reducing the underlying inflammation in adipose tissue and subsequently ameliorates insulin insensitivity[276, 277]. Endocannabinoid system plays a major role in diet intake and energy balance. Over-activity of endocannabinoid system in human obesity and in animal models of genetic and diet-induced obesity has been reported[278]. Clinical studies on treatment of obesity and metabolic syndrome with cannabinoid CB1 receptors antagonist have shown greater weight loss in obese patients compared with placebo [279]. Nevertheless, the mechanistic effect of CB1 receptor antagonist on inflammation and ATMs has not been well studied. Previous studies have shown that blockade of CB1 receptors suppressed inflammation in adipose tissue of DIO mice[250, 251]. The signals controlling the beneficiary effect of the CB1 receptor antagonists on inflammation in the adipose tissue remain poorly understood, but are likely involve reduced recruitment, local macrophage death and egress of macrophage from the inflammatory site.

In the present study, utilizing a mouse model of diet- induced obesity, we uncover a key role for SR141716A, a CB1 receptor antagonist, in the retention of macrophages in the visceral adipose tissue during obesity by triggering neuroimmune guidance cue netrin-1 and its receptor Unc5b.Here we show that Netrin-1 and its receptor Unc5b in ATMs are markedly suppressed upon SR141716A treatment in DIO mice, and investigate the effect of SR141716A beyond its effect on weight loss and diet intake by conducting the pair-fed group and body weight matched control to the SR141716A treated group. Our data demonstrates that SR141716A suppressed diet intake transiently, however weight loss and reduction in fat mass was persistent and consequently the effect of CB1 receptor blockade on inflammation is independent of its effect on weight loss and diet

96

intake. Suppression of pro-inflammatory macrophages was observed in SR141716A-treated HFD-fed group followed by down regulation of Netrin-1 and Unc5b in macrophages, which results in egression of ATMs from inflammatory adipose tissue, and subsequently improvement of insulin resistance and glucose impaired metabolism.

4.2 MATERIALS AND METHODS

Animals.

16-18 weeks old male C57BL/6J mice (Jackson Laboratory, Bar Harbor, ME) were fed a HFD consisting of 60% Kcal from fat (Research Diets Incs,New Brunswick, NJ) or the control age matched fed a LFD consisting of 10% Kcal from fat (Research Diets Incs, New Brunswick, NJ). SR141716A was obtained from NIDA and administered 10µg/kg daily oral gavage in .01% Tween 80 in DI water. All mice were maintained in the pathogen free at the AAALAC-accredited animal facility at the University of South Carolina, School of Medicine (Columbia, SC). All procedures were performed according to NIH guidelines under protocols approved by the Institutional Animal Care and Use Committee.

Analytical procedures.

The fat content in the mice was analyzed by dual-energy X-ray absorptiometry (DEXA, LUNAR, Madison, WI) scanning. The mice were anesthetized and placed in the prone position on the specimen tray to allow scanning of the entire body. For food intake measurements, mice were given a defined amount of large intact food pellet weekly.

97

Food weight was measured using a balance with a precision of 0.01 g , and cages were changed. Solid food intake was corrected for any visible spillage [282]

Metabolic parameters assessment

Fasting concentrations of glucose, insulin, total cholesterol, and triglycerides was assessed at the baseline and day 27 (prior to sacrificing day). Animals were fasted for 5 hours and blood were collected from the tip of the tail. The glucose level in whole blood was measured with glucometer (Bayer Contour, MiChawaka, IN). Insulin concentration was determined in isolated plasma using Elisa kit (abcam, Cambridge, MA). Total cholesterol (Genzyme, Kent, United Kingdom), and triglycerides (Pointe Scientific, Canton, Michigan) were determined according to the manufacturer. HOMA index was calculated for insulin resistance as previously described [283].

Tissue collection

After 4 weeks of treatment, mice were sacrificed for tissue collection. Tissues were removed, weighed, and immediately snap-frozen in liquid nitrogen and stored at −80°C or fixed in 10% formalin until analysis.

Adipocyte and adipose tissue macrophage purification.

Epididymal fat pads of mice were excised and placed in gentleMACS C Tubes (MACS Miltenyi Biotec, San Diego, CA) containing digestion medium (HSBSS,2mg/ml collagenase (Sigma-Aldrich, St. Louis, MO) and 2% BSA, and followed to be homogenized by utilizing gentleMACS Dissociator (MACS Miltenyi Biotec, San Diego,

98

CA). After incubation at 37 °C for 30 min with shaking, the cell suspension was filtered through a 100-μm filter and then spun at 300g for 5 min to separate floating adipocytes from the Stromal Vascular fraction (SVF) pellet. Isolation of F4/80 cells from SVF isolates was performed by magnetic immunoaffinity isolation with anti-F40/80 antibodies conjugated to magnetic beads (10 μl per 1×10^7 cells, EasySep™ FITC Positive Selection Kit, Stem Cells Technologies, Vancouver, BC). Cells were isolated using positive selection columns before preparation of whole-cell lysates.

Real-time Quantitative RT-PCR Analysis

RNA (0.5–1 μg) was reverse-transcribed using miScript cDNA Synthesis Kit (Qiagen, Valencia, CA), and RT-PCR analysis was conducted using SsoAdvanced™ Universal SYBR® Green Supermix kit (Bio-Rad,Hercules, CA) . The primers used are listed in Supplementary Table 4. Fold change in mRNA expression was calculated using the comparative cycle method ($2^{-\Delta\Delta Ct}$).

Gene expression profiling.

1 mg of adipose tissue from either lean or obese animals was homogenized in RNA-Solv Reagent with OBI's innovative HiBind® technology reagent (Omega Bio-tek, Norcross, GA)) and total RNA isolated as we previously described[283]. RNA quality was verified by NanoDrop 2000C (Thermo Scientific, Waltham, MA). Adipose tissue RNA (0.5-1 μg) was reverse-transcribed, and quantitative RT-PCR analysis of the four families of the axonal guidance molecules, macrophages markers (iNOS, ARG-1) was performed. Data analysis was performed using ΔΔCt-based fold change calculations.

99

miRs expression profiling and analysis.

The unique expression profile of miR assessed in F4/80 cells isolated from adipose tissue by Affymetrix GeneChip miRNA 3.0 array platform. The array contains 3100 murine-specific probes from Sanger miRBase. Total RNA were 3′-end labeled with FlashTag biotin HSR hybridization technique (Genisphere, Hatfield, PA) and was carried out according to the manufacturer's instructions (Affymetrix, Santa Clara, CA). Correlation of the hybridization signal intensities of all the expressed miRs were log transformed and visualized in the form of a heatmap. Ward's method was assessed for hierarchical clustering of differentially expressed miRs. miRs QC Tool (Affymetrix Inc), a software for data summarization, Log2 transformation, normalization and quality control, was used as described previously [284].

Bioinformatics analysis.

The differentially expressed miRs' target genes were assessed by miR target prediction algorithms miRwalk (http://www.umm.uni-heidelberg.de/apps/zmf/mirwalk/), miRmap (http://mirmap.ezlab.org).To carry out an enrichment analysis of predicted target genes of miRs in biological pathways, the commercially available analysis tool Ingenuity Pathway analysis (IPA), (Mountain View, CA, USA.), was used. IPA predicts the top affected Canonical Pathways, causal connections between differentially changed miRs and their target genes, downstream effect along with their upstream regulators. The Molecular Activity Predictor (MAP) feature of IPA was performed to predict the downstream effect of the differentially expressed miRs which were overlaid to the dataset

including miRs probes, fold changes and the p Values. Gene ontology was assessed in Cytoscape platform using CluGo app [285].

ELISA assays.

Netrin-1 (USCN Life science, Houston, TX) levels were measured in the serum or cell supernatants using mouse standards according to manufacturer's guidelines.

Migration.

The migration of macrophages to CCL19 (500 ng/ml, R&D Systems) was assessed by FluroBlok permeable inserts (Corning, Tewksbury, MA) and Cytation5 imaging (BioTek, Winooski, VT). Peritoneal macrophages were harvested from the primed mice with 1ml of 3% (wt/vol) thioglycolate to elicit peritoneal exudates with macrophage number peaking on day 4. Inter-peritoneal wash performed to collect macrophages. For tracking macrophage migration towards chemoattractants, macrophages were labeled with DiIC12(3) Fluorescent Dye (Corning, Tewksbury,MA). Macrophages were treated with conditioned media from 3T3-L1 adipocytes differentiated as described [286]. Then later, Macrophages were treated either with SR141716A (10^{-6} M) or DMSO as the vehicle [287].

101

Western blot analysis.

Western blot analyses were carried out according to standard protocols with antibodies raised against netrin-1 (R&D Systems, Minneapolis, MN), γ-tubulin (Sigma-Aldrich, St. Louis, MO) was used as loading control.

Molecular docking

The structure of the Rimonabant (SR141716A) (Compound ID: 104850) compound was downloaded from the Pubchem compound database, an open repository for small molecules and their respective experimental biological activity [288]. The 3D coordinates of the X-ray Crystal Structure of Mouse Netrin-1(PDB ID: 4OVE) [289] for Netrin-1 and the crystal structure of the UNC5H2 death domain (PDB ID: 1WMG) [300] for UNC5B were retrieved from the Protein data bank [5]. Molecular docking was performed using the Autodock 4.2 [301]. Structures were analyzed using PyMOL (PyMOL Molecular Graphics System, Version 1.7.4.5 Schrödinger, LLC).

Transfection and reporter gene assay.

Bone Marrow Derived Macrophages (BMDM) were transfected with a plasmid with a Renilla luciferase (transfection efficiency control) and 3'UTR AGAP-2 (Gene Accession: NM_001301014.1UTR Length: 808 bp (-383 - 787 bp)) of a Firefly luciferase reporter gene. Cloning details was as follow: the whole plasmid size:7097, Vector: Pezx-MT06, Promoter: SV40, Antibiotic Ampicillin, 5' Cutting Site: AsiSI,

102

EcoRI, BsiWI3' , Cutting Site :   XhoI,SpeI with sequencing Primers Forward: 5'-
GATCCGCGAGATCCTGAT-3' Reverse: 5'-CCTATTGGCGTTACTATG-3'
(GeneCopeia ™ , Rockville, MD). Firefly luciferase expression is therefore suppressed
by the corresponding endogenous miR level in the cell. The day after the cell cultures
were transfected with miR-762 miRCURY LNA™ microRNA Inhibitor(5nM) (Exiqon,
Woburn, MA). Lipofectamine® RNAiMAX Transfection Reagent (ThermoFisher
Scientific, Waltham, MA) was used for delivery of oligos into the cell.

Statistical Analysis.

For the in vivo mouse experiments, 10 mice were used per experimental group,
unless otherwise specified. For in vitro assays, all experiments were performed in
triplicate. Body weight, body composition outcomes, and metabolic outcomes were
analyzed using a repeated measures two-way ANOVA. For statistical differences, one-
way ANOVA was calculated for each experiment. Tukey's post-hoc test was performed
to analyze differences between groups. A p value of ≤ 0.05 was considered statistically
significant.

4.3 RESULTS

SR141716A Effect on body weight, calorie intake, and body composition

In consistent with previous studies, blockade of cannabionoid CB1 receptors with
SR141716A resulted in transient reduction of calorie intake and persistent weight loss in

103

diet-induced obesity mice(Fig 4.1A, 4.1B) [293,294]. The acute reduction in calorie intake with SR141716A treatment in DIO phenotype was diminished by day 9 of treatment. The average of daily calorie intake in HFD+SR group became close to the average of daily calorie intake of HFD+Vehicle group through the end of the study (Fig 4.1C). Interestingly, the weight loss with SR141716A treatment in DIO phenotype (HFD+SR) was sustainable regardless of markedly high calorie intake. In order to examine the effect of SR141716A beyond its effect on diet intake, pair-feeding was performed in pair-fed to SR141716A (PFSR) group [295]. The diet intake was restricted in PFSR group to the amount of daily diet intake of HFD+SR group.

At the baseline of study, the mice were normalized and grouped based on the fat mass composition. After 4 weeks of treatment the body composition was assessed. Reduction in the fat mass and fat percentage was significant in HFD+SR group in compare to both HFD+Vehicle and PFSR groups, while the changes in lean mass was ignorable (Table 4.1). Taken together, our data suggested that blocked of cannabinoid CB1 receptors in DIO phenotype resulted in amelioration of obesity independent of its effect on calorie intake.

SR141716A effect on metabolic profile

Fasting blood glucose, Insulin, insulin resistant index (HOMAindex), cholesterol and Triglycerides was examined at the baseline and prior to the sac day on (Day 27). Our data demonstrated improvement in metabolic parameters of DIO mice with SR141716A intervention treatment (HFD+SR) in compare to vehicle-treated DIO mice

104

(HFD+Vehicle) (Fig 4.2A-4.2E). The remarkable improvement in metabolic profile in SR141716A treated-DIO mice (HFD+SR) in compare to the pair-fed (PFSR) group was the proof of independent effect of SR141716A treatment from its effect on calorie intake.

Effect of SR141716A on adipose tissue macrophages and their microRNA profile

In order to study the anti-inflammatory effect of cannabinoid CB1 receptor antagonist on adipose tissue, we examined the M1 (pro-inflammatory) and M2 (Anti-inflammatory) macrophages profile. The lower iNOS expression along with the higher expression of Arg-1 induced the anti-inflammatory state in adipose tissue of DIO mice following SR141716A intervention treatment. Previously we have assessed the comprehensive cytokinesis both systematically and locally in DIO phenotype following treatment with SR141716A. Our study demonstrated the shift from M1 macrophages to the anti-inflammatory M2 macrophages following SR141716A treatment. Induction of anti-inflammatory state in SR141716A-treated DIO mice was constant in our study. In order to a have better understanding in underlying mechanism in attenuation of inflammation, we performed high throughput analysis of microRNA profile in adipose tissue macrophages.

For the first time we isolated the total RNA from the infiltrated macrophages in adipose tissue. The F4/80 cells were isolated from the stromal vascular fraction of adipose tissue in different groups of the study. The heatmap from the microRNA (miR) microarray expression data revealed noticeable differences in fold change intensities between the different groups (Fig 4.3A). Approximately 5.7% of miRs were either over-

expressed (36) or under-expressed (141) greater than or equal to 2 fold-change following

SR141716A treatment in DIO (HFD+SR) group in compare to vehicle-treated DIO

(HFD+Vehicle) group, while 6.09% of miRs were significantly changed in SR141716A-

treated DIO (HFD+SR) group in compare to its pair-fed (PFSR) group (164 up-regulated,

25 down-regulated) (Fig 4.3B,4.3C).

On further analysis we identified the targeted gene ontology of dysregulated miRs

using Cytoscape analysis module. Regulation of immune system processes was the main

effected pathway following SR141716A treatment in DIO phenotype (Fig 4.3D). To have

a better understanding, we performed further analysis using Ingenuity Systems IPA. The

interaction between miRs and their targeted gene following SR141716A treatment in

DIO phenotype demonstrated distinctive changes in the miR profile which skews the

adipose tissue macrophage balance to more anti-inflammatory macrophages

(M2,Arginase +) (Fig 4.3E)

Independent effect of SR141716A from diet restriction on miR profile

In order to investigate the effect of SR141716A on miR profile independent of its

effect on calorie restriction, the overlaid of the altered miR following SR141716A with

altered miR in pair-fed group were selected. Dual color bar graph and Pearson correlation

of altered miR in SR+HFD group (Log2 fold change of HFD+SR in comparison with

HFD+Vehicle) and PFSR group (Log2 fold change of HFD+SR in comparison with

PFSR), summarized the selected altered miR in HFD+SR group independent of its effect

on diet restriction (Fig 4.4A,4.4B). Interestingly, we uncovered the novel role of the

altered miR in induction of anti-inflammatory M2 macrophages by targeting the M2

related transcription factors (STAT3, STAT6, LCN2, KLF4, PPARg, SIRT1) using Ingenuity Systems IPA (Fig 4.4C). The list of corresponding targets and miR, along with their algorithm has been summarized (Table 4.2). More interestingly, for the first time we uncovered that most of the miR members of miR-466 family has been down-regulated following SR141716A treatment regardless of calorie intake. miR-466 family mimic anti-inflammatory state in adipose tissue by targeting the anti-inflammatory M2 macrophages transcription factors such as KLF4, and STAT6. RT-PCR for miR-466 family from the ATMs validated their down-regulation following SR141716A treatment (Supplementary fig 4.1A).

In order to validate the effect of miR-466 family in induction of M2 phenotype in ATMs, peritoneal macrophages were isolated following thyogicolate ip. injection. Macrophages were then cultured in conditioned media from differentiated 3T3-L1cells to adipocytes following transfection with miR-466i and miR-466f LNA [TM] power inhibitors. KLF4 and STAT6, the transcription factors of M2 macrophages, were significantly over-expressed following miR-466 inhibition (Supplementary Fif 4.1B). Thus, intervention treatment of DIO mice with SR141716A (Cannabinoid CB1 receptor antagonist) potentially restore the balance of M1 and M2 macrophages in adipose tissue.

SR141716A ameliorates ATM retention in adipose tissue

The recent studies demonstrated the potential role of the neuroimmune guidance cue Netrin-1 in promoting the defective migration of ATMs in obese phenotype [274]. Higher expression of Netrin-1 in ATMs of obese phenotype, and its interaction with Unc5b receptor resulted in ATMs retention in adipose tissue and subsequently chronic

inflammation followed by insulin resistance. Previously we demonstrated the significant less frequency and number of pro-inflammatory M1 macrophages in adipose tissue of HFD+SR treated group in compare to HFD+Vehicle group. Interestingly, we uncovered the unknown effect of SR141716A in attenuation of chronic inflammation in adipose tissue, by effecting Netrin-1 and its receptor Unc5b in ATMs. The level expression of Netrin-1 at both protein and transcription level was significantly reduced following SR141716A treatment in DIO (HFD+SR) mice in compare to vehicle-treated DIO (HFD+Vehicle) mice (Fig 4.5A, 4.5B). Subsequently, Unc5b was down-regulated in HFD+SR group in compare to HFD+Vehcile group (Fig 4.5C). Systematic changes in Netrin-1 was assessed in serum of DIO mice either treated with SR141716A or vehicle as well as age-matched LFD group. The similar level of Netrin-1 was detected in all the groups (Supplementary Fig 4.2A). Netrin-1 concentration in supernatant of the cultured BMDM in conditioned media from differentiated 3T3-L1 cells to adipocytes, revealed that treatment with SR141716A significantly reduced the Netrin-1 level in compare to vehicle treated BMDM (Supplementary Fig 4.2B). Relative expression of the Netrin family and its corresponding was examined in LFD+Vehicle, HFD+Vehicle ,and HFD+SR groups (Supplementary table 4.2)

Herein, for the first time we revealed the molecular mechanistic effect of SR141716A on macrophage retention in adipose tissue via AGAP-2, a negative regulator of Unc5b, through altered profile of miRNA. Filtering the Ingenuity Systems IPA modules to the neuroimmune guidance cue canonical pathways, demonstrated the novel series of miR in targeting upstream negative regulator of Unc5b. Assessing the down-stream effect of the interaction of AGAP-2 and altered miR following SR141716A

treatment in ATMs with MAP (Molecular Activation Predictor) module in IPA, revealed distinctive down-regulation of Unc5b in ATMs following SR141716A (Fig 4.5D).

In order to validate the direct interaction of miR-762 and Unc5b, treated Bone Marrow Derived Macrophages (BMDM) with conditioned media from differentiated 3T3-L1into adipocytes, were transfected with a plasmid with a Renilla luciferase (transfection efficiency control) and 3'UTR AGAP-2 of a Firefly luciferase reporter gene. Firefly luciferase expression is therefore; suppressed by the corresponding endogenous microRNA level in the cell. The day after the cell cultures were transfected with miR-762 miRCURY LNA™ microRNA Inhibitor(5nM). Higher activity of the reporter gene demonstrated the direct interaction of AGAP-2 and miR-762 (Fig 4.5E)

Interactions of SR141716A with Netrin-1 and UNC5B

Results from molecular docking of SR141716A with Netrin-1 showed that SR141716A show polar interaction with the SER206 present in the Netrin-1 N-terminal domain VI (Fig 4.6B and 4.6C) with a binding energy of -7.13 kcal/mol and inhibition constant (Ki) of 5.94 µM. Further, results from molecular docking of SR141716A with Unc5b death domain showed that SR141716A has a polar interaction with the LEU927 (Fig 4.6E, 4.6F and 4.6G) with a binding energy of -7.55 kcal/mol and Ki of 2.9 µM

SR141716A inhibits macrophage retention in adipose tissue

Recently it has been reported that over-secretion of netrin-1 from ATMs inhibits their egress from the adipose tissue and subsequently causes low-grade chronic inflammation which leads to metabolic dysfunction [274]. Therefore; we hypothesized that

SR141716A inhibits ATMs retention in visceral adipose tissue by promoting macrophage emigration from the adipose tissue. To test this, we isolated peritoneal macrophages from thioglycolate stimulated mice, and cultured them in the presence of conditioned media from differentiated 3T3-L1 cells into adipocytes. The peritoneal macrophages were treated either with SR141716A or DMSO as a vehicle. Then after, their migration rate towards CCL19 was measured. CCL19 is the main chemokine which is implicated in emigration of tissue macrophages towards draining lymph node. Notably, SR141716A-treated macrophages exhibit higher migration to CCL19 than DMSO-treated macrophages (Fig 4.7A), though the level expression of CCL19 receptor Ccr7 was equivalent in both groups (Fig 4.7B). According to these data, we postulated that SR141716 attenuates the over-secretion of Netrin-1 from ATMs in obese phenotype, and potentially promotes their emigration from adipose tissue, which leads to amendment of chronic inflammation in adipose tissue, and subsequently ameliorates the associated-metabolic dysfunction.

4.4 DISCUSSION

In consistent with previous studies, our study confirmed the beneficial effect of cannabinoind CB1 receptor antagonist, specifically SR141716A, as an interventional treatment in obese phenotype [296,297,298,299]. The transient reduction in calorie intake and sustained shrinkage of the fat mass, following SR141716A treatment, was demonstrated in our study and previous studies [295]. Furthermore, previously we discovered the anti-inflammatory effect of SR141716A treatment both systematically (serum) and locally

(colon, adipose tissue) in DIO phenotype. We revealed the beneficial effect of SR141716A on chronic inflammation and metabolic dysfunction in DIO phenotype, beyond its effect on restriction of calorie intake, by conducting the pair-feeding to SR141716A control. The clear link between between ATM retention, sustained chronic inflammation, and metabolic dysfunction within DIO phenotype has been well-established [300-307]. Herein, in continuation with our earlier study, we demonstrated the skew in ATMs population towards less pro-inflammatory M1 macrophages following SR141716A treatment in DIO phenotype.

The direct molecular mechanism of SR141716A, in regulating the resolution of inflammation in adipose tissue remain elusive, but is likely to comprise reduced retention, efferocytosis and macrophage death, as well as alteration in ATMs polarization. Our results uncovered a key role for dysregulated miR in ATMs following SR141716A in mediating anti-inflammatory state in adipose tissue of DIO phenotype. Notably, we identified down-regulation of miR family, miR-466 following SR141716A treatment (HFD+SR) in compare to vehicle treated DIO mice (HFD+Vehicle). miR, negative regulators of gene expression, regulates 90% of gene function including different pathways. The main target genes of the miR-466 family are KLF4 and STAT6. Previous study revealed the key role of Krüppel-like factor 4 (KLF4) in regulating macrophage polarization [308,309]. Furthermore, the loss of the function study of KLF4 in mice bearing myeloid-specific deletion of KLF4 (LysMCre/Cre*Klf4fl/fl*, designated Mye-KO) exaggerated DIO phenotype and metabolic dysfunction (glucose intolerance and insulin resistance) [310]. Interestingly, our data suggested that dysregulated family of miR-466 following SR141716A treatment was involved in the cooperative interaction of KLF4

111

and STAT6 in polarization of M2 macrophages. The effect of SR141716A on miR-466 family was beyond its effect on calorie intake.

Furthermore, we identified the unique interaction between altered miR in HFD+SR group and molecules involved in neuroimmune guidance cue pathway. However; for the first time our data uncovered that therapeutic properties of SR141716A, in attenuation of adipose tissue inflammation, is implicated in targeting Netrin-1 and its receptor Unc5b in ATMs. Recent study demonstrated the novel role of neuroimmune guidancecue, Netrin-1 and its receptor Unc5b in regulating the chemotaxis behavior of ATMs [274]. Indeed, less accumulation of ATMs in adipose tissue of HFD-fed Ntn1 [-/-] mice was identified in compare to HFD-fed wild type mice. The key regulatory role of Netrin-1 in leukocytes transmigration into tissues (intestine, kidney ,and atherosclerosis plaques) was defined earlier [311,312,313]. Indeed, abundant expression of Netrin-1 in residual macrophages of atherosclerotic plaques, exacerbate the disease state by attracting more macrophages to the site of inflammation [314]. Additionally; higher expression of Netrin-1 in endothelial cells of Apoe [-/-] , and Ldlr [-/-] mice ameliorates atherosclerosis by inhibiting the leukocyte recruitment [315]. Thus, conditional deletion of Netrin-1 and Unc5b in macrophages is desired to eliminate the off target effect of Netrin-1 deletion in other cells such as endothelial and epithelial. Outstandingly, SR141716A can be considered as an effective potential therapy in attenuation of chronic low-grade inflammation in adipose tissue, by targeting Netrin-1 and Unc5b exclusively in macrophages. Further investigation is required to identify and cover all the potential off targets of SR141716A therapy entirely.

Recently, the key functional role of Netrin-1 as the monocyte chemoattractant signals identified by monitoring the migration pattern of macrophages into and out of atherosclerotic plaques as well as adipose tissue of DIO phenotype [316,317]. Utilizing the fluorescent microspheres monocyte labeling technique in HFD-fed Ntn1^{-/-} mice, demonstrated less retention of macrophages in adipose tissue and more emigration of them into drainage lymph node (Mesynteirc lymph node) [274]. We demonstrated herein that cultured peritoneal macrophages in harvested medium from 3T3-L1 adipocytes, show higher migration to CCL19 in presence of SR141716A in compare to DMSO, despite equivalent expression of Ccr7 (CCL19 receptor). Therefore; we hypothesized that Netrin-1 in ATMs potentially was affected following SR141716A treatment, and subsequently leads to lesser frequency of macrophages in adipose tissue.

Although the implication of Netrin-1 in ATMs retention has been uncovered, but the underlying mechanism remain poorly defined. Herein, for the first time we identified the key role of AGAP-2, as the negative regulator of Unc5b in ATMs. Earlier the direct association of AGAP-2 and Unc5b in cancer cell line in a P53 dependent manner was identified [318]. The over-expressed AGAP-2 fades Unc5b expression, inversely knocked down AGAP-2 intensifies Unc5b expression. Notably, you uncovered the role of miR-762 in regulating AGAP-2 and the down-stream effect is ruling the association of Netrin-1 and Unc5b in ATMs.

Netrin-1 is an approximately 600 residue molecule (Uniprot ID: O09118) comprising of an N-terminal domain VI, three laminin-type epidermal growth factor (LE) repeats (V-1, V-2, and V-3) and a positively charged C-terminal domain [34](Figure 6a). Netrin-1 is known to show its activity through its main receptors Deleted in Colorectal

113

Carcinoma (DCC) and UNC5-homolog (UNC5H, i.e., UNC5A, UNC5B, UNC5C, UNC5D, or UNC5H1-H4) [319]. These receptors upon binding to netrin-1 induce signals leading to the activation of MAPK or PI3K proteins [320,321] whereas unbound forms of these receptors trigger apoptosis [322,323]. A previous study showed that the Ig1 domain of UNC5H2 is the primary interaction domain for the V-2 domain of netrin-1[289]. Our results, showed that SR141716A treatment has a significant change in the protein or mRNA levels of Netrin-1 and its receptor UNC5H2. Therefore, in order to check whether SR141716A has a role in blocking the Netrin-1 /UNC5H2 interaction by binding to the V-2 domain of netrin-1, we have performed molecular docking to search the entire surface of netrin-1 [324]. Results showed that SR141716A has polar interactions with the SER206 present in the Netrin-1 N-terminal domain VI (Figure 6c) indicating that SR141716A may not have a role in blocking the Netrin-1 /UNC5H2 interaction.

UNC5B on the other hand, is a 604 residue molecule (Uniprot ID: Q8K1S3) comprising of a transmembrane region followed by ZU5, UPA and death domain [325]. The complete three dimensional structure of UNC5B is not available and only the structure for death domain is available. Interaction analysis for SR141716A with netrin-1 showed that it is not interacting in the region of Netrin-1 /UNC5H2 interaction. Therefore, in order to predict the interacting residues on UNC5B with SR141716A we have performed docking to search the entire surface of UNC5B. Results showed that SR141716A has polar interactions with the LEU927 of the UNC5B death domain (Figure 6g). Further, these molecular docking analyses showed that UNC5B death domain has a lowest binding energy (-7.55 kcal/mol) indicating that it has a high binding affinity for SR141716A compared to Netrin-1 (-7.13 kcal/mol). The study provides an insight into

114

the role of SR141716A in the induction of activity for netrin-1, netrin-1 related receptors. However; further investigation is required for uncovering the potential effect of SR141716A on other neuronal immune guidance cue families such as Slit, Ephrin, Semaphorin and their related receptors in ATMs.

A

B

C
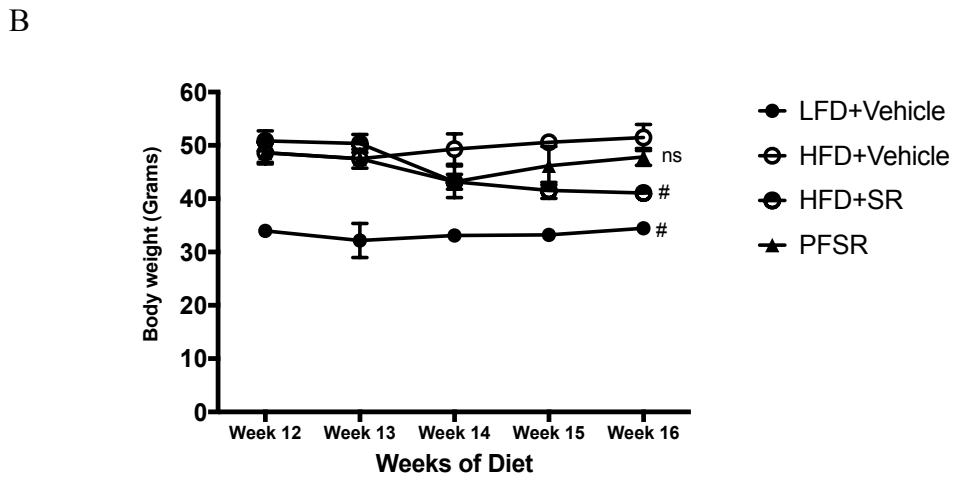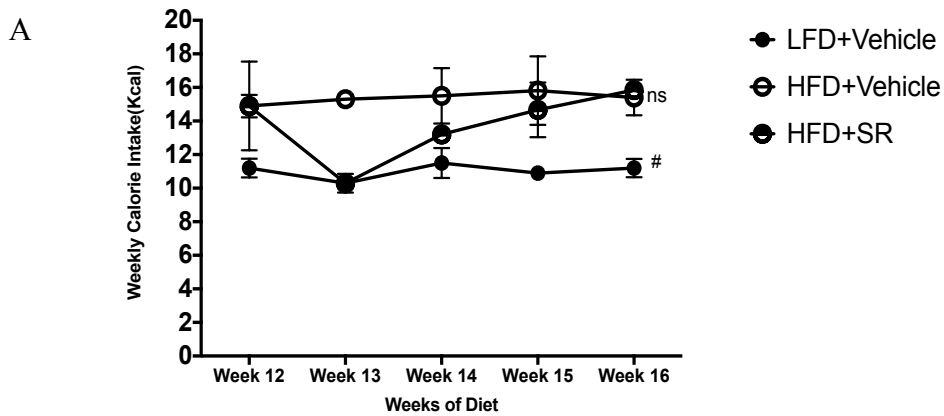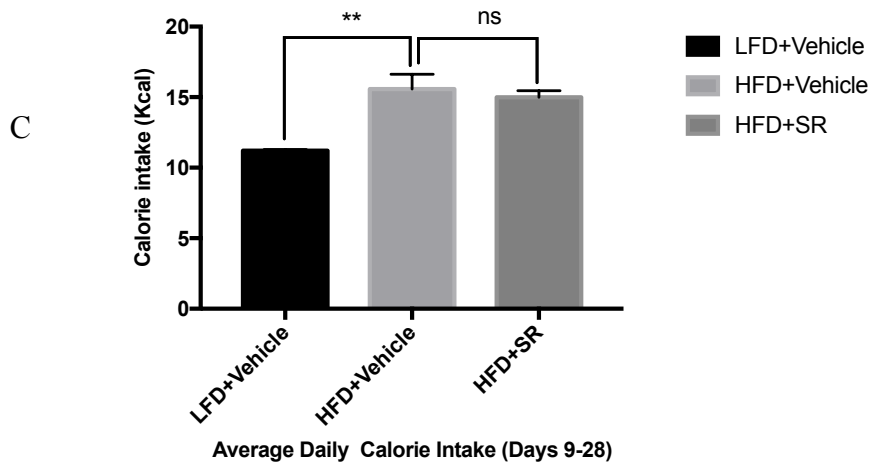
Figure 4.1

Figure 4.1 SR141716A ameliorates DIO phenotype by inducing weight loss. DIO mice were treated orally with either SR141716A (10mg/kg/day, HFD+SR) or Vehicle (.1% Tween 80) for 4 weeks and received HFD *ad libitum*. Pair-feeding to HFD+SR group was performed in PFSR group in order to consider the effect of SR141716A beyond its effect on diet intake. (A)Weekly body weight of each group of mice is shown during the whole period of treatment. (B) Weekly energy intake during 4 weeks' treatment with SR141716A in diet-induced obesity mice (C) average of daily diet intake for the period of stable diet intake (Day9-day28) (n=9-10). Repeated data were analyzed using Generalized Estimating Equation (GEE) method in SPSS. Groups were compared to the HFD+Vehicle control. Statistical significance was set with an alpha value of $**p < 0.01$, $\#p < 0.05$, ns (not significant).

116

Table 4.1 SR141716A causes significant shrinkage of fat mass. Body composition including fat mass, lean mass and fat percentage was assessed at baseline and after 4 weeks of treatment using Dual Energy X-ray absorptiometry (DEXA). Values are not sharing superscripted letters (a,b) differ significantly over time ($p < 0.05$). Values are not sharing superscripted symbols (#, @, &) differ significantly among different treated groups ($p < 0.05$).

Fat Mass (Grams)		
Diet	Week 12	Week 16
LFD+Vehicle	6.7±.49a	7.94±.38b@
HFD+vehicle	22.1±.78a	23.8±.69b#
HFD+SR	22.86±.16a	13.4±.74b&
PFSR	22.12±.29a	21.9±.92b#

Lean Mass (Grams)		
LFD+Vehicle	19.71±.37a	20.3±.62a@
HFD+vehicle	22.8±.39a	22.9±.11a#
HFD+SR	21.09±.75a	20.08±.29a#
PFSR	21.7±.28a	19.8±.36a#

Body Fat %		
LFD+Vehicle	25.369±.78a	28.11±.44b@
HFD+vehicle	49.22±.49a	50.96±.359b#
HFD+SR	52.01±.36a	40.02±.38b&
PFSR	50.47±.92a	52.51±.79b#

A

B

C

D

118

E
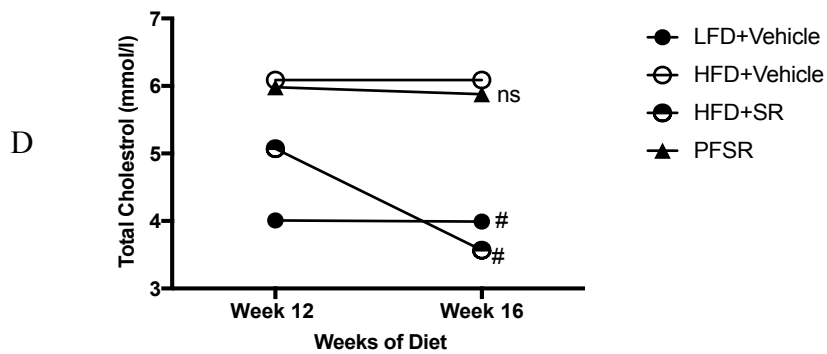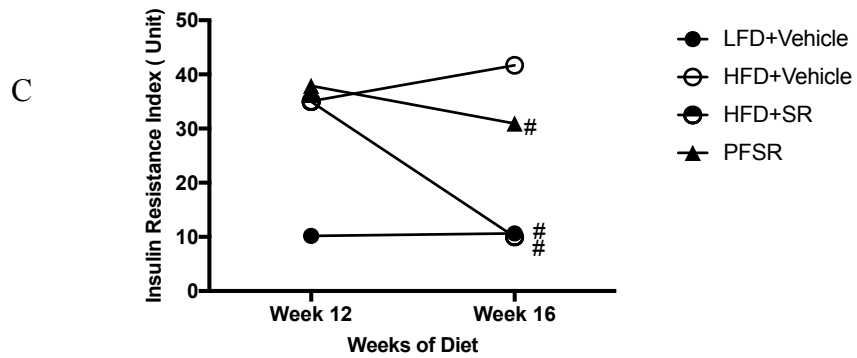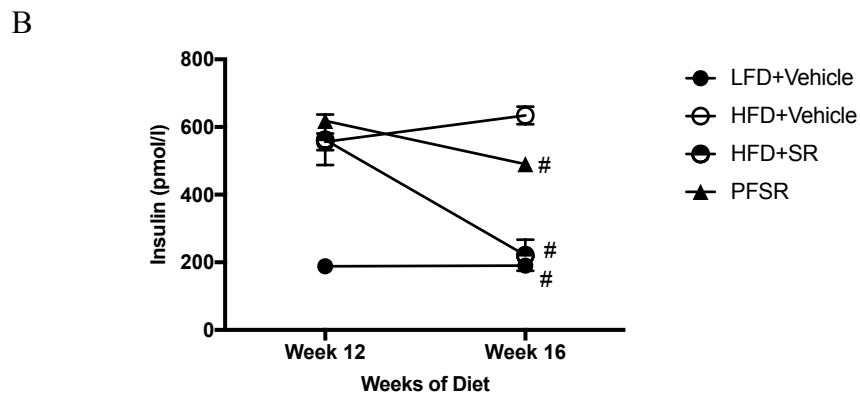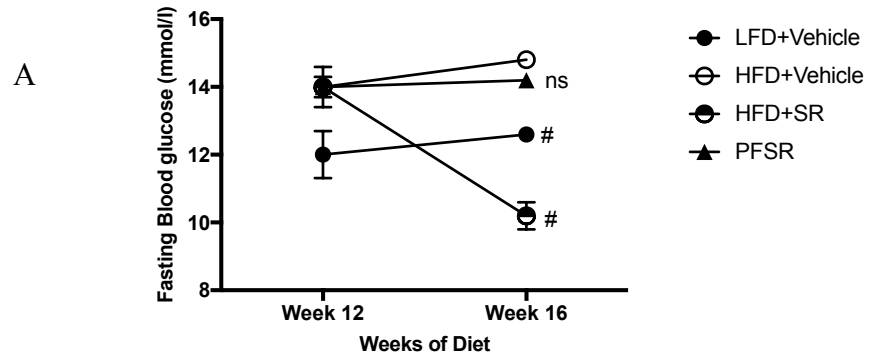
Figure 4.2

Figure 4.2 SR141716A intervention treatment ameliorates metabolic dysfunction in DIO phenotype. Fasted metabolic parameters assessed at the baseline and prior to the sacrificing day (Day 27). (A) Fasting blood glucose (B) Insulin concentration (C) HOMA index =fasting insulin(μU/ml) x fasting glucose (mmol/l) /22.5 (D) Total cholesterol concentration (E) Triglycerides concentration. Data were analyzed using one-way ANOVA, (n=9-10), significant differences from HFD+Vehicle group was demonstrated (#$p < 0.05$, ns (not significant)).

A

B

119

C

HFD+ Vehicle Vs LFD+ Vehicle

Colors:
Macrophages LFD+Vehicle
Colored by Default
-70.8782594117   258.0351940468

Macrophages HFD+Vehicle
Colored by Default
-76.40072435359   109.2656140454

Macrophates HFD+SR141716A
Colored by Default
-78.56481556403   119.2296724116

Macrophages PAIR-FED to SR141716A+Vehicle
Colored by Default
-67.11108796427   273.8331160156
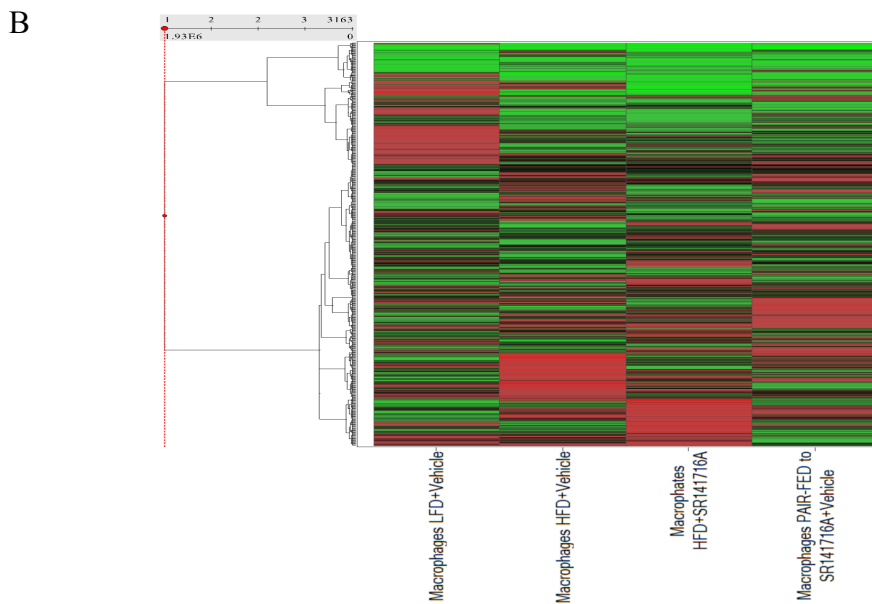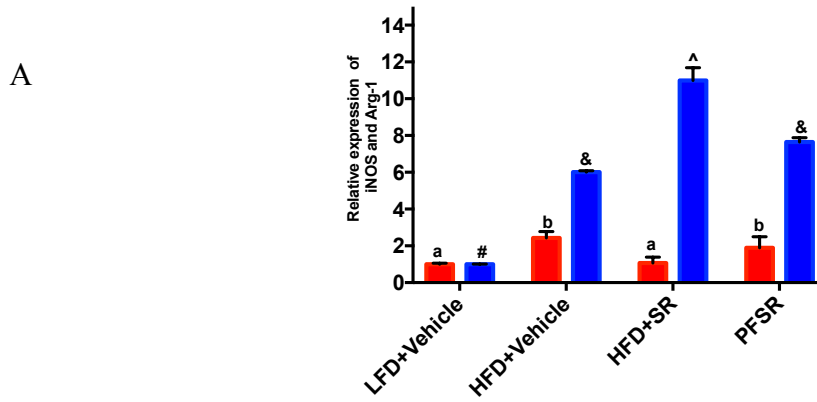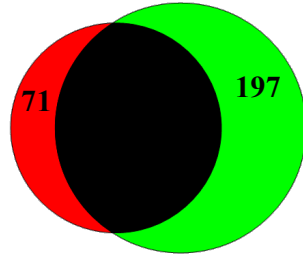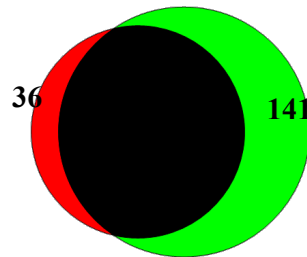
HFD+SR141716A Vs HFD + Vehicle

Pair-fed to SR141716A Vs +HFDSR141716A

D

- negative regulation of B cell activation
- positive regulation of immune response
- regulation of B cell activation
- adaptive immune response based on somatic recombination of immune receptors built from immunoglobulin superfamily domains
- leukocyte activation involved in immune response
- lymphocyte activation involved in immune response
- regulation of myeloid cell differentiation
- response to interferon-gamma
- T cell activation
- positive regulation of B cell proliferation
- lymphocyte mediated immunity *
- embryonic hemopoiesis **

120

E

Figure 4.3

Figure 4.3 SR141716A treatment in DIO phenotype skew the ATMs balance to less Pro-inflammatory M1 and more Anti-inflammatory M2 macrophages. Changes in M1 and M2 expression in ATMs were assessed following SR141716A treatment in DIO mice. (A) RT-PCR from epididymal fat mass for iNOS and ARG-1. Data were analyzed using one-way ANOVA. Groups with different super-scripted letter or symbols are significantly different from each other ($p < 0.05$). (B) Differential expression heat map of 3100 miRs between different treated group from F4/80 selected cells in adipose tissue (C) Cluster analysis of microRNAs showed that 36 miRs were up-regulated while 141 were down-regulated upon SR141716A administration compared to HFD+Vehicle group. Also 164 were up-regulated while 25 were down-regulated compared to Pair-fed to SR141716A group. (D) Go enrichment mapping. miR target genes in HFD+SR were analyzed for GO enrichment and mapped for GO category: immune system process, using Cytoscape suite with ClueGo and CluePedia plugins. Two –sided hypergeometric statistic was performed with Kappa Score threshold setting of 0.3. Enrichment depletion were calculated based on Benjamini-Hochberg Correlated *p* values of <0.05. (E) 8. Interactions between the microRNAs and their target genes were assessed by Ingenuity Pathway Analysis (IPA) software. SR141716A treatment changes the microRNA profile which skews the adipose tissue macrophage balance to more anti-inflammatory macrophages (M2, Arginase+)

121

A

B

Pearson Correlation = 0.648 (p < .001)

123

C
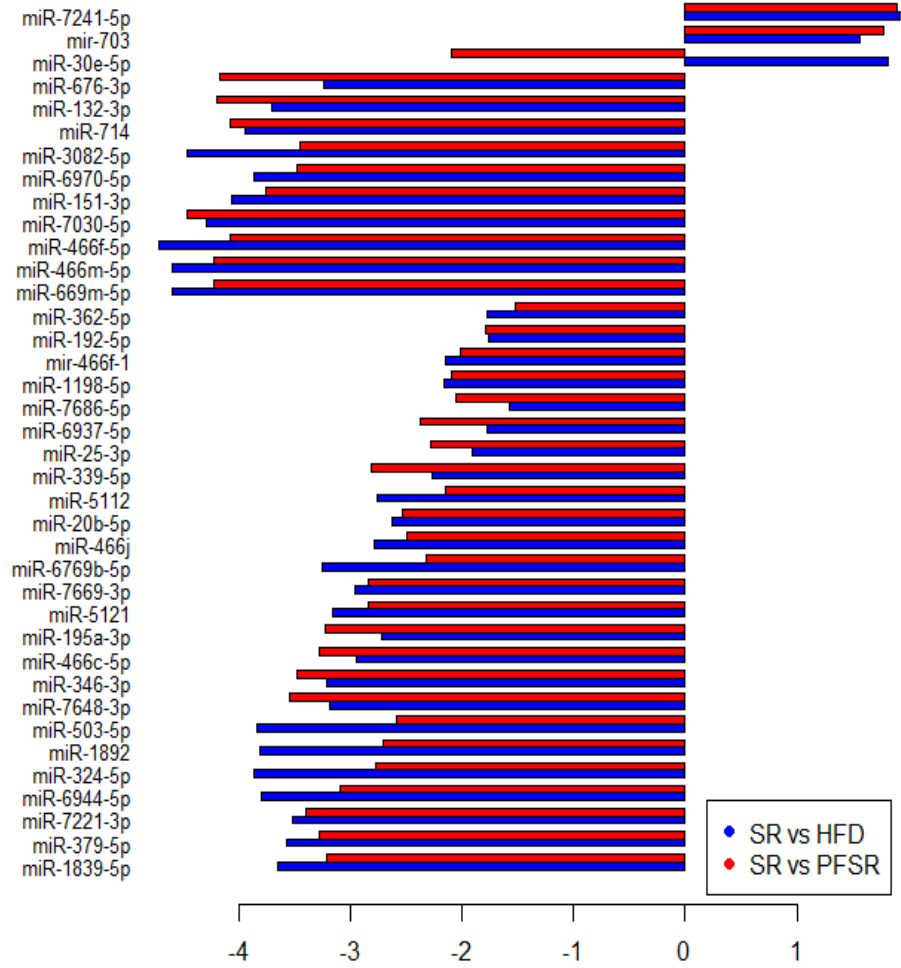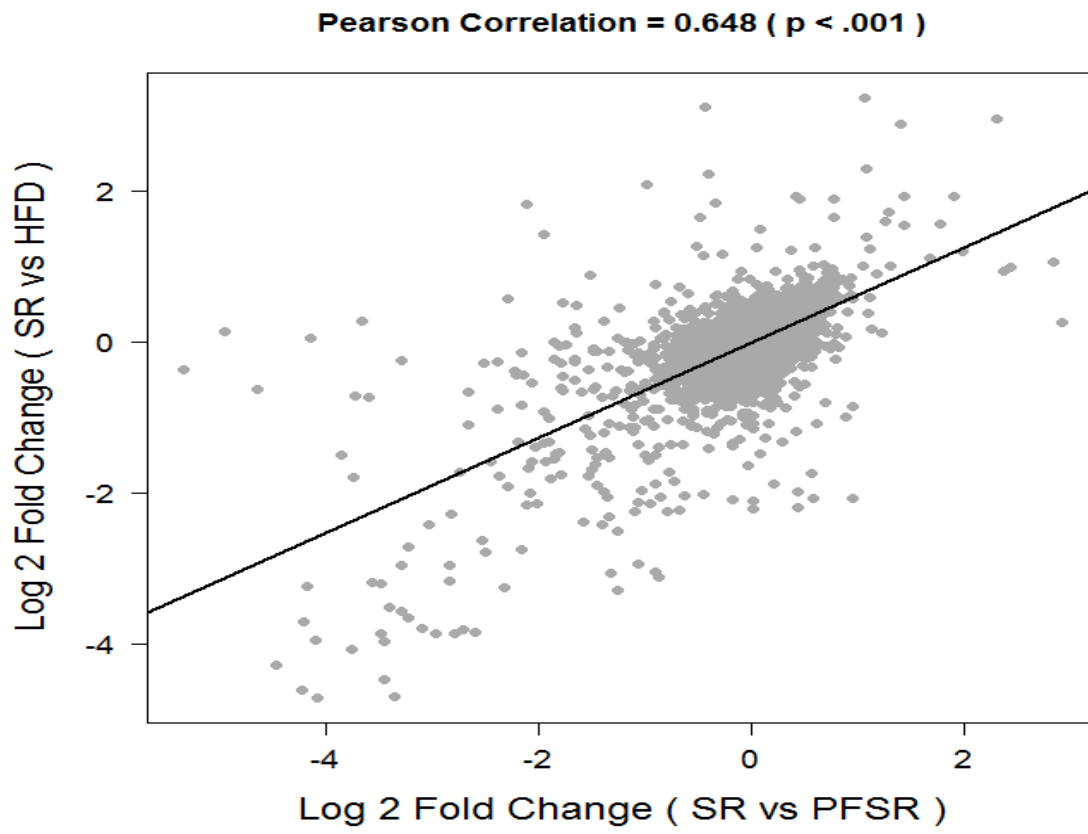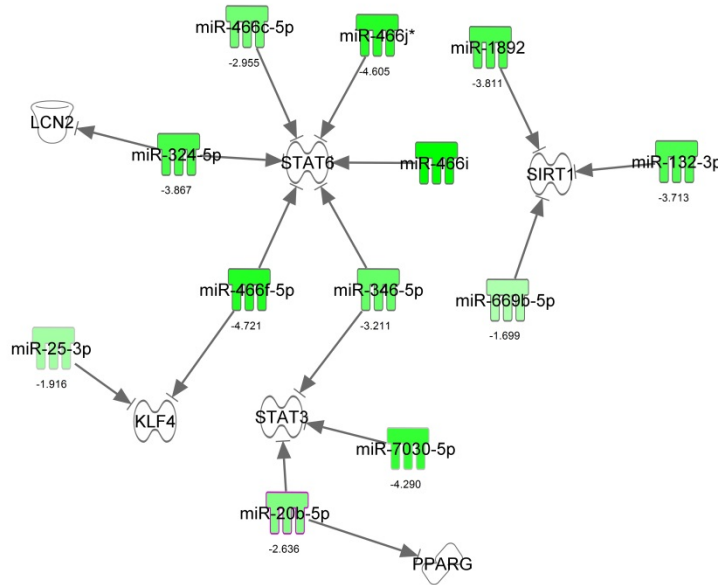
Figure 4.4

Figure 4.4 miR-466 family targets M2 polarization in DIO was down-regulated following SR141716A, the effect is beyond of SR141716A effect on diet restriction. Isolated miRs from ATMs were filtered to exclusively altered miR following SR141716A treatment (A)Dual color bar graph of modified miRs due to the effect of SR141716A treatment beyond its effect on calorie restriction. (B) Correlation plot of Log2 fold change of (HFD+SR vs HFD+Vehicle) and Log2 fold changes of (HFD+SR vs PFSR) was conducted. Correlation R ^{2}= 0.648 (univariate regression).(C) IPA analysis from filtered miRs revealed the family of miR-466 which is involved in M2 polarization in ATMs following SR141716A.

124

Table 4.2 Summary of the unique miRs targets M2 polarization in ATMs, following SR141716A treatment in DIO phenotype. The applied algorithm, down-stream effect of altered miRs following SR141716A, target genes, and the log2 fold changes was summarized in Table 2.

Target	Relevance	miRNA	Log2 FC	Algorithm
PPARg	Differentially expressed in M1 and M2. PPARg ↓=↑M1 and ↓M2	mir-20b-5p	-2.6	IPA
	∴ with treatment,PPARG ↑			
KLF4	↑ in M2 and ↓ in M1,	miR-466f-5p	-4.7	mirmap/db
	∴ with treatment,KLF4↑	miR-466f-1	-2.5	mirmap
		miR-25-3p		mirmap/db
LCN2	LCN2↓ (k.o.)=↑M1 and ↓M2	miR-324-59	-3.9	mirmap
	∴ with treatment,LCN2↑			
SIRT1	SIRT1↓ (k.o.)=↑M1 and ↓M2	miR-1892	-3.8	mirmap
	∴ with treatment,SIRT1↑	miR-669b-5p	-1.5	mirmap
		miR-132-3p	-3.7	mirwalk
STAT3	Switch to M2 assoc w. ↑Stat3	mir-20b-5p	-2.6	mirmap/db
	∴ with treatment,Stat3↑	miR-346-3p	-3.2	mirmap
		miR-7030-5p	-4.3	mirmap/db
STAT6	Switch to M2 assoc w. ↑Stat6	miR-466j-5p	-2.8	mirmap
	∴ with treatment,Stat6↑	miR-466c-5p	-3	mirmap
		miR-466f-1	-2.5	mirmap
		miR-324-5p	-3.9	mirmap

125

A

B

Ntn-1

γTubulin

Vehicle   SR141716A
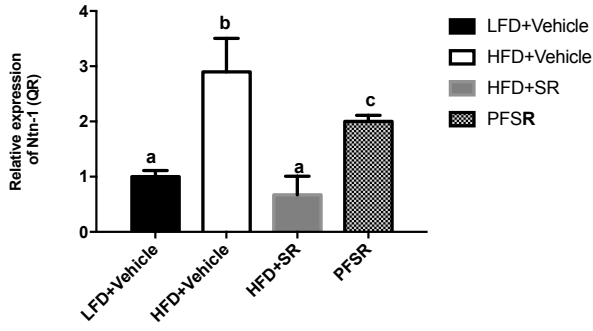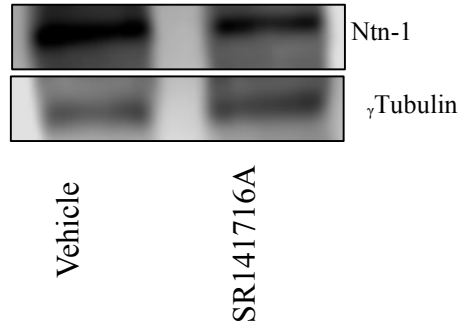
C
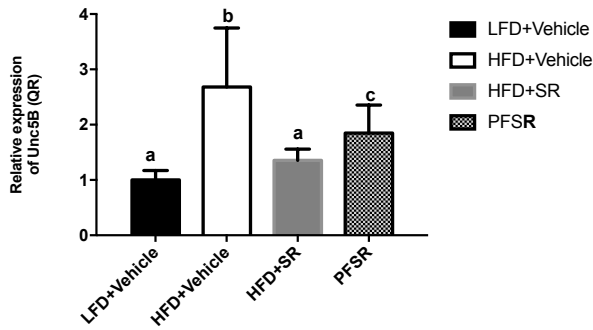
E
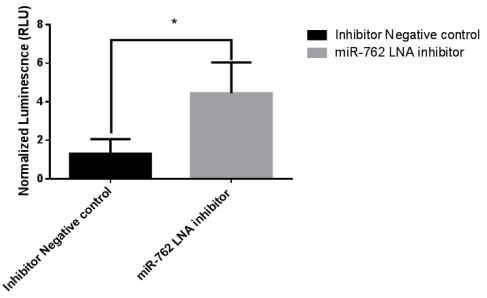
D
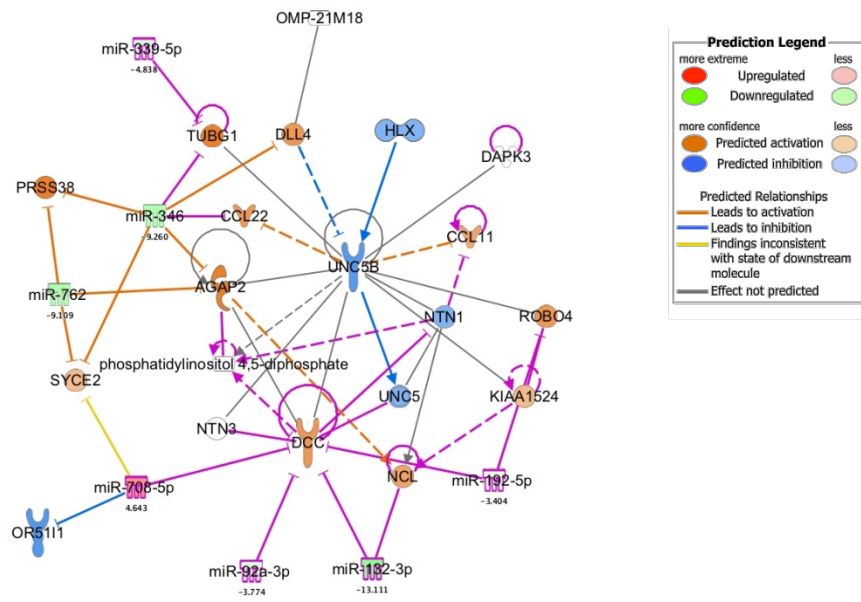
Figure 4.5

Figure 4.5 SR141716A treatment changes the miR profile which modifies the adipose tissue macrophage retention via negative regulator of neuroimmune guidance cue, AGAP-2. ATMs from different treated groups were examine for the changes in the level of nueroimmune guidance cue (A) Relative expression of Ntn-1 was assessed by RT-PCR and (B) western blot. (C) Relative expression of Unc5b was assessed by RT-PCR. (D) Interactions between the miR and their target genes were assessed by Ingenuity Pathway Analysis (IPA) software, filtered in neuroimmune guidance cue canonical pathway and MAP module was applied for down-stream effect prediction. (E) Bone Marrow Derived Macrophages (BMDM) were transfected with a plasmid with a Renilla luciferase (transfection efficiency control) and 3'UTR AGAP-2 of a Firefly luciferase reporter gene. Firefly luciferase expression is therefore suppressed by the corresponding endogenous microRNA level in the cell. The day after the cell cultures were transfected with miR-762 miRCURY LNA™ microRNA Inhibitor(5nM). Reporter gene expression was measured with a Dual Luciferase assay 24 hours after transfection. Data are shown as means $\pm$ SD. Statistical significance was set with an alpha value of *$p < 0.05$(student t-test)

A
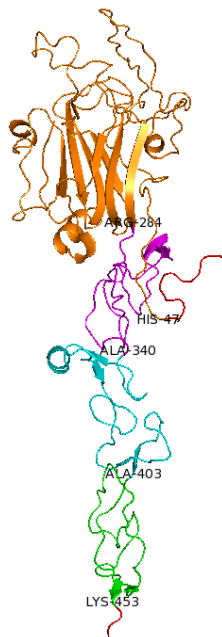
B
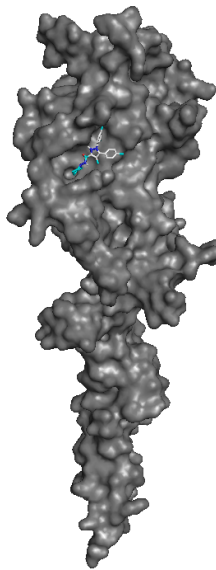
C
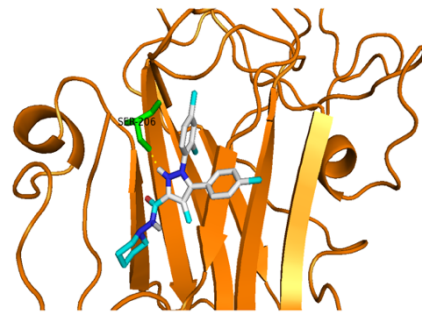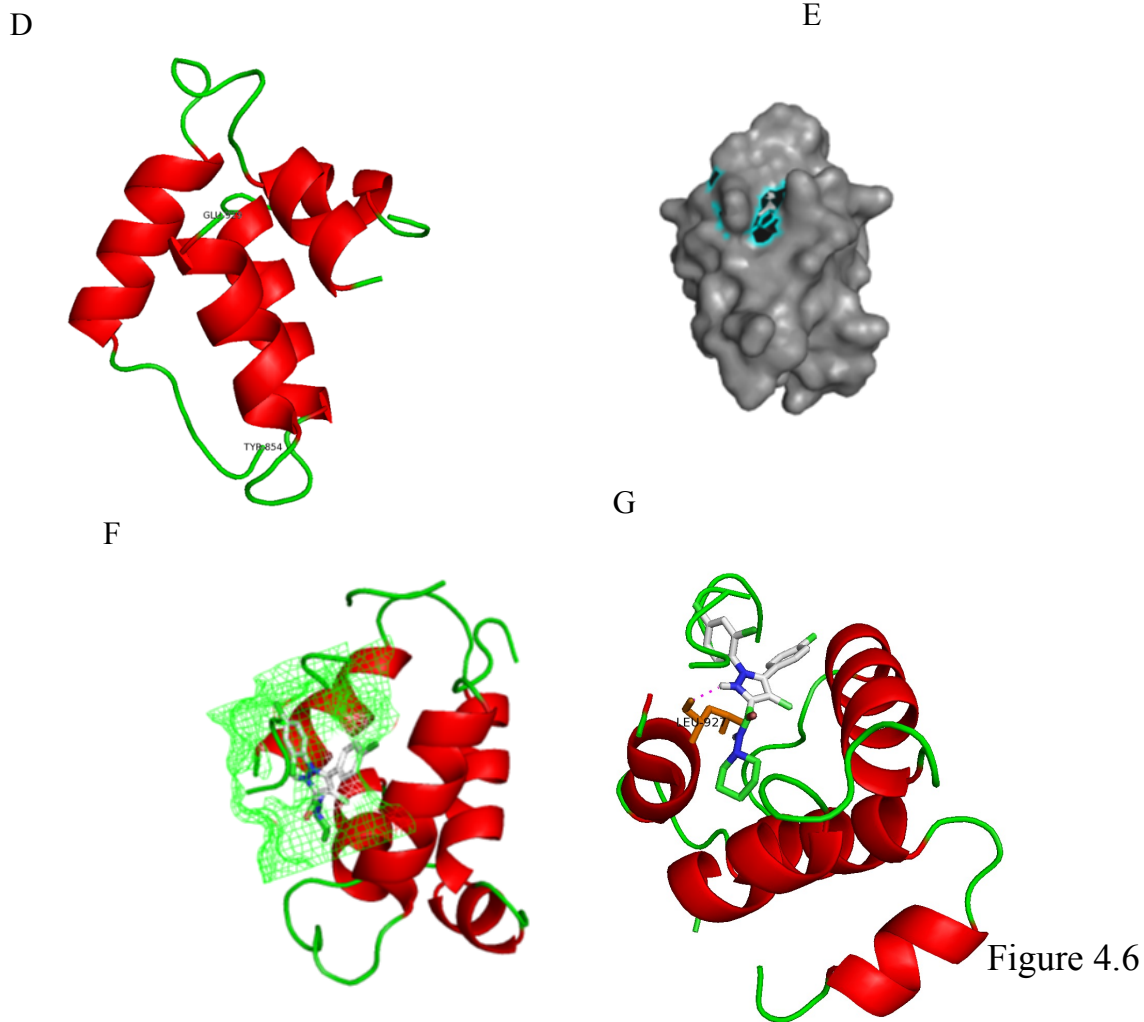
Figure 4.6 Interactions of SR141716A with Netrin-1 and UNC5B. (A) shows the three dimensional structure of Netrin-1 with N-terminal domain VI (47-284) represented in orange, Laminin epidermal growth factor (EGF) like 1 (285-340) domain represented in green color, Laminin epidermal growth factor (EGF) like 2 (341-403) domain represented in yellow color , Laminin epidermal growth factor (EGF) like 3 (404-453) domain represented in magenta color and remaining regions were coloured in grey (B) Surface model of the docked Rimonabant with Netrin-1 where Netrin-1 is shown as surface and SR141716A is shown as sticks (C) Amino acid interactions of Netrin-1 N-terminal domain VI (cartoon) and SR141716A (sticks) with polar contacts shown in yellow color dotted lines (D) shows the three dimensional structure of UNC5B death domain (854-929) with helices represented in red and loops in green color (E) Surface model of the docked SR141716A with UNC5B where UNC5B is shown as surface and SR141716A is shown as cyan color sticks (F) shows the SR141716A interacting UNC5B with the binding pocket represented in green color mesh (G) Amino acid interactions of UNC5B death domain (cartoon) and SR141716A (sticks) with polar contacts shown in magenta color dotted lines.

128
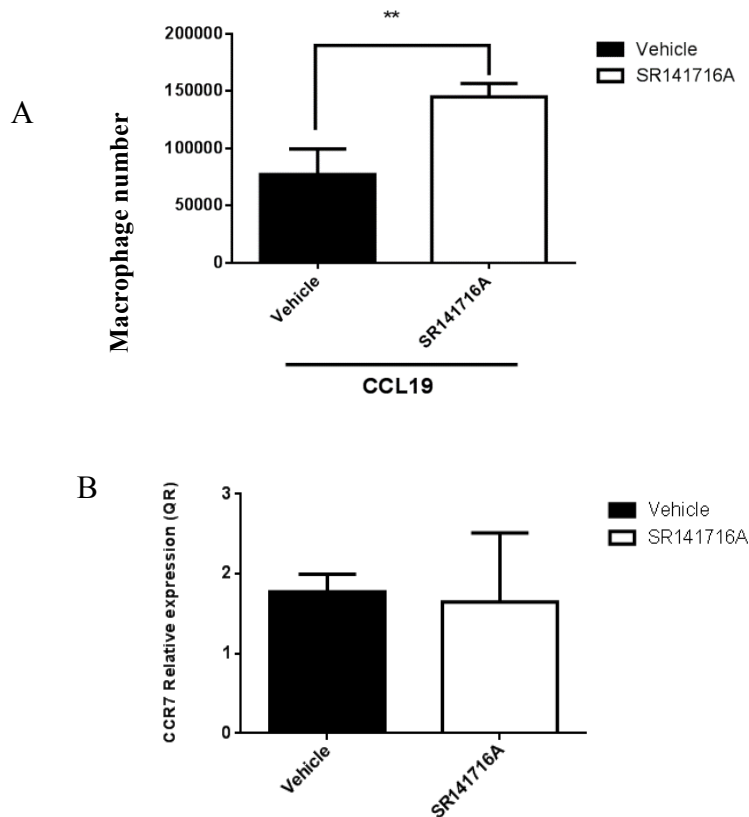
Figure 4.7

Figure 4.7 SR141716A inhibits macrophage retention in adipose tissue. (A)
Macrophage isolated from peritoneal wash of treated mice with 3%thyoglycolate.
Isolated macrophages were stained in Dilc(12)3 and treated with SR141716A or Vehicle.
Migration assay towards CCL19(500 ng/ml) was assessed by seeding $2.5*10^5$
macrophages in serum reduced conditioned medium from differentiated 3T3L-1 into
adipocytes in fluroblock plates. 12 hours later the migrated cells were quantified by
Cytation5. (B)Real-time PCR was conducted for CCR7 receptor. SR141716A does not
have any effect on the expression of CCR7 in macrophages. Data are shown as means $\pm$
SD. Statistical significance was set with an alpha value of $**p < 0.01$ (student t-test).

129

A

B
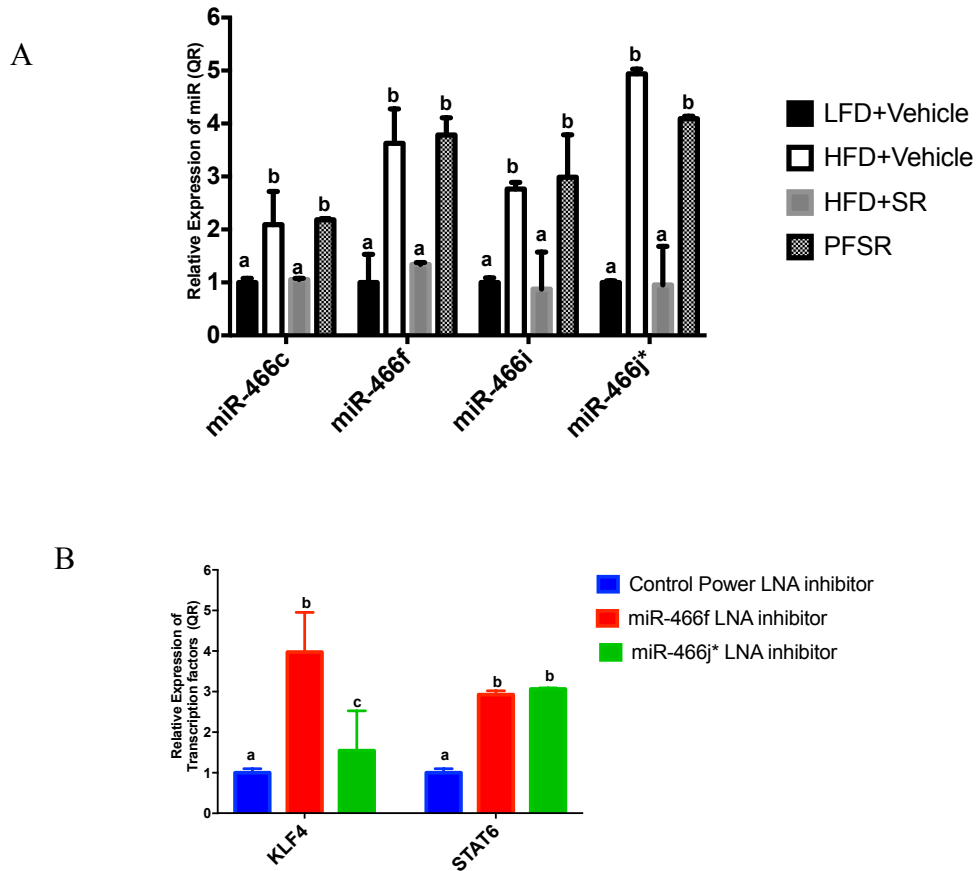
Supplementary figure 4.1

Supplementary figure 4.1 Down-regulated miR-466f and miR-466j* in DIO phenotype following SR141716A resulted in M2 polarization. ATMs were isolated from different treatment groups in our study. (A) RT-PCR for miR-466 family (B) RT-PCR for KLF4 and STAT6 after in BMDM which were transfected with LNA power inhibitors for miR-466f and mir-466j*. Vertical bars represent mean ± SD Values with different superscript letters are significantly different, (P<0.01) according to post hoc ANOVA one-way statistical analysis.

A

B

Supplementray figure 4.2
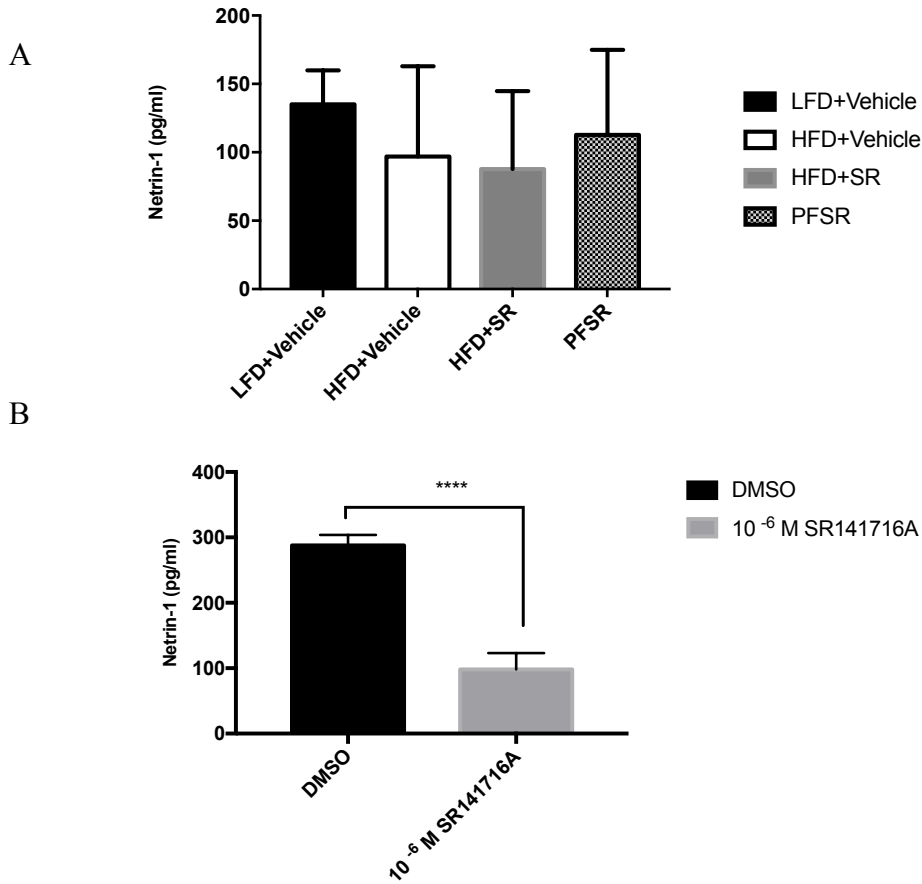
Supplementary figure 4.2 SR141716A suppressed Netrin-1 secretion from BMDM.
Systematic level of Netrin-1 was examined in serum of different study groups. (A)
Netrin-1 concentration in serum. Vertical bars represent mean ± SD. According to post
hoc ANOVA one-way statistical analysis, the differences between groups were not
significant (B) Cultured BMDM in conditioned media from 3T3-L1 adipocytes were
treated either with SR141716Aor DMSO (Vehicle). After 24 hours of treatment the
supernatant were harvested for Netrin-1 Elisa. Vertical bars represent mean ± SD. Data
were analyzed with Student t-test with ****p<.0001.

131

Supplementary Table 4.1 Primers sequences. The forward and reverse sequences of each primer used in the study.

AGAP-2	GAGCAGAACTACGCACCTCC	GTTCGGGAATTGATCGGCTCA
Adenosine A2b	AGCTAGAGACGCAAGACGC	GTGGGGGTCTGTAATGCACT
Adenosine A2a	TTCCACTCCGGTACAATGGC	CGATGGCGAATGACAGCAC
Unc5D	CAACCCGATTGCACTCAGGT	GCCTTCCTACTCTTGGACGTTC
Unc5C	GAACAAGCCTGTGAACCTGTAT	GTCTACTACGTGGTCCTTCTGA
Unc5A	GTGGAGTGGCTCCGAAATGAG	ACGCAGGTGTAGTTGGCAG
Neogenin	AATCGACAGCCCCTTCTTCTA	GGTCGCATCAGAAATACCAAGTC
DCC	ACAGCAAAAGTTACGGTAGCAG	ATGGGTTCCCCAATGACTTCA
NetrinG2	GTGATGCGCCTGAAGGATTAT	TTCTCATGGGAACAGAACCTTTC
NetrinG1	CTTCTGTGCAATGGGCAACC	GCCAAAATGTGGAGGGATGTC
Netrin4	TGTGTCAGTCCGTCGAGGT	CGGCGGTTATCCTGATAGGAAG
Netrin3	GCCGACCCCTGCTATGATG	GTTGCAGCAAATCGGAGCG

Supplementary Table 4.2 Neuronal guidance cue gene expression in HFD+Vehicle vs. LFD+Vehicle, and HFD+SR vs. HFD+Vehcile groups. The level expression of neuronal guidance cue and their receptors in epididymal fat mass of different group

Full name	RefSeq#	Gene Symbol	Fold Change HFD+Vehicle vs.LFD+Vehicle	Fold Change HFD+SR vs. HFD+Vehicle
Netrin 3	NM_010947	Ntn3	-1.0075	-1.0333
Netrin 4	NM_021320	Ntn4	-0.9038	-1.1058
Netrin G1	NM_030669	Ntng1	-1.8304	-2.0009
Netrin G2	NM_133501	Ntng2	-1.9961	-2.1862
Deleted in colorectal carcinoma	NM_007831	Dcc	-1.0039	-1.0703
Neogenin	NM_008684	Neo1	-1.9640	-1.7731
Unc-5 homolog A	NM_153131	Unc5a	-0.8229	-1.0039
Unc-5 homolog C	NM_009472	Unc5c	1.0072	0.7627
Unc-5 homolog D	NM_153135	Unc5d	-0.9501	-1.1118
Adenosine A2a receptor	NM_009630	Adora2a	-4.0051	-3.9071
Adenosine A2b receptor	NM_007413	Adora2b	1.9996	1.5548

studies.

CHAPTER V: SUMMARY AND CONCLUSION

2,3,7,8-Tetrachlorodibenzo-p-dioxin (TCDD), is an environmental contaminant and a potent ligand for AhR. Recent studies suggested that AhR activation by TCDD induces the expression of Foxp3, a marker on Tregs responsible for immunosuppression. The precise mechanisms through which AhR activation up-regulates Foxp3 expression in T cells is not clear.

In the current study, we investigated the role of microRNA (miR) and epigenetic markers in TCDD-induced expression of Foxp3 in T cells activated by Staphylococcal Enterotoxin B (SEB). We studied the effect of TCDD on purified Foxp3+Tregs from Foxp3/GFP knock-in mice injected with SEB, and treated with either vehicle or TCDD. Our studies showed that TCDD treatment decreased the percentage and numbers of SEB-activated Vβ8+ T cells while promoting Foxp3+ Vβ8+ Tregs. TCDD also suppressed pro-inflammatory cytokines (IFN-γ, TNF-α, and IL-6) and induced anti-inflammatory cytokines (IL-10, and TGF-β). High throughput miR analysis followed by *in silico* analysis demonstrated that miRs induced by TCDD regulated several epigenetic pathways, that impacted the expression of Foxp3.

Specifically, TCDD-mediated over-expression of miR-491 and miR-148a caused demethylation within the Foxp3 promoter region by targeting DNMT3a and DNMT3b. Moreover, reduction in DNMT3a and DNMT3b resulted in increased acetylation of

133

histone H3, which in turn led to promotion of the interaction with KLF10/SP-1, and consequent induction of Foxp3+.

This was also supported by the findings that TCDD down-regulated the expression of miR-31 and miR-26b and consequently induced the expression of KLF10 and SP-1, respectively. Interestingly, miR-31, was found to be complementary to the 3'-UTR of Foxp3 and CYP1A1 and induced the expression of these genes. Together, our studies demonstrate that AhR activation triggers miRs that cross-talk with multiple epigenetic pathways leading to the induction of Foxp3 and consequently, immune regulation.

In the third and forth chapters, we investigated the chronic inflammation in diet-induced obesity model. Obesity is characterized by chronic low-grade, systematic inflammation, altered gut microbiota and gut barrier disruption. The endocannabinoid system (eCB) plays a major role in the regulation of inflammation and metabolic disorders associated with obesity. In the current study, we investigated the effect of treatment of mice with SR141716A, a cannabinoid receptor1 (CB1) antagonist, on Diet Induced Obesity (DIO), specifically whether such a treatment can induce changes in gut microbiota and anti-inflammatory state in adipose tissue.

Blockade of CB1 receptor reduced plasma LPS level, circulating inflammatory cytokines and the trafficking of M1 macrophages into the adipose tissue. This decreased inflammatory tone was associated with a lower intestinal permeability and improved hyperglycemia and insulin resistance. Analysis of fecal samples using 16S rRNA metagenomic sequencing to investigate alterations in the gut microbiome, revealed that treatment with SR141716A dramatically increased the relative abundance of

134

Akkermansia muciniphila within the Verrucomicrobia phylum. Drastic reduction in immunogenic Lanchnospiraceae and Erysipelotrichaceae with SR141716A treatment was beyond its effect on the weight loss and diet intake. High level of anti-inflammatory propionate and butyrate in cecal content of SR141716A treated group was also detected. Our data suggest that blocking of CB1 receptors ameliorates obesity by restoring gut microbiome and consequently their metabolites which modulate macrophage inflammatory mediators.

Retention of Macrophages in adipose tissue is associated with high expression of neuroimmune guidance cue netrin-1 and its receptor UNC5B which are involved in chemotaxis. Suppression of pro-inflammatory macrophages was observed in SR141716A-treated HFD-fed group followed by down regulation of netrin-1 and UNC5B in macrophages. Molecular docking studies demonstrated interaction of SR141716A with both netrin-1 and UNC5B. Microarray and in silico analysis demonstrated that miRs induced by SR141716A regulated several pathways including macrophage migration. Specifically, we uncovered that SR141716A treatment down-regulated miR-466 family that regulate transcription factors such as KLF4 and STAT6 leading to promotion of M2 polarization. Also, miR-762 which was down-regulated following SR141716A treatment, was found to be complementary to the 3'-UTR of AGAP-2 gene, a negative regulator of netrin-1 receptor, UNC5B.

Thus, for the first time, we demonstrate that blockade of CB1 receptors leads to altered miR expression in adipose tissue macrophages that regulate netrin-1 and some key transcription factors leading to polarization to M2 macrophage phenotype and increased migration of such cells from adipose tissue leading to attenuation of obesity.

REFERENCES

1. Pinchuk, I. V., Beswick, E. J., & Reyes, V. E. (2010). Staphylococcal enterotoxins. Toxins, 2(8), 2177–2197.

2. Rao, R., Nagarkatti, P., & Nagarkatti, M. (2015). Role of miRNA in the regulation of inflammatory genes in staphylococcal enterotoxin B-induced acute inflammatory lung injury and mortality. Toxicological Sciences: An Official Journal of the Society of Toxicology.

3. Henghold, W. B. (2004). Other biologic toxin bioweapons: ricin, staphylococcal enterotoxin B, and trichothecene mycotoxins. Dermatologic Clinics, 22(3), 257–262.

4. Baker, M. D., & Acharya, K. R. (2004). Superantigens: structure-function relationships. International Journal of Medical Microbiology: IJMM, 293(7-8), 529–537.

5. Rieder, S. A., Nagarkatti, P., & Nagarkatti, M. (2012). Multiple anti-inflammatory pathways triggered by resveratrol lead to amelioration of staphylococcal enterotoxin B-induced lung injury. British Journal of Pharmacology, 167(6), 1244–1258.

6. Rao, R., Rieder, S. A., Nagarkatti, P., & Nagarkatti, M. (2014). Staphylococcal enterotoxin B-induced microRNA-155 targets SOCS1 to promote acute inflammatory lung injury. Infection and Immunity, 82(7), 2971–2979.

136

7. Fraser, J. D. (1989). High-affinity binding of staphylococcal enterotoxins A and B to HLA-DR. Nature, 339(6221), 221–223.

8. Krakauer, T., and Stiles, B.G. (2013). The staphylococcal enterotoxin (SE) family: SEB and siblings. Virulence *4*, 759–773.

9. Puneet, P., Moochhala, S., and Bhatia, M. (2005). Chemokines in acute respiratory distress syndrome. Am. J. Physiol. Lung Cell Mol. Physiol. *288*, L3–L15.

10. Miyara, M., Amoura, Z., Parizot, C., Badoual, C., Dorgham, K., Trad, S., Nochy, D., Debré, P., Piette, J.-C., and Gorochov, G. (2005). Global Natural Regulatory T Cell Depletion in Active Systemic Lupus Erythematosus. J Immunol *175*, 8392–8400.

11. Morgan, M.E., Sutmuller, R.P.M., Witteveen, H.J., van Duivenvoorde, L.M., Zanelli, E., Melief, C.J.M., Snijders, A., Offringa, R., de Vries, R.R.P., and Toes, R.E.M. (2003). CD25+ cell depletion hastens the onset of severe disease in collagen-induced arthritis. Arthritis & Rheumatism *48*, 1452–1460.

12. Huter, E.N., Punkosdy, G.A., Glass, D.D., Cheng, L.I., Ward, J.M., and Shevach, E.M. (2008). TGFβ-induced FoxP3+ Regulatory T Cells Rescue Scurfy Mice. Eur J Immunol *38*, 1814–1821.

13. Lahl, K., Loddenkemper, C., Drouin, C., Freyer, J., Arnason, J., Eberl, G., Hamann, A., Wagner, H., Huehn, J., and Sparwasser, T. (2007). Selective depletion of Foxp3+ regulatory T cells induces a scurfy-like disease. J Exp Med *204*, 57–63.

14. Atkinson, S.M., Hoffmann, U., Hamann, A., Bach, E., Danneskiold-Samsøe, N.B., Kristiansen, K., Serikawa, K., Fox, B., Kruse, K., Haase, C., et al. (2016). Depletion of regulatory T cells leads to an exacerbation of delayed-type hypersensitivity arthritis in C57BL/6 mice that can be counteracted by IL-17 blockade. Dis Model Mech *9*, 427–440.

15. Kelchtermans, H., De Klerck, B., Mitera, T., Van Balen, M., Bullens, D., Billiau, A., Leclercq, G., and Matthys, P. (2005). Defective CD4+CD25+ regulatory T cell functioning in collagen-induced arthritis: an important factor in pathogenesis, counter-regulated by endogenous IFN-γ. Arthritis Res Ther *7*, R402–R415.

16. Sakaguchi, S., Sakaguchi, N., Asano, M., Itoh, M., and Toda, M. (1995). Immunologic self-tolerance maintained by activated T cells expressing IL-2 receptor alpha-chains (CD25). Breakdown of a single mechanism of self-tolerance causes various autoimmune diseases. J. Immunol. *155*, 1151–1164.

17. Sullivan, K.E., McDonald-McGinn, D., and Zackai, E.H. (2002). CD4(+) CD25(+) T-cell production in healthy humans and in patients with thymic hypoplasia. Clin. Diagn. Lab. Immunol. *9*, 1129–1131.

18. Brunkow, M.E., Jeffery, E.W., Hjerrild, K.A., Paeper, B., Clark, L.B., Yasayko, S.A., Wilkinson, J.E., Galas, D., Ziegler, S.F., and Ramsdell, F. (2001). Disruption of a new forkhead/winged-helix protein, scurfin, results in the fatal lymphoproliferative disorder of the scurfy mouse. Nat. Genet. *27*, 68–73.

19. Lyon, M.F., Peters, J., Glenister, P.H., Ball, S., and Wright, E. (1990). The scurfy mouse mutant has previously unrecognized hematological abnormalities and

resembles Wiskott-Aldrich syndrome. Proc. Natl. Acad. Sci. U.S.A. *87*, 2433–2437.

20. Bensinger, S.J., Bandeira, A., Jordan, M.S., Caton, A.J., and Laufer, T.M. (2001). Major histocompatibility complex class II-positive cortical epithelium mediates the selection of CD4(+)25(+) immunoregulatory T cells. J. Exp. Med. *194*, 427–438.

21. Fontenot, J.D., and Rudensky, A.Y. (2005). A well adapted regulatory contrivance: regulatory T cell development and the forkhead family transcription factor Foxp3. Nat. Immunol. *6*, 331–337.

22. Chen, W. (2011). Tregs in immunotherapy: opportunities and challenges. Immunotherapy *3*, 911–914.

23. Fontenot, J.D., Rasmussen, J.P., Gavin, M.A., and Rudensky, A.Y. (2005). A function for interleukin 2 in Foxp3-expressing regulatory T cells. Nat. Immunol. *6*, 1142–1151.

24. D'Cruz, L.M., and Klein, L. (2005). Development and function of agonist-induced CD25+Foxp3+ regulatory T cells in the absence of interleukin 2 signaling. Nat. Immunol. *6*, 1152–1159.

25. Hori, S., Nomura, T., and Sakaguchi, S. (2003). Control of regulatory T cell development by the transcription factor Foxp3. Science *299*, 1057–1061.

26. Fontenot, J.D., Gavin, M.A., and Rudensky, A.Y. (2003). Foxp3 programs the development and function of CD4+CD25+ regulatory T cells. Nat. Immunol. *4*, 330–336.

27. Rubtsov, Y.P., Niec, R.E., Josefowicz, S., Li, L., Darce, J., Mathis, D., Benoist, C., and Rudensky, A.Y. (2010). Stability of the regulatory T cell lineage in vivo. Science *329*, 1667–1671.

28. Feng, Y., Arvey, A., Chinen, T., van der Veeken, J., Gasteiger, G., and Rudensky, A.Y. (2014). Control of the inheritance of regulatory T cell identity by a cis element in the Foxp3 locus. Cell *158*, 749–763.

29. Li, B., Samanta, A., Song, X., Iacono, K.T., Bembas, K., Tao, R., Basu, S., Riley, J.L., Hancock, W.W., Shen, Y., et al. (2007). FOXP3 interactions with histone acetyltransferase and class II histone deacetylases are required for repression. Proc. Natl. Acad. Sci. U.S.A. *104*, 4571–4576.

30. Chen, Z., Barbi, J., Bu, S., Yang, H.-Y., Li, Z., Gao, Y., Jinasena, D., Fu, J., Lin, F., Chen, C., et al. (2013). The ubiquitin ligase Stub1 negatively modulates regulatory T cell suppressive activity by promoting degradation of the transcription factor Foxp3. Immunity *39*, 272–285.

31. van Loosdregt, J., Fleskens, V., Fu, J., Brenkman, A.B., Bekker, C.P.J., Pals, C.E.G.M., Meerding, J., Berkers, C.R., Barbi, J., Gröne, A., et al. (2013). Stabilization of the transcription factor Foxp3 by the deubiquitinase USP7 increases Treg-cell-suppressive capacity. Immunity *39*, 259–271.

32. von Boehmer, H. (2005). Mechanisms of suppression by suppressor T cells. Nat. Immunol. *6*, 338–344.

33. Esser, C., Rannug, A., & Stockinger, B. (2009). The aryl hydrocarbon receptor in immunity. Trends in Immunology, 30(9), 447–454.

140

34. Marshall, N. B., & Kerkvliet, N. I. (2010). Dioxin and immune regulation: emerging role of aryl hydrocarbon receptor in the generation of regulatory T cells. Annals of the New York Academy of Sciences, 1183, 25–37

35. Singh, N.P., Singh, U.P., Singh, B., Price, R.L., Nagarkatti, M., and Nagarkatti, P.S. (2011). Activation of aryl hydrocarbon receptor (AhR) leads to reciprocal epigenetic regulation of Foxp3 and IL-17 expression and amelioration of experimental colitis. PLoS ONE 6, e23522.

36. Quintana, F.J., Basso, A.S., Iglesias, A.H., Korn, T., Farez, M.F., Bettelli, E., Caccamo, M., Oukka, M., and Weiner, H.L. (2008). Control of Treg and TH17 cell differentiation by the aryl hydrocarbon receptor. Nature *453*, 65–71.

37. Kerkvliet, N.I., Steppan, L.B., Vorachek, W., Oda, S., Farrer, D., Wong, C.P., Pham, D., and Mourich, D.V. (2009). Activation of aryl hydrocarbon receptor by TCDD prevents diabetes in NOD mice and increases Foxp3+ T cells in pancreatic lymph nodes. Immunotherapy *1*, 539–547.

38. Alberti, K.G.M.M., Eckel, R.H., Grundy, S.M., Zimmet, P.Z., Cleeman, J.I., Donato, K.A., Fruchart, J.-C., James, W.P.T., Loria, C.M., Smith, S.C., et al. (2009). Harmonizing the metabolic syndrome: a joint interim statement of the International Diabetes Federation Task Force on Epidemiology and Prevention; National Heart, Lung, and Blood Institute; American Heart Association; World Heart Federation; International Atherosclerosis Society; and International Association for the Study of Obesity. Circulation 120, 1640–1645.

39. Flegal, K.M., Carroll, M.D., Ogden, C.L., and Curtin, L.R. (2010). Prevalence and trends in obesity among US adults, 1999-2008. JAMA 303, 235–241.

141

40. Prevalence of obesity and trends in body mass index among US children and adolescents, 1999-2010. - PubMed - NCBI.

41. Chawla, A., Nguyen, K.D., and Goh, Y.P.S. (2011). Macrophage-mediated inflammation in metabolic disease. Nat. Rev. Immunol. 11, 738–749.

42. Enos, R.T., Velázquez, K.T., McClellan, J.L., Cranford, T.L., Walla, M.D., and Murphy, E.A. (2014). Reducing the dietary omega-6:omega-3 utilizing α-linolenic acid; not a sufficient therapy for attenuating high-fat-diet-induced obesity development nor related detrimental metabolic and adipose tissue inflammatory outcomes. PLoS ONE 9, e94897.

43. Weisberg, S.P., McCann, D., Desai, M., Rosenbaum, M., Leibel, R.L., and Ferrante, A.W. (2003). Obesity is associated with macrophage accumulation in adipose tissue. J. Clin. Invest. 112, 1796–1808.

44. O'Rourke, R.W., White, A.E., Metcalf, M.D., Olivas, A.S., Mitra, P., Larison, W.G., Cheang, E.C., Varlamov, O., Corless, C.L., Roberts, C.T., et al. (2011). Hypoxia-induced inflammatory cytokine secretion in human adipose tissue stromovascular cells. Diabetologia 54, 1480–1490.

45. Hotamisligil, G.S., Shargill, N.S., and Spiegelman, B.M. (1993). Adipose expression of tumor necrosis factor-alpha: direct role in obesity-linked insulin resistance. Science 259, 87–91.

46. Vandanmagsar, B., Youm, Y.-H., Ravussin, A., Galgani, J.E., Stadler, K., Mynatt, R.L., Ravussin, E., Stephens, J.M., and Dixit, V.D. (2011). The NLRP3 inflammasome instigates obesity-induced inflammation and insulin resistance. Nat. Med. 17, 179–188.

142

47. Wen, H., Gris, D., Lei, Y., Jha, S., Zhang, L., Huang, M.T.-H., Brickey, W.J., and Ting, J.P.-Y. (2011). Fatty acid-induced NLRP3-ASC inflammasome activation interferes with insulin signaling. Nat. Immunol. 12, 408–415.

48. Esser, N., L'homme, L., De Roover, A., Kohnen, L., Scheen, A.J., Moutschen, M., Piette, J., Legrand-Poels, S., and Paquot, N. (2013). Obesity phenotype is related to NLRP3 inflammasome activity and immunological profile of visceral adipose tissue. Diabetologia 56, 2487–2497.

49. Gordon, S., and Taylor, P.R. (2005). Monocyte and macrophage heterogeneity. Nat. Rev. Immunol. 5, 953–964.

50. Mantovani, A., Sica, A., Sozzani, S., Allavena, P., Vecchi, A., and Locati, M. (2004). The chemokine system in diverse forms of macrophage activation and polarization. Trends Immunol. 25, 677–686.

51. Gordon, S. (2003). Alternative activation of macrophages. Nat. Rev. Immunol. 3, 23–35.

52. Odegaard, J.I., Ricardo-Gonzalez, R.R., Goforth, M.H., Morel, C.R., Subramanian, V., Mukundan, L., Red Eagle, A., Vats, D., Brombacher, F., Ferrante, A.W., et al. (2007). Macrophage-specific PPARgamma controls alternative activation and improves insulin resistance. Nature 447, 1116–1120.

53. Yang, X., Wang, X., Liu, D., Yu, L., Xue, B., and Shi, H. (2014). Epigenetic regulation of macrophage polarization by DNA methyltransferase 3b. Mol. Endocrinol. 28, 565–574.

54. Di Marzo, V. (2006). A brief history of cannabinoid and endocannabinoid pharmacology as inspired by the work of British scientists. Trends Pharmacol. Sci. *27*, 134–140.

55. Howlett, A.C., Breivogel, C.S., Childers, S.R., Deadwyler, S.A., Hampson, R.E., and Porrino, L.J. (2004). Cannabinoid physiology and pharmacology: 30 years of progress. Neuropharmacology *47, Supplement 1*, 345–358.

56. V. Di Marzo (Ed.), Cannabinoids, Kluwer-Plenum (2004), The pharmacology and therapeutic potential of cannabidiol. pp. 32–83

57. Matsuda, L. A., S. J. Lolait, M. J. Brownstein, A. C. Young, and T. I. Bonner. 1990. Structure of a cannabinoid receptor and functional expression of the cloned cDNA. *Nature* 346: 561-564.

58. Munro, S., Thomas, K.L., and Abu-Shaar, M. (1993). Molecular characterization of a peripheral receptor for cannabinoids. Nature *365*, 61–65.

59. Zygmunt, P. M., J. Petersson, D. A. Andersson, H. Chuang, M. Sorgard, V. Di Marzo, D. Julius, and E. D. Hogestatt. 1999. Vanilloid receptors on sensory nerves mediate the vasodilator action of anandamide. *Nature* 400: 452-457.

60. Mezey, E., Z. E. Toth, D. N. Cortright, M. K. Arzubi, J. E. Krause, R. Elde, A. Guo, P. M. Blumberg, and A. Szallasi. 2000. Distribution of mRNA for vanilloid receptor subtype 1 (VR1), and VR1-like immunoreactivity, in the central nervous system of the rat and human. *Proceedings of the National Academy of Sciences of the United States of America* 97: 3655-3660.

61. Saunders, C. I., R. G. Fassett, and D. P. Geraghty. 2009. Up-regulation of TRPV1 in mononuclear cells of end-stage kidney disease patients increases susceptibility

to N-arachidonoyl-dopamine (NADA)-induced cell death. *Biochim Biophys Acta* 1792: 1019-1026.

62. Moldrich, G., and T. Wenger. 2000. Localization of the CB1 cannabinoid receptor in the rat brain. An immunohistochemical study. *Peptides* 21: 1735-1742.

63. Parolaro, D. 1999. Presence and functional regulation of cannabinoid receptors in immune cells. *Life Sci* 65: 637-644.

64. Onaivi, E. S., H. Ishiguro, J. P. Gong, S. Patel, A. Perchuk, P. A. Meozzi, L. Myers, Z. Mora, P. Tagliaferro, E. Gardner, A. Brusco, B. E. Akinshola, Q. R. Liu, B. Hope, S. Iwasaki, T. Arinami, L. Teasenfitz, and G. R. Uhl. 2006. Discovery of the presence and functional expression of cannabinoid CB2 receptors in brain. *Annals of the New York Academy of Sciences* 1074: 514-536.

65. de Fonseca, F.R., and Schneider, M. (2008). The endogenous cannabinoid system and drug addiction: 20 years after the discovery of the CB1 receptor. Addict Biol *13*, 143–146.

66. Brown, A.J. (2007). Novel cannabinoid receptors. Br. J. Pharmacol. *152*, 567–575.

67. Barnett-Norris, J., D. P. Hurst, D. L. Lynch, F. Guarnieri, A. Makriyannis, and P. H. Reggio. 2002. Conformational memories and the endocannabinoid binding site at the cannabinoid CB1 receptor. *Journal of medicinal chemistry* 45: 3649-3659.

68. Song, Z. H., and T. I. Bonner. 1996. A lysine residue of the cannabinoid receptor is critical for receptor recognition by several agonists but not WIN55212-2. *Mol Pharmacol* 49: 891-896.

69. Bouaboula, M., D. Dussossoy, and P. Casellas. 1999. Regulation of peripheral cannabinoid receptor CB2 phosphorylation by the inverse agonist SR 144528. Implications for receptor biological responses. *J Biol Chem* 274: 20397-20405.

70. Song, Z. H., C. A. Slowey, D. P. Hurst, and P. H. Reggio. 1999. The difference between the CB(1) and CB(2) cannabinoid receptors at position 5.46 is crucial for the selectivity of WIN55212-2 for CB(2). *Mol Pharmacol* 56: 834-840.

71. Feng, W., and Z. H. Song. 2003. Effects of D3.49A, R3.50A, and A6.34E mutations on ligand binding and activation of the cannabinoid-2 (CB2) receptor. *Biochem Pharmacol* 65: 1077-1085.

72. Rossi, S., G. Bernardi, and D. Centonze. 2010. The endocannabinoid system in the inflammatory and neurodegenerative processes of multiple sclerosis and of amyotrophic lateral sclerosis. *Exp Neurol* 224: 92-102.

73. Devane, W. A., L. Hanus, A. Breuer, R. G. Pertwee, L. A. Stevenson, G. Griffin, D. Gibson, A. Mandelbaum, A. Etinger, and R. Mechoulam. 1992. Isolation and structure of a brain constituent that binds to the cannabinoid receptor. *Science* 258: 1946-1949.

74. di Tomaso, E., Beltramo, M., and Piomelli, D. (1996). Brain cannabinoids in chocolate. Nature *382*, 677–678.

75. Martin, B.R., Mechoulam, R., and Razdan, R.K. (1999). Discovery and characterization of endogenous cannabinoids. Life Sciences *65*, 573–595.

76. Tanasescu, R., and C. S. Constantinescu. 2010. Cannabinoids and the immune system: an overview. *Immunobiology* 215: 588-597.

77. Grotenhermen, F. (2005). Cannabinoids. Current Drug Target -CNS & Neurological Disorders *4*, 507–530.

78. Stella, N., Schweitzer, P., and Piomelli, D. (1997). A second endogenous cannabinoid that modulates long-term potentiation. Nature *388*, 773–778.

79. Savinainen, J.R., Järvinen, T., Laine, K., and Laitinen, J.T. (2001). Despite substantial degradation, 2-arachidonoylglycerol is a potent full efficacy agonist mediating CB(1) receptor-dependent G-protein activation in rat cerebellar membranes. Br. J. Pharmacol. *134*, 664–672.

80. Cravatt, B. F., and A. H. Lichtman. 2004. The endogenous cannabinoid system and its role in nociceptive behavior. *J Neurobiol* 61: 149-160.

81. Ueda, N. 2002. Endocannabinoid hydrolases. *Prostaglandins & other lipid mediators* 68-69: 521-534.

82. Bisogno, T., Ligresti, A., and Di Marzo, V. (2005). The endocannabinoid signalling system: biochemical aspects. Pharmacol. Biochem. Behav. *81*, 224–238.

83. Ralevic, V. (2003). Cannabinoid modulation of peripheral autonomic and sensory neurotransmission. Eur. J. Pharmacol. *472*, 1–21.

84. Porter, A.C., Sauer, J.-M., Knierman, M.D., Becker, G.W., Berna, M.J., Bao, J., Nomikos, G.G., Carter, P., Bymaster, F.P., Leese, A.B., et al. (2002). Characterization of a novel endocannabinoid, virodhamine, with antagonist activity at the CB1 receptor. J. Pharmacol. Exp. Ther. *301*, 1020–1024.

85. Dinh, T. P., T. F. Freund, and D. Piomelli. 2002. A role for monoglyceride lipase in 2-arachidonoylglycerol inactivation. *Chemistry and physics of lipids* 121: 149-158.

86. ElSohly, M.A., Gul, W., Wanas, A.S., and Radwan, M.M. (2014). Synthetic cannabinoids: Analysis and metabolites. Life Sciences *97*, 78–90.

87. Lauritsen, K.J., and Rosenberg, H. (2016). Comparison of outcome expectancies for synthetic cannabinoids and botanical marijuana. Am J Drug Alcohol Abuse *42*, 377–384.

88. Fong, T.M., and Heymsfield, S.B. (2009). Cannabinoid-1 receptor inverse agonists: current understanding of mechanism of action and unanswered questions. Int J Obes (Lond) *33*, 947–955.

89. Cahill, K., and Ussher, M. (2007). Cannabinoid type 1 receptor antagonists (rimonabant) for smoking cessation. Cochrane Database Syst Rev CD005353.

90. Maldonado, R., Valverde, O., and Berrendero, F. (2006). Involvement of the endocannabinoid system in drug addiction. Trends Neurosci. *29*, 225–232.

91. Deadwyler, S.A., Goonawardena, A.V., and Hampson, R.E. (2007). Short-term memory is modulated by the spontaneous release of endocannabinoids: evidence from hippocampal population codes. Behav Pharmacol *18*, 571–580.

92. Huestis, M.A., Gorelick, D.A., Heishman, S.J., Preston, K.L., Nelson, R.A., Moolchan, E.T., and Frank, R.A. (2001). Blockade of effects of smoked marijuana by the CB1-selective cannabinoid receptor antagonist SR141716. Arch. Gen. Psychiatry *58*, 322–328.

148

93. Aquila, S., Guido, C., Santoro, A., Gazzerro, P., Laezza, C., Baffa, M.F., Andò, S., and Bifulco, M. (2010). Rimonabant (SR141716) induces metabolism and acquisition of fertilizing ability in human sperm. Br. J. Pharmacol. *159*, 831–841.

94. Galiègue, S., Mary, S., Marchand, J., Dussossoy, D., Carrière, D., Carayon, P., Bouaboula, M., Shire, D., Le Fur, G., and Casellas, P. (1995). Expression of central and peripheral cannabinoid receptors in human immune tissues and leukocyte subpopulations. Eur. J. Biochem. *232*, 54–61.

95. Ortega-Gutiérrez, S., Molina-Holgado, E., Arévalo-Martín, A., Correa, F., Viso, A., López-Rodríguez, M.L., Di Marzo, V., and Guaza, C. (2005). Activation of the endocannabinoid system as therapeutic approach in a murine model of multiple sclerosis. FASEB J. *19*, 1338–1340.

96. Ligresti, A., Cascio, M.G., Pryce, G., Kulasegram, S., Beletskaya, I., De Petrocellis, L., Saha, B., Mahadevan, A., Visintin, C., Wiley, J.L., et al. (2006). New potent and selective inhibitors of anandamide reuptake with antispastic activity in a mouse model of multiple sclerosis. Br. J. Pharmacol. *147*, 83–91.

97. Pandey, R., Mousawy, K., Nagarkatti, M., and Nagarkatti, P. (2009). Endocannabinoids and immune regulation. Pharmacol Res *60*, 85–92.

98. McKallip, R.J., Lombard, C., Fisher, M., Martin, B.R., Ryu, S., Grant, S., Nagarkatti, P.S., and Nagarkatti, M. (2002). Targeting CB2 cannabinoid receptors as a novel therapy to treat malignant lymphoblastic disease. Blood *100*, 627–634.

99. Gill, S.R., Pop, M., Deboy, R.T., Eckburg, P.B., Turnbaugh, P.J., Samuel, B.S., Gordon, J.I., Relman, D.A., Fraser-Liggett, C.M., and Nelson, K.E. (2006).

Metagenomic analysis of the human distal gut microbiome. Science *312*, 1355–1359.

100.   Spor, A., Koren, O., and Ley, R. (2011). Unravelling the effects of the environment and host genotype on the gut microbiome. Nat. Rev. Microbiol. *9*, 279–290.

101.   Wu, G.D., Chen, J., Hoffmann, C., Bittinger, K., Chen, Y.-Y., Keilbaugh, S.A., Bewtra, M., Knights, D., Walters, W.A., Knight, R., et al. (2011). Linking long-term dietary patterns with gut microbial enterotypes. Science *334*, 105–108.

102.   Yatsunenko, T., Rey, F.E., Manary, M.J., Trehan, I., Dominguez-Bello, M.G., Contreras, M., Magris, M., Hidalgo, G., Baldassano, R.N., Anokhin, A.P., et al. (2012). Human gut microbiome viewed across age and geography. Nature *486*, 222–227.

103.   David, L.A., Maurice, C.F., Carmody, R.N., Gootenberg, D.B., Button, J.E., Wolfe, B.E., Ling, A.V., Devlin, A.S., Varma, Y., Fischbach, M.A., et al. (2014). Diet rapidly and reproducibly alters the human gut microbiome. Nature *505*, 559–563.

104.   Dethlefsen, L., and Relman, D.A. (2011). Incomplete recovery and individualized responses of the human distal gut microbiota to repeated antibiotic perturbation. Proc. Natl. Acad. Sci. U.S.A. *108 Suppl 1*, 4554–4561.

105.   Sturlan, S., Oberhuber, G., Beinhauer, B.G., Tichy, B., Kappel, S., Wang, J., and Rogy, M.A. (2001). Interleukin-10-deficient mice and inflammatory bowel disease associated cancer development. Carcinogenesis *22*, 665–671.

106.   Koren, O., Goodrich, J.K., Cullender, T.C., Spor, A., Laitinen, K.,
Bäckhed, H.K., Gonzalez, A., Werner, J.J., Angenent, L.T., Knight, R., et al.
(2012). Host Remodeling of the Gut Microbiome and Metabolic Changes during
Pregnancy. Cell *150*, 470–480.

107.   Markle, J.G.M., Frank, D.N., Mortin-Toth, S., Robertson, C.E., Feazel,
L.M., Rolle-Kampczyk, U., von Bergen, M., McCoy, K.D., Macpherson, A.J.,
and Danska, J.S. (2013). Sex differences in the gut microbiome drive hormone-
dependent regulation of autoimmunity. Science *339*, 1084–1088.

108.   Paun, A., Yau, C., and Danska, J.S. (2016). Immune recognition and
response to the intestinal microbiome in type 1 diabetes. J. Autoimmun.

109.   Tsurumaki, M., Kotake, M., Iwasaki, M., Saito, M., Tanaka, K., Aw, W.,
Fukuda, S., and Tomita, M. (2015). The application of omics technologies in the
functional evaluation of inulin and inulin-containing prebiotics dietary
supplementation. Nutr Diabetes *5*, e185.

110.   Le Chatelier, E., Nielsen, T., Qin, J., Prifti, E., Hildebrand, F., Falony, G.,
Almeida, M., Arumugam, M., Batto, J.-M., Kennedy, S., et al. (2013). Richness
of human gut microbiome correlates with metabolic markers. Nature *500*, 541–
546.

111.   Round, J.L., and Mazmanian, S.K. (2009). The gut microbiota shapes
intestinal immune responses during health and disease. Nat. Rev. Immunol. *9*,
313–323.

112.   Bevins, C.L., and Salzman, N.H. (2011). Paneth cells, antimicrobial peptides and maintenance of intestinal homeostasis. Nat. Rev. Microbiol. *9*, 356–368.

113.   Hooper, L.V., and Macpherson, A.J. (2010). Immune adaptations that maintain homeostasis with the intestinal microbiota. Nat. Rev. Immunol. *10*, 159–169.

114.   Macpherson, A.J., Geuking, M.B., Slack, E., Hapfelmeier, S., and McCoy, K.D. (2012). The habitat, double life, citizenship, and forgetfulness of IgA. Immunol. Rev. *245*, 132–146.

115.   Bartel, D. P. 2009. MicroRNAs: target recognition and regulatory functions. *Cell* 136: 215-233.

116.   Lee, R. C., R. L. Feinbaum, and V. Ambros. 1993. The C. elegans heterochronic gene lin-4 encodes small RNAs with antisense complementarity to lin-14. *Cell* 75: 843-854.

117.   Rieder, S. A., Nagarkatti, P., & Nagarkatti, M. (2012). Multiple anti-inflammatory pathways triggered by resveratrol lead to amelioration of staphylococcal enterotoxin B-induced lung injury. British Journal of Pharmacology, 167(6), 1244–1258.

118.   Rao, R., Rieder, S. A., Nagarkatti, P., & Nagarkatti, M. (2014). Staphylococcal enterotoxin B-induced microRNA-155 targets SOCS1 to promote acute inflammatory lung injury. Infection and Immunity, 82(7), 2971–2979.

119.   Huang, Y., Shen, X.J., Zou, Q., Wang, S.P., Tang, S.M., Zhang, G.Z., (2011). Biological functions of microRNAs: a review. J. Physiol. Biochem. 67, 129–139.

120.   Pasquinelli, A.E., (2012). MicroRNAs and their targets: recognition, regulation and an emerging reciprocal relationship. Nat. Rev. Genet. 13, 271–282.

121.   Wang, H. Y., & Wang, R.-F. (2007). Regulatory T cells and cancer. Current Opinion in Immunology, 19(2), 217–223.

122.   Sakaguchi, S., & Powrie, F. (2007). Emerging challenges in regulatory T cell function and biology. Science (New York, N.Y.), 317(5838), 627–629.

123.   Fontenot, J. D., Rasmussen, J. P., Williams, L. M., Dooley, J. L., Farr, A. G., & Rudensky, A. Y. (2005). Regulatory T cell lineage specification by the forkhead transcription factor Foxp3. Immunity, 22(3), 329–341.

124.   Fontenot, J. D., Gavin, M. A., & Rudensky, A. Y. (2003). Foxp3 programs the development and function of CD4+CD25+ regulatory T cells. Nature Immunology, 4(4), 330–336.

125.   Esser, C., Rannug, A., & Stockinger, B. (2009). The aryl hydrocarbon receptor in immunity. Trends in Immunology, 30(9), 447–454.

126.   Marshall, N. B., & Kerkvliet, N. I. (2010). Dioxin and immune regulation: emerging role of aryl hydrocarbon receptor in the generation of regulatory T cells. Annals of the New York Academy of Sciences, 1183, 25–37

127.   Singh, N.P., Singh, U.P., Singh, B., Price, R.L., Nagarkatti, M., and Nagarkatti, P.S. (2011). Activation of aryl hydrocarbon receptor (AhR) leads to

reciprocal epigenetic regulation of Foxp3 and IL-17 expression and amelioration of experimental colitis. PLoS ONE 6, e23522.

128.   Nicodeme, E., Jeffrey, K. L., Schaefer, U., Beinke, S., Dewell, S., Chung, C.-W.Tarakhovsky, A. (2010). Suppression of inflammation by a synthetic histone mimic. Nature, 468(7327), 1119–1123.

129.   Medzhitov, R., & Horng, T. (2009). Transcriptional control of the inflammatory response. Nature Reviews.

130.   Li, C., Ebert, P. J. R., & Li, Q.-J. (2013). T cell receptor (TCR) and transforming growth factor β (TGF-β) signaling converge on DNA (cytosine-5)-methyltransferase to control forkhead box protein 3 (Foxp3) locus methylation and inducible regulatory T cell differentiation. The Journal of Biological Chemistry, 288(26), 19127–19139.

131.   Busbee, P. B., Nagarkatti, M., & Nagarkatti, P. S. (2014). Natural indoles, indole-3-carbinol and 3,3'-diindolymethane, inhibit T cell activation by staphylococcal enterotoxin B through epigenetic regulation involving HDAC expression. Toxicology and Applied Pharmacology, 274(1), 7–16.

132.   Ng, H. H., Zhang, Y., Hendrich, B., Johnson, C. A., Turner, B. M., Erdjument-Bromage, H., Bird, A. (1999). MBD2 is a transcriptional repressor belonging to the MeCP1 histone deacetylase complex. Nature Genetics, 23(1), 58–61.

133.   Feng, Q., & Zhang, Y. (2001). The MeCP1 complex represses transcription through preferential binding, remodeling, and deacetylating methylated nucleosomes. Genes & Development

134.   Haberland, M., Montgomery, R. L., & Olson, E. N. (2009). The many roles of histone deacetylases in development and physiology: implications for disease and therapy. Nature Reviews. Genetics, 10(1), 32–42.

135.   Rea, S., Eisenhaber, F., O'Carroll, D., Strahl, B. D., Sun, Z. W., Schmid, M. Jenuwein, T. (2000). Regulation of chromatin structure by site-specific histone H3 methyltransferases. Nature, 406(6796), 593–599.

136.   Pryputniewicz, S.J., Nagarkatti, M., and Nagarkatti, P.S. (1998). Differential induction of apoptosis in activated and resting T cells by 2,3,7,8-tetrachlorodibenzo-p-dioxin (TCDD) and its repercussion on T cell responsiveness. Toxicology *129*, 211–226.

137.   Rao, R., Nagarkatti, P.S., and Nagarkatti, M. (2015). Δ(9) Tetrahydrocannabinol attenuates Staphylococcal enterotoxin B-induced inflammatory lung injury and prevents mortality in mice by modulation of miR-17-92 cluster and induction of T-regulatory cells. Br. J. Pharmacol. *172*, 1792–1806

138.   Singh, N.P., Singh, U.P., Guan, H., Nagarkatti, P., and Nagarkatti, M. (2012). Prenatal exposure to TCDD triggers significant modulation of microRNA expression profile in the thymus that affects consequent gene expression. PLoS ONE *7*, e45054.

139.   Liu, X.S., Chopp, M., Zhang, R.L., Tao, T., Wang, X.L., Kassis, H., Hozeska-Solgot, A., Zhang, L., Chen, C., and Zhang, Z.G. (2011). MicroRNA profiling in subventricular zone after stroke: MiR-124a regulates proliferation of neural progenitor cells through Notch signaling pathway. PLoS ONE 6, e23461.

140.   Yang, X., Hegde, V.L., Rao, R., Zhang, J., Nagarkatti, P.S., and Nagarkatti, M. (2014). Histone modifications are associated with Δ9-tetrahydrocannabinol-mediated alterations in antigen-specific T cell responses. J. Biol. Chem. *289*, 18707–18718.

141.   Lal, G., Zhang, N., van der Touw, W., Ding, Y., Ju, W., Bottinger, E.P., Reid, S.P., Levy, D.E., and Bromberg, J.S. (2009). Epigenetic regulation of Foxp3 expression in regulatory T cells by DNA methylation. J. Immunol. *182*, 259–273.

142.   Florquin, S., & Aaldering, L. (1997). Superantigens: a tool to gain new insight into cellular immunity. Research in Immunology, 148(6), 373–386.

143.   Hasleton, P. S., & Roberts, T. E. (1999). Adult respiratory distress syndrome - an update. Histopathology, 34(4), 285–294.

144.   Wang, L., Liu, Y., Beier, U. H., Han, R., Bhatti, T. R., Akimova, T., & Hancock, W. W. (2013). Foxp3+ T-regulatory cells require DNA methyltransferase 1 expression to prevent development of lethal autoimmunity. Blood, 121(18), 3631–3639.

145.   Bird, A., Taggart, M., Frommer, M., Miller, O. J., & Macleod, D. (1985). A fraction of the mouse genome that is derived from islands of nonmethylated, CpG-rich DNA. Cell, 40(1), 91–99.

146.   Höller, M., Westin, G., Jiricny, J., & Schaffner, W. (1988). Sp1 transcription factor binds DNA and activates transcription even when the binding site is CpG methylated. Genes & Development, 2(9), 1127–1135.

147.   Brandeis, M., Frank, D., Keshet, I., Siegfried, Z., Mendelsohn, M., Names, A. Cedar, H. (1994). Spl elements protect a CpG island from de novo methylation. Nature, 371(6496), 435–438

148.   Subramaniam, M., Hawse, J. R., Rajamannan, N. M., Ingle, J. N., & Spelsberg, T. C. (2010). Functional role of KLF10 in multiple disease processes. BioFactors (Oxford, England), 36(1), 8–18.

149.   Dweep, H., Gretz, N., & Sticht, C. (2014). miRWalk database for miRNA-target interactions. Methods in Molecular Biology (Clifton, N.J.), 1182, 289–305.

150.   Ji Diana Lee, Y., Kim, V., Muth, D. C., & Witwer, K. W. (2015). Validated MicroRNA Target Databases: An Evaluation. Drug Development Research, 76(7), 389–396.

151.   Pinchuk, I. V., Beswick, E. J., & Reyes, V. E. (2010). Staphylococcal enterotoxins. Toxins, 2(8), 2177–2197.

152.   Henghold, W. B. (2004). Other biologic toxin bioweapons: ricin, staphylococcal enterotoxin B, and trichothecene mycotoxins. Dermatologic Clinics, 22(3), 257–262.

153.   Baker, M. D., & Acharya, K. R. (2004). Superantigens: structure-function relationships. International Journal of Medical Microbiology: IJMM, 293(7-8), 529–537.

154.   Rieder, S. A., Nagarkatti, P., & Nagarkatti, M. (2012). Multiple anti-inflammatory pathways triggered by resveratrol lead to amelioration of staphylococcal enterotoxin B-induced lung injury. British Journal of Pharmacology, 167(6), 1244–1258.

155.   Rao, R., Rieder, S. A., Nagarkatti, P., & Nagarkatti, M. (2014). Staphylococcal enterotoxin B-induced microRNA-155 targets SOCS1 to promote acute inflammatory lung injury. Infection and Immunity, 82(7), 2971–2979.

156.   Fraser, J. D. (1989). High-affinity binding of staphylococcal enterotoxins A and B to HLA-DR. Nature, 339(6221), 221–223.

157.   Busbee, P.B., Rouse, M., Nagarkatti, M., and Nagarkatti, P.S. (2013). Use of natural AhR ligands as potential therapeutic modalities against inflammatory disorders. Nutr. Rev. *71*, 353–369.

158.   Esser, C., and Rannug, A. (2015). The aryl hydrocarbon receptor in barrier organ physiology, immunology, and toxicology. Pharmacol. Rev. *67*, 259–279.

159.   Nagarkatti, P.S., Sweeney, G.D., Gauldie, J., and Clark, D.A. (1984). Sensitivity to suppression of cytotoxic T cell generation by 2,3,7,8-tetrachlorodibenzo-p-dioxin (TCDD) is dependent on the Ah genotype of the murine host. Toxicol. Appl. Pharmacol. *72*, 169–176.

160.   Hori, S., Nomura, T., and Sakaguchi, S. (2003). Control of regulatory T cell development by the transcription factor Foxp3. Science *299*, 1057–1061.

161.   Marshall, N.B., Vorachek, W.R., Steppan, L.B., Mourich, D.V., and Kerkvliet, N.I. (2008). Functional characterization and gene expression analysis of CD4+ CD25+ regulatory T cells generated in mice treated with 2,3,7,8-tetrachlorodibenzo-p-dioxin. J. Immunol. *181*, 2382–2391.

162.   Singh, N.P., Singh, U.P., Singh, B., Price, R.L., Nagarkatti, M., and Nagarkatti, P.S. (2011). Activation of aryl hydrocarbon receptor (AhR) leads to reciprocal epigenetic regulation of FoxP3 and IL-17 expression and amelioration of experimental colitis. PLoS ONE *6*, e23522.

163.   Zhan, Q., Fang, Y., Deng, X., Chen, H., Jin, J., Lu, X.Shen, B. (2015). The Interplay Between miR-148a and DNMT1 Might be exploited for Pancreatic Cancer Therapy. Cancer Investigation, 33(7), 267–275.

164.   Wu, M.-Y., Fu, J., Xiao, X., Wu, J., & Wu, R.-C. (2014). MiR-34a regulates therapy resistance by targeting HDAC1 and HDAC7 in breast cancer. Cancer Letters, 354(2), 311–319.

165.   Ptashne, M. (2007). On the use of the word "epigenetic." Current Biology: CB, 17(7), R233–236.

166.   Lim, L. P., Lau, N. C., Garrett-Engele, P., Grimson, A., Schelter, J. M., Castle, J.Johnson, J. M. (2005). Microarray analysis shows that some microRNAs downregulate large numbers of target mRNAs. Nature, 433(7027), 769–773.

167.   Slotkin, R. K., & Martienssen, R. (2007). Transposable elements and the epigenetic regulation of the genome. Nature Reviews. Genetics, 8(4), 272–285.

168.   Kim, H.-P., and Leonard, W.J. (2007). CREB/ATF-dependent T cell receptor–induced FoxP3 gene expression: a role for DNA methylation. J Exp Med *204*, 1543–1551.

169.   Janson, P.C.J., Winerdal, M.E., Marits, P., Thörn, M., Ohlsson, R., and Winqvist, O. (2008). FOXP3 promoter demethylation reveals the committed Treg population in humans. PLoS ONE *3*, e1612.

170.   Macleod, D., Charlton, J., Mullins, J., & Bird, A. P. (1994). Sp1 sites in the mouse aprt gene promoter are required to prevent methylation of the CpG island. Genes & Development, 8(19), 2282–2292.

171.   Venuprasad, K., Huang, H., Harada, Y., Elly, C., Subramaniam, M.,
Spelsberg, T.,Liu, Y.-C. (2008). The E3 ubiquitin ligase Itch regulates expression
of transcription factor Foxp3 and airway inflammation by enhancing the function
of transcription factor TIEG1. Nature Immunology, 9(3), 245–253.

172.   Turnbaugh, P.J., Ley, R.E., Mahowald, M.A., Magrini, V., Mardis, E.R.,
and Gordon, J.I. (2006). An obesity-associated gut microbiome with increased
capacity for energy harvest. Nature *444*, 1027–1031.

173.   Turnbaugh, P.J., Bäckhed, F., Fulton, L., and Gordon, J.I. (2008). Diet-
induced obesity is linked to marked but reversible alterations in the mouse distal
gut microbiome. Cell Host Microbe *3*, 213–223.

174.   Vijay-Kumar, M., Aitken, J.D., Carvalho, F.A., Cullender, T.C., Mwangi,
S., Srinivasan, S., Sitaraman, S.V., Knight, R., Ley, R.E., and Gewirtz, A.T.
(2010). Metabolic syndrome and altered gut microbiota in mice lacking Toll-like
receptor 5. Science *328*, 228–231.

175.   Gill, S.R., Pop, M., Deboy, R.T., Eckburg, P.B., Turnbaugh, P.J., Samuel,
B.S., Gordon, J.I., Relman, D.A., Fraser-Liggett, C.M., and Nelson, K.E. (2006).
Metagenomic analysis of the human distal gut microbiome. Science *312*, 1355–
1359.

176.   Koren, O., Goodrich, J.K., Cullender, T.C., Spor, A., Laitinen, K.,
Bäckhed, H.K., Gonzalez, A., Werner, J.J., Angenent, L.T., Knight, R., et al.
(2012). Host Remodeling of the Gut Microbiome and Metabolic Changes during
Pregnancy. Cell *150*, 470–480.

160

177.   Markle, J.G.M., Frank, D.N., Mortin-Toth, S., Robertson, C.E., Feazel, L.M., Rolle-Kampczyk, U., von Bergen, M., McCoy, K.D., Macpherson, A.J., and Danska, J.S. (2013). Sex differences in the gut microbiome drive hormone-dependent regulation of autoimmunity. Science *339*, 1084–1088.

178.   Paun, A., Yau, C., and Danska, J.S. (2016). Immune recognition and response to the intestinal microbiome in type 1 diabetes. J. Autoimmun.

179.   Tsurumaki, M., Kotake, M., Iwasaki, M., Saito, M., Tanaka, K., Aw, W., Fukuda, S., and Tomita, M. (2015). The application of omics technologies in the functional evaluation of inulin and inulin-containing prebiotics dietary supplementation. Nutr Diabetes *5*, e185.

180.   Le Chatelier, E., Nielsen, T., Qin, J., Prifti, E., Hildebrand, F., Falony, G., Almeida, M., Arumugam, M., Batto, J.-M., Kennedy, S., et al. (2013). Richness of human gut microbiome correlates with metabolic markers. Nature *500*, 541–546.

181.   Bevins, C.L., and Salzman, N.H. (2011). Paneth cells, antimicrobial peptides and maintenance of intestinal homeostasis. Nat. Rev. Microbiol. *9*, 356–368.

182.   Cani, P.D., Amar, J., Iglesias, M.A., Poggi, M., Knauf, C., Bastelica, D., Neyrinck, A.M., Fava, F., Tuohy, K.M., Chabo, C., et al. (2007). Metabolic Endotoxemia Initiates Obesity and Insulin Resistance. Diabetes *56*, 1761–1772.

183.   Cani, P.D., Possemiers, S., Wiele, T.V. de, Guiot, Y., Everard, A., Rottier, O., Geurts, L., Naslain, D., Neyrinck, A., Lambert, D.M., et al. (2009). Changes

in gut microbiota control inflammation in obese mice through a mechanism involving GLP-2-driven improvement of gut permeability. Gut *58*, 1091–1103.

184.   Ghoshal, S., Witta, J., Zhong, J., de Villiers, W., and Eckhardt, E. (2009). Chylomicrons promote intestinal absorption of lipopolysaccharides. J. Lipid Res. *50*, 90–97.

185.   Wright, S.D., Ramos, R.A., Tobias, P.S., Ulevitch, R.J., and Mathison, J.C. (1990). CD14, a receptor for complexes of lipopolysaccharide (LPS) and LPS binding protein. Science *249*, 1431–1433.

186.   Dentener, M.A., Bazil, V., Von Asmuth, E.J., Ceska, M., and Buurman, W.A. (1993).

187.   Involvement of CD14 in lipopolysaccharide-induced tumor necrosis factor-alpha, IL-6 and IL-8 release by human monocytes and alveolar macrophages. J. Immunol. *150*, 2885–2891.

188.   Engeli, S., Böhnke, J., Feldpausch, M., Gorzelniak, K., Janke, J., Bátkai, S., Pacher, P., Harvey-White, J., Luft, F.C., Sharma, A.M., et al. (2005). Activation of the Peripheral Endocannabinoid System in Human Obesity. Diabetes *54*, 2838–2843.

189.   Dysregulation of the peripheral and adipose tissue endocannabinoid system in human abdominal obesity. ***Diabetes***

190.   Starowicz, K.M., Cristino, L., Matias, I., Capasso, R., Racioppi, A., Izzo, A.A., and Di Marzo, V. (2008). Endocannabinoid dysregulation in the pancreas and adipose tissue of mice fed with a high-fat diet. Obesity (Silver Spring) *16*, 553–565.

162

191.	D'Eon, T.M., Pierce, K.A., Roix, J.J., Tyler, A., Chen, H., and Teixeira, S.R. (2008). The Role of Adipocyte Insulin Resistance in the Pathogenesis of Obesity-Related Elevations in Endocannabinoids. Diabetes *57*, 1262–1268.

192.	Izzo, A.A., Piscitelli, F., Capasso, R., Aviello, G., Romano, B., Borrelli, F., Petrosino, S., and Di Marzo, V. (2009). Peripheral endocannabinoid dysregulation in obesity: relation to intestinal motility and energy processing induced by food deprivation and re-feeding. Br. J. Pharmacol. *158*, 451–461.

193.	Muccioli, G.G., Naslain, D., Bäckhed, F., Reigstad, C.S., Lambert, D.M., Delzenne, N.M., and Cani, P.D. (2010). The endocannabinoid system links gut microbiota to adipogenesis. Mol. Syst. Biol. *6*, 392.

194.	Liu, J., Batkai, S., Pacher, P., Harvey-White, J., Wagner, J.A., Cravatt, B.F., Gao, B., and Kunos, G. (2003). Lipopolysaccharide induces anandamide synthesis in macrophages via CD14/MAPK/phosphoinositide 3-kinase/NF-kappaB independently of platelet-activating factor. J. Biol. Chem. *278*, 45034–45039.

195.	Klein, T.W. (2005). Cannabinoid-based drugs as anti-inflammatory therapeutics. Nat Rev Immunol *5*, 400–411.

196.	Di Marzo, V., and Després, J.-P. (2009). CB1 antagonists for obesity--what lessons have we learned from rimonabant? Nat Rev Endocrinol *5*, 633–638.

197.	Di Marzo, V., Goparaju, S.K., Wang, L., Liu, J., Bátkai, S., Járai, Z., Fezza, F., Miura, G.I., Palmiter, R.D., Sugiura, T., et al. (2001). Leptin-regulated endocannabinoids are involved in maintaining food intake. Nature *410*, 822–825.

163

198.   Wang, Q., Perrard, X.D., Perrard, J.L., Mansoori, A., Smith, C.W., Ballantyne, C.M., and Wu, H. (2011). Effect of the cannabinoid receptor-1 antagonist rimonabant on inflammation in mice with diet-induced obesity. Obesity (Silver Spring) *19*, 505–513.

199.   Jourdan, T., Djaouti, L., Demizieux, L., Gresti, J., Vergès, B., and Degrace, P. (2010). CB1 antagonism exerts specific molecular effects on visceral and subcutaneous fat and reverses liver steatosis in diet-induced obese mice. Diabetes *59*, 926–934.

200.   Bergholm, R., Sevastianova, K., Santos, A., Kotronen, A., Urjansson, M., Hakkarainen, A., Lundbom, J., Tiikkainen, M., Rissanen, A., Lundbom, N., et al. (2013). CB1 blockade-induced weight loss over 48 weeks decreases liver fat in proportion to weight loss in humans. Int J Obes *37*, 699–703.

201.   Després, J.-P. (2006). How effective is rimonabant at promoting and maintaining weight loss in patients with obesity? Nat Clin Pract End Met *2*, 428–429.

202.   Pi-Sunyer, F.X., Aronne, L.J., Heshmati, H.M., Devin, J., Rosenstock, J., and RIO-North America Study Group (2006). Effect of rimonabant, a cannabinoid-1 receptor blocker, on weight and cardiometabolic risk factors in overweight or obese patients: RIO-North America: a randomized controlled trial. JAMA *295*, 761–775.

203.   Lentzsch, S., Gries, M., Janz, M., Bargou, R., Dörken, B., and Mapara, M.Y. (2003). Macrophage inflammatory protein 1-alpha (MIP-1 alpha) triggers

migration and signaling cascades mediating survival and proliferation in multiple myeloma (MM) cells. Blood *101*, 3568–3573.

204.   Brenchley, J.M., Price, D.A., Schacker, T.W., Asher, T.E., Silvestri, G., Rao, S., Kazzaz, Z., Bornstein, E., Lambotte, O., Altmann, D., et al. (2006). Microbial translocation is a cause of systemic immune activation in chronic HIV infection. Nat Med *12*, 1365–1371.

205.   Könner, A.C., Janoschek, R., Plum, L., Jordan, S.D., Rother, E., Ma, X., Xu, C., Enriori, P., Hampel, B., Barsh, G.S., et al. (2007). Insulin action in AgRP-expressing neurons is required for suppression of hepatic glucose production. Cell Metab. *5*, 438–449.

206.   Enos, R.T., Velázquez, K.T., McClellan, J.L., Cranford, T.L., Walla, M.D., and Murphy, E.A. (2014). Reducing the Dietary Omega-6:Omega-3 Utilizing α-Linolenic Acid; Not a Sufficient Therapy for Attenuating High-Fat-Diet-Induced Obesity Development Nor Related Detrimental Metabolic and Adipose Tissue Inflammatory Outcomes. PLOS ONE *9*, e94897.

207.   Enos, R.T., Davis, J.M., Velázquez, K.T., McClellan, J.L., Day, S.D., Carnevale, K.A., and Murphy, E.A. (2013). Influence of dietary saturated fat content on adiposity, macrophage behavior, inflammation, and metabolism: composition matters. J Lipid Res *54*, 152–163.

208.   Matthews, D.R., Hosker, J.P., Rudenski, A.S., Naylor, B.A., Treacher, D.F., and Turner, R.C. (1985). Homeostasis model assessment: insulin resistance and beta-cell function from fasting plasma glucose and insulin concentrations in man. Diabetologia *28*, 412–419.

209.   Chassaing, B., Koren, O., Goodrich, J.K., Poole, A.C., Srinivasan, S., Ley, R.E., and Gewirtz, A.T. (2015). Dietary emulsifiers impact the mouse gut microbiota promoting colitis and metabolic syndrome. Nature *519*, 92–96.

210.   Sido, J.M., Nagarkatti, P.S., and Nagarkatti, M. (2016). Production of endocannabinoids by activated T cells and B cells modulates inflammation associated with delayed type hypersensitivity. Eur. J. Immunol.

211.   Fadrosh, D.W., Ma, B., Gajer, P., Sengamalay, N., Ott, S., Brotman, R.M., and Ravel, J. (2014). An improved dual-indexing approach for multiplexed 16S rRNA gene sequencing on the Illumina MiSeq platform. Microbiome *2*, 1–7.

212.   Caporaso, J.G., Kuczynski, J., Stombaugh, J., Bittinger, K., Bushman, F.D., Costello, E.K., Fierer, N., Peña, A.G., Goodrich, J.K., Gordon, J.I., et al. (2010). QIIME allows analysis of high-throughput community sequencing data. Nature Methods *7*, 335–336.

213.   Trompette, A., Gollwitzer, E.S., Yadava, K., Sichelstiel, A.K., Sprenger, N., Ngom-Bru, C., Blanchard, C., Junt, T., Nicod, L.P., Harris, N.L., et al. (2014). Gut microbiota metabolism of dietary fiber influences allergic airway disease and hematopoiesis. Nat Med *20*, 159–166.

214.   Zhao, G., Nyman, M., and Åke Jönsson, J. (2006). Rapid determination of short-chain fatty acids in colonic contents and faeces of humans and rats by acidified water-extraction and direct-injection gas chromatography. Biomed. Chromatogr. *20*, 674–682

215.   Poirier, B., Bidouard, J.-P., Cadrouvele, C., Marniquet, X., Staels, B., O'Connor, S.E., Janiak, P., and Herbert, J.-M. (2005). The anti-obesity effect of

rimonabant is associated with an improved serum lipid profile. Diabetes Obes Metab *7*, 65–72.

216.   Jbilo, O., Ravinet-Trillou, C., Arnone, M., Buisson, I., Bribes, E., Péleraux, A., Pénarier, G., Soubrié, P., Le Fur, G., Galiègue, S., et al. (2005). The CB1 receptor antagonist rimonabant reverses the diet-induced obesity phenotype through the regulation of lipolysis and energy balance. FASEB J. *19*, 1567–1569.

217.   Meng, F., and Lowell, C.A. (1997). Lipopolysaccharide (LPS)-induced macrophage activation and signal transduction in the absence of Src-family kinases Hck, Fgr, and Lyn. J. Exp. Med. *185*, 1661–1670.

218.   Everard, A., Belzer, C., Geurts, L., Ouwerkerk, J.P., Druart, C., Bindels, L.B., Guiot, Y., Derrien, M., Muccioli, G.G., Delzenne, N.M., et al. (2013). Cross-talk between Akkermansia muciniphila and intestinal epithelium controls diet-induced obesity. Proc. Natl. Acad. Sci. U.S.A. *110*, 9066–9071.

219.   Derrien, M., Vaughan, E.E., Plugge, C.M., and de Vos, W.M. (2004). Akkermansia muciniphila gen. nov., sp. nov., a human intestinal mucin-degrading bacterium. Int. J. Syst. Evol. Microbiol. *54*, 1469–1476.

220.   Santacruz, A., Collado, M.C., García-Valdés, L., Segura, M.T., Martín-Lagos, J.A., Anjos, T., Martí-Romero, M., Lopez, R.M., Florido, J., Campoy, C., et al. (2010). Gut microbiota composition is associated with body weight, weight gain and biochemical parameters in pregnant women. Br. J. Nutr. *104*, 83–92.

221.   Hansen, C.H.F., Krych, L., Nielsen, D.S., Vogensen, F.K., Hansen, L.H., Sørensen, S.J., Buschard, K., and Hansen, A.K. (2012). Early life treatment with

167

vancomycin propagates Akkermansia muciniphila and reduces diabetes incidence in the NOD mouse. Diabetologia *55*, 2285–2294.

222.   Derrien, M., Van Baarlen, P., Hooiveld, G., Norin, E., Müller, M., and de Vos, W.M. (2011). Modulation of Mucosal Immune Response, Tolerance, and Proliferation in Mice Colonized by the Mucin-Degrader Akkermansia muciniphila. Front Microbiol *2*, 166.

223.   van Passel, M.W.J., Kant, R., Zoetendal, E.G., Plugge, C.M., Derrien, M., Malfatti, S.A., Chain, P.S.G., Woyke, T., Palva, A., de Vos, W.M., et al. (2011). The genome of Akkermansia muciniphila, a dedicated intestinal mucin degrader, and its use in exploring intestinal metagenomes. PLoS ONE *6*, e16876.

224.   Cani, P.D., Possemiers, S., Wiele, T.V. de, Guiot, Y., Everard, A., Rottier, O., Geurts, L., Naslain, D., Neyrinck, A., Lambert, D.M., et al. (2009). Changes in gut microbiota control inflammation in obese mice through a mechanism involving GLP-2-driven improvement of gut permeability. Gut *58*, 1091–1103.

225.   Harris, K., Kassis, A., Major, G., ve, Chou, C.J., Harris, K., Kassis, A., Major, G., ve, and Chou, C.J. (2012). Is the Gut Microbiota a New Factor Contributing to Obesity and Its Metabolic Disorders?, Is the Gut Microbiota a New Factor Contributing to Obesity and Its Metabolic Disorders? Journal of Obesity, Journal of Obesity *2012, 2012*, e879151.

226.   Zhang, H., DiBaise, J.K., Zuccolo, A., Kudrna, D., Braidotti, M., Yu, Y., Parameswaran, P., Crowell, M.D., Wing, R., Rittmann, B.E., et al. (2009). Human gut microbiota in obesity and after gastric bypass. PNAS *106*, 2365–2370.

227.   Martínez, I., Perdicaro, D.J., Brown, A.W., Hammons, S., Carden, T.J., Carr, T.P., Eskridge, K.M., and Walter, J. (2013). Diet-Induced Alterations of Host Cholesterol Metabolism Are Likely To Affect the Gut Microbiota Composition in Hamsters. Appl. Environ. Microbiol. *79*, 516–524.

228.   Kaakoush, N.O. (2015). Insights into the Role of Erysipelotrichaceae in the Human Host. Front Cell Infect Microbiol *5*.

229.   Després, J.-P., Golay, A., Sjöström, L., and Rimonabant in Obesity-Lipids Study Group (2005). Effects of rimonabant on metabolic risk factors in overweight patients with dyslipidemia. N. Engl. J. Med. *353*, 2121–2134.

230.   Schäfer, A., Pfrang, J., Neumüller, J., Fiedler, S., Ertl, G., and Bauersachs, J. (2008). The cannabinoid receptor-1 antagonist rimonabant inhibits platelet activation and reduces pro-inflammatory chemokines and leukocytes in Zucker rats. Br. J. Pharmacol. *154*, 1047–1054.

231.   Cota, D., Sandoval, D.A., Olivieri, M., Prodi, E., D'Alessio, D.A., Woods, S.C., Seeley, R.J., and Obici, S. (2009). Food intake-independent effects of CB1 antagonism on glucose and lipid metabolism. Obesity (Silver Spring) *17*, 1641–1645.

232.   Talukdar, S., Oh, D.Y., Bandyopadhyay, G., Li, D., Xu, J., McNelis, J., Lu, M., Li, P., Yan, Q., Zhu, Y., et al. (2012). Neutrophils mediate insulin resistance in mice fed a high-fat diet through secreted elastase. Nat. Med. *18*, 1407–1412.

233.   Verty, A.N.A., Allen, A.M., and Oldfield, B.J. (2009). The Effects of Rimonabant on Brown Adipose Tissue in Rat: Implications for Energy Expenditure. Obesity *17*, 254–261.

234.   Bellocchio, L., Cervino, C., Vicennati, V., Pasquali, R., and Pagotto, U. (2008). Cannabinoid type 1 receptor: another arrow in the adipocytes' bow. J. Neuroendocrinol. *20 Suppl 1*, 130–138.

235.   Shi, D., Zhan, X., Yu, X., Jia, M., Zhang, Y., Yao, J., Hu, X., and Bao, Z. (2014). Inhibiting CB1 receptors improves lipogenesis in an in vitro non-alcoholic fatty liver disease model. Lipids Health Dis *13*, 173.

236.   Côté, M., Matias, I., Lemieux, I., Petrosino, S., Alméras, N., Després, J.-P., and Di Marzo, V. (2007). Circulating endocannabinoid levels, abdominal adiposity and related cardiometabolic risk factors in obese men. Int J Obes (Lond) *31*, 692–699.

237.   Trillou, C.R., Arnone, M., Delgorge, C., Gonalons, N., Keane, P., Maffrand, J.-P., and Soubrié, P. (2003). Anti-obesity effect of SR141716, a CB1 receptor antagonist, in diet-induced obese mice. American Journal of Physiology - Regulatory, Integrative and Comparative Physiology *284*, R345–R353.

238.   Ravinet Trillou, C., Delgorge, C., Menet, C., Arnone, M., and Soubrié, P. (2004). CB1 cannabinoid receptor knockout in mice leads to leanness, resistance to diet-induced obesity and enhanced leptin sensitivity. Int J Obes Relat Metab Disord *28*, 640–648.

239.   Caesar, R., Tremaroli, V., Kovatcheva-Datchary, P., Cani, P.D., and Bäckhed, F. (2015). Crosstalk between Gut Microbiota and Dietary Lipids

170

Aggravates WAT Inflammation through TLR Signaling. Cell Metab. *22*, 658–668.

240.   Seki, E., De Minicis, S., Osterreicher, C.H., Kluwe, J., Osawa, Y., Brenner, D.A., and Schwabe, R.F. (2007). TLR4 enhances TGF-beta signaling and hepatic fibrosis. Nat. Med. *13*, 1324–1332.

241.   Cani, P.D., Neyrinck, A.M., Fava, F., Knauf, C., Burcelin, R.G., Tuohy, K.M., Gibson, G.R., and Delzenne, N.M. (2007). Selective increases of bifidobacteria in gut microflora improve high-fat-diet-induced diabetes in mice through a mechanism associated with endotoxaemia. Diabetologia *50*, 2374–2383.

242.   Round, J.L., and Mazmanian, S.K. (2009). The gut microbiome shapes intestinal immune responses during health and disease. Nat Rev Immunol *9*, 313–323.

243.   Everard, A., Lazarevic, V., Derrien, M., Girard, M., Muccioli, G.G., Neyrinck, A.M., Possemiers, S., Holle, A.V., François, P., Vos, W.M. de, et al. (2011). Responses of Gut Microbiota and Glucose and Lipid Metabolism to Prebiotics in Genetic Obese and Diet-Induced Leptin-Resistant Mice. Diabetes *60*, 2775–2786.

244.   Derrien, M., Vaughan, E.E., Plugge, C.M., and de Vos, W.M. (2004). Akkermansia muciniphila gen. nov., sp. nov., a human intestinal mucin-degrading bacterium. Int. J. Syst. Evol. Microbiol. *54*, 1469–1476.

245.   Roopchand, D.E., Carmody, R.N., Kuhn, P., Moskal, K., Rojas-Silva, P., Turnbaugh, P.J., and Raskin, I. (2015). Dietary Polyphenols Promote Growth of

the Gut Bacterium Akkermansia muciniphila and Attenuate High-Fat Diet-Induced Metabolic Syndrome. Diabetes *64*, 2847–2858.

246.   Li, J., Sung, C.Y.J., Lee, N., Ni, Y., Pihlajamäki, J., Panagiotou, G., and El-Nezami, H. (2016). Probiotics modulated gut microbiota suppresses hepatocellular carcinoma growth in mice. PNAS *113*, E1306–E1315.

247.   Dao, M.C., Everard, A., Aron-Wisnewsky, J., Sokolovska, N., Prifti, E., Verger, E.O., Kayser, B.D., Levenez, F., Chilloux, J., Hoyles, L., et al. (2016). Akkermansia muciniphila and improved metabolic health during a dietary intervention in obesity: relationship with gut microbiome richness and ecology. Gut *65*, 426–436.

248.   Kang, C.-S., Ban, M., Choi, E.-J., Moon, H.-G., Jeon, J.-S., Kim, D.-K., Park, S.-K., Jeon, S.G., Roh, T.-Y., Myung, S.-J., et al. (2013). Extracellular vesicles derived from gut microbiota, especially Akkermansia muciniphila, protect the progression of dextran sulfate sodium-induced colitis. PLoS ONE *8*, e76520

249.   Alard, J., Lehrter, V., Rhimi, M., Mangin, I., Peucelle, V., Abraham, A.-L., Mariadassou, M., Maguin, E., Waligora-Dupriet, A.-J., Pot, B., et al. (2015). Beneficial metabolic effects of selected probiotics on diet-induced obesity and insulin resistance in mice are associated with improvement of dysbiotic gut microbiota. Environ. Microbiol.

250.   Gersemann, M., Becker, S., Kübler, I., Koslowski, M., Wang, G., Herrlinger, K.R., Griger, J., Fritz, P., Fellermann, K., Schwab, M., et al. (2009).

Differences in goblet cell differentiation between Crohn's disease and ulcerative colitis. Differentiation *77*, 84–94.

251.   Besten, G. den, Bleeker, A., Gerding, A., Eunen, K. van, Havinga, R., Dijk, T.H. van, Oosterveer, M.H., Jonker, J.W., Groen, A.K., Reijngoud, D.-J., et al. (2015). Short-Chain Fatty Acids Protect Against High-Fat Diet–Induced Obesity via a PPARγ-Dependent Switch From Lipogenesis to Fat Oxidation. Diabetes *64*, 2398–2408.

252.   Park, J.-S., Lee, E.-J., Lee, J.-C., Kim, W.-K., and Kim, H.-S. (2007). Anti-inflammatory effects of short chain fatty acids in IFN-gamma-stimulated RAW 264.7 murine macrophage cells: involvement of NF-kappaB and ERK signaling pathways. Int. Immunopharmacol. *7*, 70–77.

253.   Ji, J., Shu, D., Zheng, M., Wang, J., Luo, C., Wang, Y., Guo, F., Zou, X., Lv, X., Li, Y., et al. (2016). Microbial metabolite butyrate facilitates M2 macrophage polarization and function. Sci Rep *6*, 24838

254.   Lukovac, S., Belzer, C., Pellis, L., Keijser, B.J., Vos, W.M. de, Montijn, R.C., and Roeselers, G. (2014). Differential Modulation by Akkermansia muciniphila and Faecalibacterium prausnitzii of Host Peripheral Lipid Metabolism and Histone Acetylation in Mouse Gut Organoids. mBio *5*, e01438–14.

255.   Psichas, A., Sleeth, M.L., Murphy, K.G., Brooks, L., Bewick, G.A., Hanyaloglu, A.C., Ghatei, M.A., Bloom, S.R., and Frost, G. (2015). The short chain fatty acid propionate stimulates GLP-1 and PYY secretion via free fatty acid receptor 2 in rodents. Int J Obes *39*, 424–429

173

256. Alberti, K.G.M.M., Eckel, R.H., Grundy, S.M., Zimmet, P.Z., Cleeman, J.I., Donato, K.A., Fruchart, J.-C., James, W.P.T., Loria, C.M., Smith, S.C., et al. (2009). Harmonizing the metabolic syndrome: a joint interim statement of the International Diabetes Federation Task Force on Epidemiology and Prevention; National Heart, Lung, and Blood Institute; American Heart Association; World Heart Federation; International Atherosclerosis Society; and International Association for the Study of Obesity. Circulation 120, 1640–1645.

257. Flegal, K.M., Carroll, M.D., Ogden, C.L., and Curtin, L.R. (2010). Prevalence and trends in obesity among US adults, 1999-2008. JAMA 303, 235– 241.

258. Prevalence of obesity and trends in body mass index among US children and adolescents, 1999-2010. - PubMed - NCBI.

259. Chawla, A., Nguyen, K.D., and Goh, Y.P.S. (2011). Macrophage-mediated inflammation in metabolic disease. Nat. Rev. Immunol. 11, 738–749.

260. Enos, R.T., Velázquez, K.T., McClellan, J.L., Cranford, T.L., Walla, M.D., and Murphy, E.A. (2014). Reducing the dietary omega-6:omega-3 utilizing α-linolenic acid; not a sufficient therapy for attenuating high-fat-diet-induced obesity development nor related detrimental metabolic and adipose tissue inflammatory outcomes. PLoS ONE 9, e94897.

174

261.   Weisberg, S.P., McCann, D., Desai, M., Rosenbaum, M., Leibel, R.L., and Ferrante, A.W. (2003). Obesity is associated with macrophage accumulation in adipose tissue. J. Clin. Invest. 112, 1796–1808.

262.   O'Rourke, R.W., White, A.E., Metcalf, M.D., Olivas, A.S., Mitra, P., Larison, W.G., Cheang, E.C., Varlamov, O., Corless, C.L., Roberts, C.T., et al. (2011). Hypoxia-induced inflammatory cytokine secretion in human adipose tissue stromovascular cells. Diabetologia 54, 1480–1490.

263.   Hotamisligil, G.S., Shargill, N.S., and Spiegelman, B.M. (1993). Adipose expression of tumor necrosis factor-alpha: direct role in obesity-linked insulin resistance. Science 259, 87–91.

264.   Vandanmagsar, B., Youm, Y.-H., Ravussin, A., Galgani, J.E., Stadler, K., Mynatt, R.L., Ravussin, E., Stephens, J.M., and Dixit, V.D. (2011). The NLRP3 inflammasome instigates obesity-induced inflammation and insulin resistance. Nat. Med. 17, 179–188.

265.   Wen, H., Gris, D., Lei, Y., Jha, S., Zhang, L., Huang, M.T.-H., Brickey, W.J., and Ting, J.P.-Y. (2011). Fatty acid-induced NLRP3-ASC inflammasome activation interferes with insulin signaling. Nat. Immunol. 12, 408–415.

266.   Esser, N., L'homme, L., De Roover, A., Kohnen, L., Scheen, A.J.,

Moutschen, M., Piette, J., Legrand-Poels, S., and Paquot, N. (2013). Obesity

phenotype is related to NLRP3 inflammasome activity and immunological profile

of visceral adipose tissue. Diabetologia 56, 2487–2497.

267.   Gordon, S., and Taylor, P.R. (2005). Monocyte and macrophage

heterogeneity. Nat. Rev. Immunol. 5, 953–964.

268.   Mantovani, A., Sica, A., Sozzani, S., Allavena, P., Vecchi, A., and Locati,

M. (2004). The chemokine system in diverse forms of macrophage activation and

polarization. Trends Immunol. 25, 677–686.

269.   Gordon, S. (2003). Alternative activation of macrophages. Nat. Rev.

Immunol. 3, 23–35.

270.   Odegaard, J.I., Ricardo-Gonzalez, R.R., Goforth, M.H., Morel, C.R.,

Subramanian, V., Mukundan, L., Red Eagle, A., Vats, D., Brombacher, F.,

Ferrante, A.W., et al. (2007). Macrophage-specific PPARgamma controls

alternative activation and improves insulin resistance. Nature 447, 1116–1120.

271.   Yang, X., Wang, X., Liu, D., Yu, L., Xue, B., and Shi, H. (2014).

Epigenetic regulation of macrophage polarization by DNA methyltransferase 3b.

Mol. Endocrinol. 28, 565–574.

272.   Suzuki, K., Kumanogoh, A., and Kikutani, H. (2008). Semaphorins and their receptors in immune cell interactions. Nat. Immunol. 9, 17–23.

273.   Takamatsu, H., and Kumanogoh, A. (2012). Diverse roles for semaphorin-plexin signaling in the immune system. Trends Immunol. 33, 127–135.

274.   Ramkhelawon, B., Hennessy, E.J., Ménager, M., Ray, T.D., Sheedy, F.J., Hutchison, S., Wanschel, A., Oldebeken, S., Geoffrion, M., Spiro, W., et al. (2014). Netrin-1 promotes adipose tissue macrophage retention and insulin resistance in obesity. Nat. Med. 20, 377–384.

275.   Shimizu, I., Yoshida, Y., Moriya, J., Nojima, A., Uemura, A., Kobayashi, Y., and Minamino, T. (2013). Semaphorin3E-induced inflammation contributes to insulin resistance in dietary obesity. Cell Metab. 18, 491–504.

276.   Ziccardi, P., Nappo, F., Giugliano, G., Esposito, K., Marfella, R., Cioffi, M., D'Andrea, F., Molinari, A.M., and Giugliano, D. (2002). Reduction of inflammatory cytokine concentrations and improvement of endothelial functions in obese women after weight loss over one year. Circulation 105, 804–809.

277.   Yang, W.S., Lee, W.J., Funahashi, T., Tanaka, S., Matsuzawa, Y., Chao, C.L., Chen, C.L., Tai, T.Y., and Chuang, L.M. (2001). Weight reduction increases

177

plasma levels of an adipose-derived anti-inflammatory protein, adiponectin. J. Clin. Endocrinol. Metab. 86, 3815–3819.

278.   Perkins, J.M., and Davis, S.N. (2008). Endocannabinoid system overactivity and the metabolic syndrome: prospects for treatment. Curr. Diab. Rep. 8, 12–19.

279.   Pi-Sunyer, F.X., Aronne, L.J., Heshmati, H.M., Devin, J, Rosenstock, J., and RIO-North America Study Group (2006). Effect of rimonabant, a cannabinoid-1 receptor blocker, on weight and cardiometabolic risk factors in overweight or obese patients: RIO-North America: a randomized controlled trial. JAMA 295, 761–775.

280.   Jbilo, O., Ravinet-Trillou, C., Arnone, M., Buisson, I., Bribes, E., Péleraux, A., Pénarier, G., Soubrié, P., Le Fur, G., Galiègue, S., et al. (2005). The CB1 receptor antagonist rimonabant reverses the diet-induced obesity phenotype through the regulation of lipolysis and energy balance. FASEB J. 19, 1567–1569.

281.   Wang, Q., Perrard, X.D., Perrard, J.L., Mansoori, A., Smith, C.W., Ballantyne, C.M., and Wu, H. (2011). Effect of the cannabinoid receptor-1 antagonist rimonabant on inflammation in mice with diet-induced obesity. Obesity (Silver Spring) 19, 505–513.

282. Bachman, E.S., Dhillon, H., Zhang, C.-Y., Cinti, S., Bianco, A.C., Kobilka, B.K., and Lowell, B.B. (2002). betaAR signaling required for diet-induced thermogenesis and obesity resistance. Science 297, 843–845.

283. Enos, R.T., Davis, J.M., Velázquez, K.T., McClellan, J.L., Day, S.D., Carnevale, K.A., and Murphy, E.A. (2013). Influence of dietary saturated fat content on adiposity, macrophage behavior, inflammation, and metabolism: composition matters. J. Lipid Res. 54, 152–163.

284. Liu, X.S., Chopp, M., Zhang, R.L., Tao, T., Wang, X.L., Kassis, H., Hozeska-Solgot, A., Zhang, L., Chen, C., and Zhang, Z.G. (2011). MicroRNA profiling in subventricular zone after stroke: MiR-124a regulates proliferation of neural progenitor cells through Notch signaling pathway. PLoS ONE 6, e23461.

285. Bindea, G., Mlecnik, B., Hackl, H., Charoentong, P., Tosolini, M., Kirilovsky, A., Fridman, W.-H., Pagès, F., Trajanoski, Z., and Galon, J. (2009). ClueGO: a Cytoscape plug-in to decipher functionally grouped gene ontology and pathway annotation networks. Bioinformatics 25, 1091–1093.

286. Maianti, J.P., McFedries, A., Foda, Z.H., Kleiner, R.E., Du, X.Q., Leissring, M.A., Tang, W.-J., Charron, M.J., Seeliger, M.A., Saghatelian, A., et al. (2014). Anti-diabetic activity of insulin-degrading enzyme inhibitors mediated by multiple hormones. Nature 511, 94–98.

179

287.   Sacerdote, P., Martucci, C., Vaccani, A., Bariselli, F., Panerai, A.E.,

Colombo, A., Parolaro, D., and Massi, P. (2005). The nonpsychoactive

component of marijuana cannabidiol modulates chemotaxis and IL-10 and IL-12

production of murine macrophages both in vivo and in vitro. J. Neuroimmunol.

159, 97–105.

288.   Kim, S., Thiessen, P.A., Bolton, E.E., Chen, J., Fu, G., Gindulyte, A.,

Han, L., He, J., He, S., Shoemaker, B.A., et al. (2016). PubChem Substance and

Compound databases. Nucleic Acids Res. *44*, D1202–D1213.

289.   Grandin, M., Meier, M., Delcros, J.G., Nikodemus, D., Reuten, R., Patel,

T.R., Goldschneider, D., Orriss, G., Krahn, N., Boussouar, A., et al. (2016).

Structural Decoding of the Netrin-1/UNC5 Interaction and its Therapeutical

Implications in Cancers. Cancer Cell *29*, 173–185.

290.   Handa N, Kukimoto-Niino M, Akasaka R, Murayama K, Terada T, Inoue

M, Yabuki T, Aoki M, Seki E, Matsuda T *et al*. (2006) .Structure of the UNC5H2

death domain. Acta crystallographica Section D, Biological crystallography 62,

1502-1509.

291.   Dutta, S., Burkhardt, K., Young, J., Swaminathan, G.J., Matsuura, T., Henrick, K., Nakamura, H., and Berman, H.M. (2009). Data deposition and annotation at the worldwide protein data bank. Mol. Biotechnol. *42*, 1–13.

292.   Morris GM, Huey R, Lindstrom W, Sanner MF, Belew RK, Goodsell DS, Olson AJ., et al. (2009). AutoDock4 and AutoDockTools4: Automated docking with selective receptor flexibility. Journal of computational chemistry.30, 2785-2791.

293.   Poirier, B., Bidouard, J.-P., Cadrouvele, C., Marniquet, X., Staels, B., O'Connor, S.E., Janiak, P., and Herbert, J.-M. (2005). The anti-obesity effect of rimonabant is associated with an improved serum lipid profile. Diabetes Obes Metab *7*, 65–72.

294.   .Jbilo, O., Ravinet-Trillou, C., Arnone, M., Buisson, I., Bribes, E., Péleraux, A., Pénarier, G., Soubrié, P., Le Fur, G., Galiègue, S., et al. (2005). The CB1 receptor antagonist rimonabant reverses the diet-induced obesity phenotype through the regulation of lipolysis and energy balance. FASEB J. *19*, 1567–1569.

295.   Wang, Q., Perrard, X.D., Perrard, J.L., Mansoori, A., Smith, C.W., Ballantyne, C.M., and Wu, H. (2011). Effect of the cannabinoid receptor-1 antagonist rimonabant on inflammation in mice with diet-induced obesity. Obesity (Silver Spring) *19*, 505–513.

181

296.   Després, J.-P., Golay, A., Sjöström, L., and Rimonabant in Obesity-Lipids Study Group (2005). Effects of rimonabant on metabolic risk factors in overweight patients with dyslipidemia. N. Engl. J. Med. *353*, 2121–2134.

297.   Jbilo, O., Ravinet-Trillou, C., Arnone, M., Buisson, I., Bribes, E., Péleraux, A., Pénarier, G., Soubrié, P., Le Fur, G., Galiègue, S., et al. (2005). The CB1 receptor antagonist rimonabant reverses the diet-induced obesity phenotype through the regulation of lipolysis and energy balance. FASEB J. *19*, 1567–1569.

298.   Schäfer, A., Pfrang, J., Neumüller, J., Fiedler, S., Ertl, G., and Bauersachs, J. (2008). The cannabinoid receptor-1 antagonist rimonabant inhibits platelet activation and reduces pro-inflammatory chemokines and leukocytes in Zucker rats. Br. J. Pharmacol. *154*, 1047–1054.

299.   Cota, D., Sandoval, D.A., Olivieri, M., Prodi, E., D'Alessio, D.A., Woods, S.C., Seeley, R.J., and Obici, S. (2009). Food intake-independent effects of CB1 antagonism on glucose and lipid metabolism. Obesity (Silver Spring) *17*, 1641–1645.

300.   Fujisaka, S., Usui, I., Bukhari, A., Ikutani, M., Oya, T., Kanatani, Y., Tsuneyama, K., Nagai, Y., Takatsu, K., Urakaze, M., et al. (2009). Regulatory

182

Mechanisms for Adipose Tissue M1 and M2 Macrophages in Diet-Induced Obese Mice. Diabetes *58*, 2574–2582.

301.   Weisberg, S.P., McCann, D., Desai, M., Rosenbaum, M., Leibel, R.L., and Ferrante, A.W. (2003). Obesity is associated with macrophage accumulation in adipose tissue. J. Clin. Invest. *112*, 1796–1808.

302.   Xu, H., Barnes, G.T., Yang, Q., Tan, G., Yang, D., Chou, C.J., Sole, J., Nichols, A., Ross, J.S., Tartaglia, L.A., et al. (2003). Chronic inflammation in fat plays a crucial role in the development of obesity-related insulin resistance. Journal of Clinical Investigation *112*, 1821–1830.

303.   Kamei, N., Tobe, K., Suzuki, R., Ohsugi, M., Watanabe, T., Kubota, N., Ohtsuka-Kowatari, N., Kumagai, K., Sakamoto, K., Kobayashi, M., et al. (2006). Overexpression of Monocyte Chemoattractant Protein-1 in Adipose Tissues Causes Macrophage Recruitment and Insulin Resistance. J. Biol. Chem. *281*, 26602–26614.

304.   Kanda, H. (2006). MCP-1 contributes to macrophage infiltration into adipose tissue, insulin resistance, and hepatic steatosis in obesity. Journal of Clinical Investigation *116*, 1494–1505.

305.   Hotamisligil, G.S. (2006). Inflammation and metabolic disorders. Nature *444*, 860–867.

183

306. Qatanani, M., and Lazar, M.A. (2007). Mechanisms of obesity-associated insulin resistance: many choices on the menu. Genes Dev. *21*, 1443–1455.

307. Weisberg, S.P., Hunter, D., Huber, R., Lemieux, J., Slaymaker, S., Vaddi, K., Charo, I., Leibel, R.L., and Ferrante, A.W. (2006). CCR2 modulates inflammatory and metabolic effects of high-fat feeding. J. Clin. Invest. *116*, 115–124.

308. Odegaard, J.I., Ricardo-Gonzalez, R.R., Red Eagle, A., Vats, D., Morel, C.R., Goforth, M.H., Subramanian, V., Mukundan, L., Ferrante, A.W., and Chawla, A. (2008). Alternative M2 Activation of Kupffer Cells by PPARδ Ameliorates Obesity-Induced Insulin Resistance. Cell Metabolism *7*, 496–507.

309. 54.Eisenstein, A., Carroll, S.H., Johnston-Cox, H., Farb, M., Gokce, N., and Ravid, K. (2014). An Adenosine Receptor-Krüppel-like Factor 4 Protein Axis Inhibits Adipogenesis. J. Biol. Chem. *289*, 21071–21081.

310. Liao, X., Sharma, N., Kapadia, F., Zhou, G., Lu, Y., Hong, H., Paruchuri, K., Mahabeleshwar, G.H., Dalmas, E., Venteclef, N., et al. (2011). Krüppel-like factor 4 regulates macrophage polarization. Journal of Clinical Investigation *121*, 2736–2749.

311.   Wang, W., Reeves, W.B., Pays, L., Mehlen, P., and Ramesh, G. (2009). Netrin-1 overexpression protects kidney from ischemia reperfusion injury by suppressing apoptosis. Am. J. Pathol. *175*, 1010–1018.

312.   Ly, N.P., Komatsuzaki, K., Fraser, I.P., Tseng, A.A., Prodhan, P., Moore, K.J., and Kinane, T.B. (2005). Netrin-1 inhibits leukocyte migration in vitro and in vivo. Proc. Natl. Acad. Sci. U.S.A. *102*, 14729–14734.

313.   Rosenberger, P., Schwab, J.M., Mirakaj, V., Masekowsky, E., Mager, A., Morote-Garcia, J.C., Unertl, K., and Eltzschig, H.K. (2009). Hypoxia-inducible factor-dependent induction of netrin-1 dampens inflammation caused by hypoxia. Nat. Immunol. *10*, 195–202.

314.   van Gils, J.M., Derby, M.C., Fernandes, L.R., Ramkhelawon, B., Ray, T.D., Rayner, K.J., Parathath, S., Distel, E., Feig, J.L., Alvarez-Leite, J.I., et al. (2012). The neuroimmune guidance cue netrin-1 promotes atherosclerosis by inhibiting the emigration of macrophages from plaques. Nat. Immunol. *13*, 136–143.

315.   Khan, J.A., Cao, M., Kang, B.Y., Liu, Y., Mehta, J.L., and Hermonat, P.L. (2011). Systemic human Netrin-1 gene delivery by adeno-associated virus type 8 alters leukocyte accumulation and atherogenesis in vivo. Gene Ther *18*, 437–444.

185

316.   Tacke, F., Alvarez, D., Kaplan, T.J., Jakubzick, C., Spanbroek, R., Llodra, J., Garin, A., Liu, J., Mack, M., van Rooijen, N., et al. (2007). Monocyte subsets differentially employ CCR2, CCR5, and CX3CR1 to accumulate within atherosclerotic plaques. J. Clin. Invest. *117*, 185–194.

317.   Feig, J.E., Pineda-Torra, I., Sanson, M., Bradley, M.N., Vengrenyuk, Y., Bogunovic, D., Gautier, E.L., Rubinstein, D., Hong, C., Liu, J., et al. (2010). LXR promotes the maximal egress of monocyte-derived cells from mouse aortic plaques during atherosclerosis regression. J. Clin. Invest. *120*, 4415–4424.

318.   He, K., Jang, S.-W., Joshi, J., Yoo, M.-H., and Ye, K. (2011). Akt-phosphorylated PIKE-A inhibits UNC5B-induced apoptosis in cancer cell lines in a p53-dependent manner. Mol Biol Cell *22*, 1943–1954.

319.   Leonardo, E.D., Hinck, L., Masu, M., Keino-Masu, K., Ackerman, S.L., and Tessier-Lavigne, M. (1997). Vertebrate homologues of C. elegans UNC-5 are candidate netrin receptors. Nature *386*, 833–838.

320.   Forcet, C., Stein, E., Pays, L., Corset, V., Llambi, F., Tessier-Lavigne, M., and Mehlen, P. (2002). Netrin-1-mediated axon outgrowth requires deleted in colorectal cancer-dependent MAPK activation. Nature *417*, 443–447.

321.   Ming, G., Song, H., Berninger, B., Inagaki, N., Tessier-Lavigne, M., and Poo, M. (1999). Phospholipase C-gamma and phosphoinositide 3-kinase mediate cytoplasmic signaling in nerve growth cone guidance. Neuron *23*, 139–148.

322.   Llambi, F., Causeret, F., Bloch-Gallego, E., and Mehlen, P. (2001). Netrin-1 acts as a survival factor via its receptors UNC5H and DCC. EMBO J. *20*, 2715–2722.

323.   Llambi, F., Lourenço, F.C., Gozuacik, D., Guix, C., Pays, L., Del Rio, G., Kimchi, A., and Mehlen, P. (2005). The dependence receptor UNC5H2 mediates apoptosis through DAP-kinase. EMBO J *24*, 1192–1201.

324.   Hetényi, C., and van der Spoel, D. (2002). Efficient docking of peptides to proteins without prior knowledge of the binding site. Protein Sci. *11*, 1729–1737.

325.   Yasunaga, M., Ipsaro, J.J., and Mondragón, A. (2012). Structurally similar but functionally diverse ZU5 domains in human erythrocyte ankyrin. J. Mol. Biol. *417*, 336–350.